

THERMOMECHANICAL CHARACTERIZATION AND MODELING
OF SHAPE MEMORY POLYMERS

A Thesis

by

BRENT LOUIS VOLK

Submitted to the Office of Graduate Studies of
Texas A&M University
in partial fulfillment of the requirements for the degree of

MASTER OF SCIENCE

May 2009

Major Subject: Aerospace Engineering

THERMOMECHANICAL CHARACTERIZATION AND MODELING
OF SHAPE MEMORY POLYMERS

A Thesis

by

BRENT LOUIS VOLK

Submitted to the Office of Graduate Studies of
Texas A&M University
in partial fulfillment of the requirements for the degree of

MASTER OF SCIENCE

Approved by:

| | |
|---------------------|----------------------|
| Chair of Committee, | Dimitris C. Lagoudas |
| Committee Members, | Zoubeida Ounaies |
| | Duncan Maitland |
| | Yi-Chao Chen |
| Head of Department, | Dimitris C. Lagoudas |

May 2009

Major Subject: Aerospace Engineering

ABSTRACT

Thermomechanical Characterization and Modeling
of Shape Memory Polymers. (May 2009)

Brent Louis Volk, B.S., Texas A&M University

Chair of Advisory Committee: Dr. Dimitris C. Lagoudas

This work focuses on the thermomechanical characterization and constitutive model calibration of shape memory polymers (SMPs). These polymers have the ability to recover seemingly permanent large deformations under the appropriate thermomechanical load path. In this work, a contribution is made to both existing experimental and modeling efforts. First, an experimental investigation is conducted which subjects SMPs to a thermomechanical load path that includes varying the value of applied deformations and temperature rates. Specifically, SMPs are deformed to tensile extensions of 10% to 100% at temperature rates varying from 1°C/min to 5°C/min, and the complete shape recovery profile is captured. The results from this experimental investigation show that the SMP in question can recover approximately 95% of the value of the applied deformation, independent of the temperature rate during the test.

The data obtained in the experimental investigation are then used to calibrate, in one-dimension, two constitutive models which have been developed to describe and predict the material response of SMPs. The models include a model in terms of general deformation gradients, thus making it capable of handling large deformations. In addition, the data are used to calibrate a linearized version of the constitutive model for small deformations. The material properties required for calibrating the constitutive models are derived from portions of the experimental results, and the model is then used to predict the shape memory effect for an SMP undergoing various

levels of deformation. The model predictions are shown to match well with the experimental data.

To Abby - my wife, my best friend, and my biggest supporter

ACKNOWLEDGMENTS

First, I would like to thank Dr. Lagoudas for his guidance and support as my advisor. He taught me to actually *think* about the problem at hand rather than just trying to blindly solve equations without understanding the corresponding physical significance. In addition, I would like to thank Dr. Chen for his support during this research. His work in developing the model paved the way for this research, and he provided valuable insight into proposing and designing the necessary experiments. Additional thanks go to my other committee members, Dr. Maitland and Dr. Ounaies, whose discussions, questions, and expertise have helped me overcome technical challenges and provided a fresh outlook on many research objectives.

In addition, I would like to thank Karen Whitley and the other NASA Langley Research Center employees with whom I worked for two summers. Their guidance and support was invaluable in completing the experimental portion of this work. They constantly allowed me the freedom to perform new experiments, helped me understand the results, and provided me the first opportunity to present my work to other engineers and scientists. I would also like to thank the National Science Foundation Integrative Graduate Education and Research Traineeship (NSF IGERT) fellowship program for helping to support my graduate school education.

My friends and colleagues deserve a great deal of thanks as well. My fellow researchers Parikshith Kumar, Olivier Bertacchini, Francis Phillips, and Justin Schick have provided a number of suggestions and good technical conversations which have further progressed this work. Special thanks is extended to Darren Hartl, who was my officemate from day one and has been my inspiration and role model for graduate school. He has constantly challenged me to think about the fundamental questions behind my work, and has helped me take a better approach to new challenges. Grati-

tude is extended to all of my friends, particularly my college roommates Brian Green, James Kress, Tyler Waite, and Corley Walters who have been the greatest friends and kept me level headed when things got stressful.

Finally, I would like to extend thanks to my family. I would like to thank my parents and grandparents for always supporting my dreams and providing the resources I needed to always reach my goals. I would like to thank Grandpa Lowry for teaching, inspiring, and being a role model for me more than he will ever get credit for. In addition, I would also like to thank my brother and best friend Eric and my brother Chris for always supporting their younger brother. Thank you to Abby for being everything a husband could ever ask for.

TABLE OF CONTENTS

| CHAPTER | | Page |
|---------|----------------------------------------------------------------------------------------------------------|------|
| I | INTRODUCTION | 1 |
| | A. Shape Memory Effect | 2 |
| | B. Literature Review | 4 |
| | 1. Experimental Efforts | 4 |
| | 2. Modeling Efforts | 6 |
| | C. Research Objectives and Outline of Research | 8 |
| II | THERMOMECHANICAL CHARACTERIZATION OF THE SHAPE MEMORY EFFECT OF A SHAPE MEMORY POLY- MER | 11 |
| | A. Experimental Procedures | 11 |
| | 1. Specimen Type and Preparation | 11 |
| | 2. Experimental Setup | 13 |
| | 3. Test Matrix and Experimental Parameters | 15 |
| | B. Results | 17 |
| | 1. 10% Applied Extension Experiment and Compar- ison to SME Thermomechanical Cycle | 18 |
| | 2. Repeatability of Experiments | 21 |
| | 3. Influence of Increasing Applied Extension | 23 |
| | a. Stress-Extension Relationship During Loading Above T_g | 25 |
| | b. Stress Increase Due to Constrained Cooling | 25 |
| | c. Shape Recovery Behavior During Heating at Zero Load | 27 |
| | 4. Influence of Experimental Parameters on the Total Amount of Recoverable Deformation | 28 |
| | C. Conclusions | 31 |
| III | MODEL CALIBRATION | 33 |
| | A. Description of the Chen and Lagoudas Constitutive Model | 33 |
| | B. Calibration of the Constitutive Model as Linearized for Small Deformations | 35 |
| | 1. Derivation of Linearized Model | 36 |

| CHAPTER | Page |
|-------------------------------------------------------------------------------------------------|------|
| 2. Assumptions Made in Calibrating the Model | 37 |
| 3. Determination of Calibration Parameters from Ex- perimental Data | 39 |
| 4. Axial Strain Constitutive Equation as Applied to SME Thermomechanical Load Path | 42 |
| 5. Prediction of Experimental Load Path and Discussion | 47 |
| C. Calibration of the Constitutive Model for Large Deformations | 54 |
| 1. Assumption of a Neo-Hookean Material | 55 |
| 2. Constitutive Equation as Applied to SME with Uniaxial Tension | 57 |
| 3. Determination of Calibration Parameters | 59 |
| 4. Reduction of Large Deformation Model for Small Deformations | 64 |
| 5. Axial Stretch Equation as Applied to the SME Thermomechanical Load Path | 66 |
| 6. Prediction of Experimental Load Path and Discussion | 71 |
| D. Conclusions | 80 |
| IV CONCLUSIONS | 84 |
| REFERENCES | 87 |
| APPENDIX A | 91 |
| APPENDIX B | 99 |
| VITA | 111 |

LIST OF TABLES

| TABLE | | Page |
|-------|--------------------------------------------------------------------------------------------------------------|------|
| I | Shape Memory Polymer Test Matrix. Tests with Full Results Not Presented Denoted by “*” | 18 |
| II | Effect of Increasing Temperature Rate on the Percentage of Recoverable Extension/Applied Extension | 29 |
| III | Deformation Gradients for Material Particles with Various Reference and Deformed Configurations | 34 |
| IV | Calibration Parameters Derived from 10% Applied Extension Experimental Data | 43 |
| V | Necessary Calibration Parameters for the Large Deformation Constitutive Model | 63 |

LIST OF FIGURES

| FIGURE | Page |
|--------|---------------------------------------------------------------------------------------------------------------------------|
| 1 | Thermomechanical Cycle for Shape Memory Effect in SMPs 4 |
| 2 | Shape Memory Polymer Specimens 13 |
| 3 | Experimental Setup 15 |
| 4 | Thermomechanical Analyzer Results Indicating a Glass Transition Temperature of 60°C 17 |
| 5 | Results from Experiment with 10% Applied Extension and a Temperature Rate of 3°C/min 19 |
| 6 | Stress-Extension Relationship from the End of Specimen Cooling to the End of Observed Stress Increase 21 |
| 7 | Repeatability of Experiments Presented: 10% Applied Extension Experiments with a Temperature Rate of 3°C/min 22 |
| 8 | 10%, 50%, and 100% Applied Extension Experiments with Temperature Rate of 2°C/min 24 |
| 9 | Stress-Extension Results for Tensile Tests with Applied Strains of 10%, 50%, and 100% 26 |
| 10 | Stress Increase vs. Temperature During Constrained Cooling for All Values of Applied Extension 26 |
| 11 | Extension Recovery vs. Temperature for Tensile Tests with Applied Strains of 10%, 50%, and 100% 28 |
| 12 | 25% Applied Extension Experiments with Temperature Rate Increased from 1°C/min to 5°C/min 30 |
| 13 | Recoverable Extension as a Percentage of Applied Extension for All Experiments 31 |

| FIGURE | Page |
|--------|--------------------------------------------------------------------------------------------------------------|
| 14 | Heating Curve Maintaining Zero Load 40 |
| 15 | Elastic Moduli as Calculated from 10% Applied Extension Experimental Results 41 |
| 16 | Frozen Volume Fraction as a Normalization of the Extension Recovery Profile 42 |
| 17 | Strain-Stress-Temperature Prediction for SME with 10% Applied Tensile Strain 48 |
| 18 | Stress-Strain Prediction for SME with 10% Applied Tensile Strain 49 |
| 19 | Stress-Temperature Prediction for SME with 10% Applied Tensile Strain 49 |
| 20 | Strain-Temperature Prediction for SME with 10% Applied Tensile Strain 51 |
| 21 | Strain-Stress-Temperature Prediction for 10%, 25%, 50%, and 100% Applied Tensile Strain 52 |
| 22 | Stress-Strain Prediction for 10%, 25%, 50%, and 100% Applied Tensile Strain 53 |
| 23 | Stress-Temperature Prediction for 10%, 25%, 50%, and 100% Applied Tensile Strain 53 |
| 24 | Strain-Temperature Prediction for 10%, 25%, 50%, and 100% Applied Tensile Strain 54 |
| 25 | Poisson's Ratios for Shape Memory Polymer 60 |
| 26 | Elastic Moduli as Calculated from 25% Applied Extension Results 62 |
| 27 | Frozen Volume Fraction as a Normalization of the Extension Recovery Profile 62 |
| 28 | Comparison of Stretch-Stress-Temperature Predictions for SME with 10% Applied Tensile Extension 71 |
| 29 | Stretch-Stress-Temperature Prediction for SME with Stretch Equal to 1.25 73 |

| FIGURE | Page |
|--------|------------------------------------------------------------------------------------------|
| 30 | Stress-Stretch Prediction for SME with Stretch Equal to 1.25 73 |
| 31 | Stress-Temperature Prediction for SME with Stretch Equal to 1.25 74 |
| 32 | Stretch-Temperature Prediction for SME with Stretch Equal to 1.25 76 |
| 33 | Stretch-Stress-Temperature Prediction for SME with Stretch Equal to 1.5 77 |
| 34 | Stretch-Stress-Temperature Prediction for SME with Stretch Equal to 2.0 77 |
| 35 | Stress-Stretch Prediction for SME with Stretch Equal to 1.5 and 2.0 78 |
| 36 | Stress-Temperature Prediction for SME with Stretch Equal to 1.5 and 2.0 79 |
| 37 | Stretch-Temperature Prediction for SME with Stretch Equal to 1.5 and 2.0 80 |

CHAPTER I

INTRODUCTION

Shape memory polymers (SMPs) are polymers capable of recovering an applied deformation through thermal, optical, and/or electrical actuation. SMPs represent a relatively new class of shape memory materials, which also include shape memory alloys (SMAs) and shape memory ceramics. Shape memory materials have been heavily researched, developed, and utilized in a wide range of applications, including cutting-edge technologies in the aerospace, medical, and oil exploration industries [1, 2, 3].

Although both SMPs and SMAs have the ability to recover an apparently permanent deformation, SMPs possess the unique ability to recover extensions of up to 400% [4]. In addition, SMPs are lightweight, inexpensive, and possess excellent manufacturability characteristics as compared to SMAs, but typically have stiffness and strength values two to three orders of magnitude lower than their metal counterparts [5, 6, 7, 8, 9, 10]. Considering these characteristics, SMPs present a viable solution for applications, such as space and biomedical, which demand large deformations at reduced force levels. Other possible applications for shape memory polymers include biodegradable sutures, repairable automobile skins, satellites and deployable space systems [6, 9, 11]. An example of a potential application is the concept of a morphing wing using active materials. Such an application was investigated by Toensmeir, in which the morphing wings were expected to adjust the surface area based on the current flight conditions, with a possible area increase of 300%. In this project, SMPs and composites using a shape memory polymer as the matrix material were considered as

The journal model is *International Journal of Engineering Science*.

possible choices for the skin of the wing [12].

Additional research efforts have focused on increasing the naturally low stiffness and low recovery stress of SMPs by developing composites, many of which incorporate shape memory polymer as the matrix material [11, 13, 14, 15, 16]. Related efforts by Manzo and Garcia [17] as well as McKnight and Henry [18, 19] have attempted to incorporate SMPs in applications with other shape memory materials, such as SMAs, to develop morphing or reconfigurable structures which have a variable stiffness. For example, Manzo and Garcia proposed a tri-phase composite material which included both SMAs and SMPs. By controlling the temperature of the individual phases, particularly that of the SMP, the effective stiffness of the composite was changed. Additionally, McKnight and Henry proposed the use of SMPs in reconfigurable cellular and morphing wing structures. The use of SMPs allowed for variable stiffness structure capable of undergoing large deformations.

A. Shape Memory Effect

The shape memory effect (SME) is the ability for shape memory materials to recover a seemingly permanent applied deformation through thermal cycling. Depending on the structure of the molecular chains in the shape memory polymer, the SME is triggered by heating through either the glass transition temperature (T_g) or the melting temperature (T_m). The SMPs of interest in this work are chemically cross-linked thermosets for which the cross-linked regions maintain the permanent shape of the polymer. In these SMPs, the glass transition temperature serves as the transition temperature necessary for shape recovery.

At temperatures above T_g , the polymer is in the rubber (active) phase, and the stiffness is lower than when the material is at a temperature below T_g . Consequently,

large scale deformations are possible for a SMP in the rubber phase as the polymer chains are able to move and stretch easier due to the relatively low stiffness. On the other hand, when the temperature $T < T_g$ and the polymer is in the glass (frozen) phase, large-scale motions are prevented due to the increased stiffness of the polymer. As a result, only small, elastic motions are possible. Furthermore, a material which undergoes deformation in the rubber phase can be ‘frozen’ by maintaining the deformation while cooling to the glass phase. Once in the glass phase, the polymers affected by the deformation process are frozen indefinitely until subsequent heating.

The complete thermomechanical cycle allowing for the shape memory effect is summarized in the following steps. Additionally, Fig. 1 presents the thermomechanical cycle in strain-stress-temperature space and relates it to the schematic molecular representation of the shape memory effect.

1. Deform the SMP at $T > T_g$ (rubber phase) to the desired value of deformation. By loading in the rubber phase, large deformations (strains) can be generated as the molecular chains are stretched. The entropy of the system is reduced due to the imposed deformation.
2. Hold the deformation constant, and cool to below T_g . The deformation is stored as the stiff glass phase prevents the molecular chains from moving, and the new configuration is termed the ‘temporary shape.’
3. Unload the specimen at $T < T_g$ (glass phase) to a predetermined stress level (i.e. zero stress). The decrease in strain due to elastic unloading in the glass phase is often negligible.
4. Hold the stress level constant, and heat the material to above T_g . The molecular chains are free to move, and the polymer returns to the original, permanent

shape - a state of higher entropy than the temporary shape.

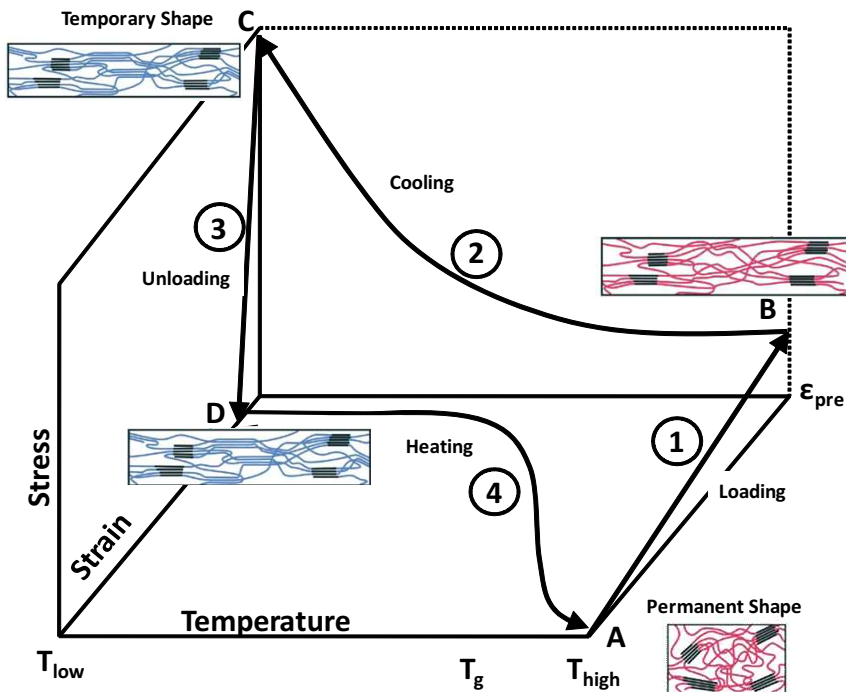


Fig. 1. Thermomechanical Cycle for Shape Memory Effect in SMPs

B. Literature Review

1. Experimental Efforts

With the ability to recover seemingly permanent large deformations, shape memory polymers have been the focus of a wide range of experimental research efforts, particularly over the previous decade, as researchers attempt to better understand the material response and capabilities. Although a broad scope of research efforts have been and continue to be performed involving SMPs, this section focuses on the research efforts present in the literature which are relevant to the research in this

work.

Initial experimental efforts by Tobushi et al. provided data from small deformation experiments, with applied extensions of 2%, 4%, and 10% [7]. The tests investigated the stress-strain relationship of thin film, polyurethane SMPs. The results obtained during this experimental investigation represented one of the first attempts to capture the entire shape memory effect of SMPs. In particular, the stress due to constrained cooling and the shape recovery upon subsequent heating was noted for the three different values of applied extension.

Additional efforts by Tobushi et al. involved deforming the thin films to extensions of 20% and 100% [8]. The thermomechanical response of specimens loaded at different temperatures was captured. In addition, the stress-strain relationship upon loading was observed to be nonlinear for extensions greater than approximately 20%. The preliminary cyclic effects on the shape recovery were investigated, and a shift in the stress-strain-temperature results was noted for subsequent thermomechanical cycles. In particular, the accumulated amount of irrecoverable deformation continued to increase for each of the ten thermomechanical cycles, and Tobushi noted that the SMPs recovered approximately 98% of the applied deformation during each thermomechanical cycle.

Extensive efforts were also conducted by Liu et al. on the thermomechanical behavior of SMPs for small deformations [5]. These experiments characterized dog-bone shaped specimens, and the data was subsequently used to calibrate and validate the proposed constitutive model. The experiments performed by Liu not only aimed to obtain the material properties above and below the glass transition temperature, but also characterize the thermomechanical response when deformed to a range of values, up to 9% in magnitude, of applied tensile and compressive strains. In these experiments, both the stress increase due to constrained cooling and the nonlinear

strain-temperature relationship during zero load recovery were captured and observed to occur in a smooth, nonlinear manner.

Recent experimental efforts have shifted from the characterization of the response due to small deformations to the large deformation response of SMPs processed in a dogbone shape. For instance, Baer et al. [20] tested polyurethane SMP specimens to tensile extensions of 20% and 100% for use in medical applications. In these experiments, the SMP recovered approximately 90% of the applied deformation, and the effects of cyclic deformation at a range of temperatures were investigated. The results from the cyclic deformation study indicated the greatest shift in material response from the first cycle to the second cycle with an apparent training, or stabilization in material response, occurring from the second to fifth cycles.

Additionally, Atli et al. thermomechanically characterized SMPs for applied tensile strains up to 75% for dogbone specimens[21]. The experiments performed by Atli are similar in principle to those presented in this work such that the same VeriflexTM shape memory polymer is used and subjected to a similar thermomechanical load path. Due to experimental apparatus limitations, however, the complete shape recovery profile during heating was not captured by Atli.

2. Modeling Efforts

A number of modeling research efforts have attempted to predict the shape memory behavior in SMPs observed experimentally. Most existing models, however, have focused on the response of the material due to small deformations ($\leq \pm 10\%$ nominal strain).

For instance, early one-dimensional modeling efforts by Tobushi and Bhattacharyya represented SMPs as a discrete spring-dashpot system [7, 22, 23]. In some of the first proposed models, Tobushi incorporates thermal expansion, viscoelasticity, and non-

linear elastic terms. Another model incorporating the viscoelastic response of SMPs when subjected to small deformations was proposed by Hong et al. [24]. In the study by Hong, the relaxation modulus was obtained at various temperatures, and was used as input to the model. A more recent rheological model has been developed by Srinivasa and Gosh [25], which also uses a spring-dashpot analogy based on a Gibbs potential approach. This model derives the state equations from the equations of motion and subsequently solves the resulting differential equations for the state of the material. Although the aforementioned models present a useful physical analogy to the deformation mechanisms in the material, many fail to meet the desired accuracy of the material response and often do not present a very general framework for arbitrary thermomechanical deformations.

In a model proposed by Rao [26], the shape memory behavior was approached from and related to the formation of the crystalline phase of the polymer. Specifically, the model incorporated variables which accounted for the rubber phase, the semicrystalline phase, the crystallization process, and the melting process. The model proposed that the formation of the crystalline phase ‘stored’ the deformation, and the subsequent ‘melting’ of the crystalline phase returned the material to its original shape.

Another model which predicted the small deformation material response was proposed by Liu et al. [5]. This model additively decomposes the strain into thermal, elastic, and stored components and utilizes two internal variables - namely the frozen volume fraction and the stored strain - to describe the evolution of the microstructure. The model assumes that deformation which is in the material is then ‘frozen’ and thus contributes to the term accounting for the stored strain. Upon subsequent heating, the stored deformation is then released, and the material returns to its original, permanent shape.

More recently, a three-dimensional SMP constitutive model has been developed by Chen and Lagoudas which can account for the nonlinear material response due to large deformations [27, 28]. This model, proposed on the framework of thermoelasticity, adapts similar concepts to the model proposed by Liu et al. such that it incorporates the concepts of stored strain and a frozen volume fraction. The constitutive equation proposed by this model, in its general form, can be interpreted as essentially a rule of mixtures with contributions due to deformations in the frozen and active phase as well as a contribution due to deformations which are frozen upon cooling. Additionally, Chen and Lagoudas linearized this model and then used small deformation data produced by Liu and Gall to calibrate the model and analyze its validity. The large deformation model, however, remained previously uncalibrated due to the lack of sufficient data.

C. Research Objectives and Outline of Research

The review of the literature and state of the current research in SMPs indicates there is significant opportunity for furthering both the experimental and modeling body of knowledge in the field. For instance, there have been few successful experimental efforts which captured the large deformation response of shape memory polymers. As such, the first objective of the research in this work is to perform a thorough experimental investigation of the large deformation shape memory effect in SMPs. This effort will use an advanced visual-photographic strain measurement device and is intended to be one of the first to capture the entire shape recovery profile for large values of applied deformation.

The experiments presented in this work aim to expand on the knowledge about SMPs previously observed by Tobushi, Liu, Atli, and others by investigating a rela-

tively large range of applied deformations as well as temperature rates, as applied to the commercially available VeriflexTM. The material is subjected to a series of tensile tests for applied extensions of 10%, 25%, 50%, and 100% under temperature rates ranging from 1°C/min to 5°C/min. It is important to note that *extension*, or *nominal strain*, is defined and used hereafter as the change in the length of the material divided by the initial length. Additionally, the *stress* referred to in the experimental portion of this work is the *first Piola-Kirchoff stress* which is defined by the applied load divided by the initial cross-sectional area.

In addition to the experimental objectives, the other primary objective of this research is to use to large deformation data obtained experimentally to calibrate a large deformation constitutive model for SMPs. While many models have been calibrated for small deformations, there exists no models which have been calibrated which can accurately describe the large deformation response of these active materials. As a result, this work will calibrate the Chen and Lagoudas constitutive model in one-dimension. The successful calibration of this model will represent the first step toward implementing such a model into a more general, finite-element framework for the analysis and optimization of complex structures in which SMPs are to be used.

In Chapter II, the details of the thermomechanical tests are presented. First, the experimental setup, including the 3-D Vision Image Correlation (VIC 3D) system, a visual-photographic apparatus used to measure the distributed two-dimensional strain field, is presented. Specifically, the method used to prepare the specimens, the parameters of the shape memory effect (SME) thermomechanical load path, and the test matrix is presented. The results from the thermomechanical tests are then presented and analyzed to determine the influence on the material response due to increasing applied deformation and temperature rates.

In Chapter III, the constitutive models developed by Chen and Lagoudas are

calibrated using the data obtained in Chapter II. First, the constitutive model linearized for infinitesimal strains is calibrated using the data from the 10% applied extension case, and the model is used to predict the material response for values of strain of 25%, 50%, and 100%. These predictions are empirically compared to the experimental results for extensions of the same magnitude. Next, the general constitutive model capable of handling large deformations is calibrated using data from the 25% extension experiments. Assuming a neo-Hookean material undergoing uniaxial deformation, the model is simplified to an equation for the axial stretch of the material. The model is then used to predict the material response for stretch values of 1.25, 1.50, and 2.0 and compared to the experimental results.

CHAPTER II

THERMOMECHANICAL CHARACTERIZATION OF THE SHAPE MEMORY EFFECT OF A SHAPE MEMORY POLYMER

A general introduction to shape memory polymers (SMPs) and the shape memory effect (SME) was provided in Chapter I. In the current chapter, the thermomechanical experimental investigation of the shape memory effect of a SMP is presented. The experimental procedures, including the material used, experimental setup, and test matrix are presented. The results are then analyzed to gain a better understanding of the material behavior and the manner in which it is affected by changes in experimental parameters.

A. Experimental Procedures

This section presents the experimental procedures necessary to test the SMP specimens. Included in the procedures is the preparation of the specimens for use with a visual strain measurement system. The details of this strain measurement system and the other components of the experimental apparatus are presented. In addition, the experiments performed in this study are outlined in the form of a test matrix.

1. Specimen Type and Preparation

The shape memory polymer used for testing was the commercially available VeriflexTM produced by Cornerstone Research Group, Inc.(CRG). VeriflexTM is a thermoset, polystyrene-based SMP whose exact composition has been retained by CRG. The material was received in the form of 0.6 m x 0.6 m (24.0 in x 24.0 in) pre-cured sheets. In this work, the focus was on the shape memory effect under tensile loading, and the size of the specimens was adapted from the ASTM D638 Standard Test

Method for the Tensile Properties of Plastics [29].

The resulting samples were in a dogbone shape with a 57.0 mm (2.25 in) gauge length and a 12.7 mm x 3.2 mm (0.50 in x 0.125 in) cross-sectional area in the gauge region. The total length of the specimens was 114.0 mm (4.50 in). Figure 2a presents a schematic of a shape memory polymer dogbone specimen. A water jet cutting procedure, performed at NASA Langley Research Center, was used to cut the specimens from the bulk material. Small regions of local damage were seen at the end of the specimen which coincided with where the water jet started and finished cutting. The concentrations, however, were relatively small in size and at the edge furthest from the gauge region; thus, these regions were assumed to have no impact on the material response as observed within the gauge area.

After the specimens were processed to the desired specifications, they were then prepared for thermomechanical characterization using the Vision Image Correlation (VIC) 3D system - an optical strain measurement system. The VIC 3D system requires a high-contrast 'speckled' pattern on the surface of the gauge area. This pattern is photographed at each time step and then processed in such a way to calculate the displacements and strains of the material. Because the specimens were transparent in nature, a white base coat was first applied to the specimens. Then, a random, black speckled pattern was applied and resulted in a contrast sufficient for the system to correlate images. Figure 2b presents a specimen ready for experimentation using the VIC system.

The material was received, processed, and stored until testing at room temperature and at atmospheric pressure. The specimens were tested over a period of two years with no noticeable change in shape recovery behavior. This observation implies the material is not significantly affected by changing atmospheric conditions or environmental aging on this time scale. Furthermore, each specimen was only subjected

to a single thermomechanical cycle. As such, the results presented in this work represent the behavior of pristine specimens, and may not be representative of a ‘trained’ material for use as an actuator.

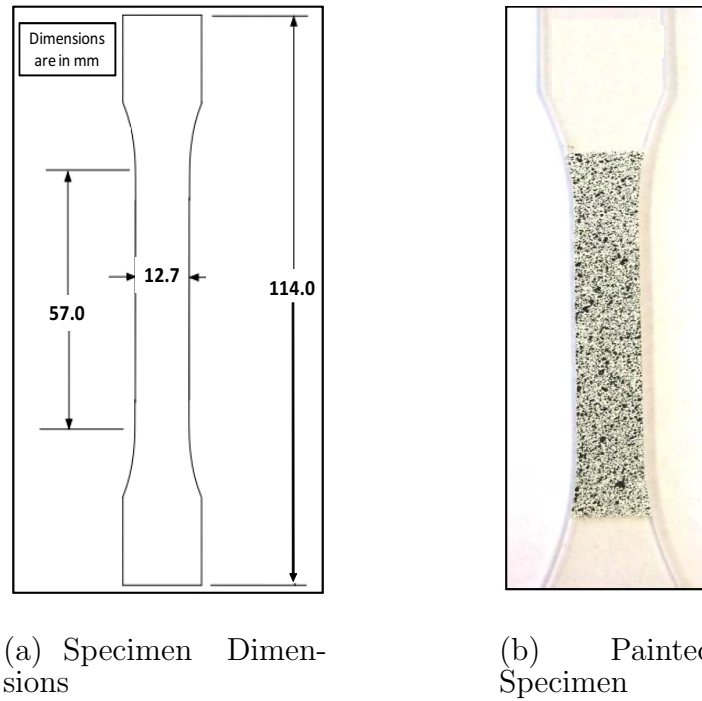


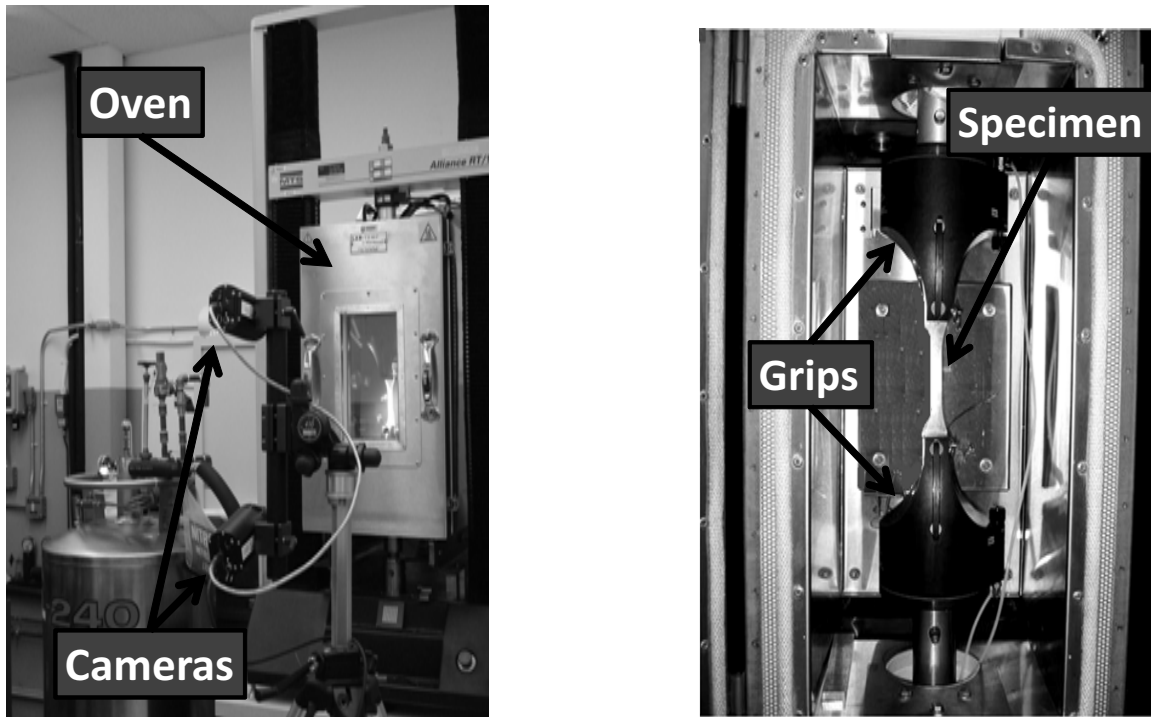
Fig. 2. Shape Memory Polymer Specimens

2. Experimental Setup

All of the thermomechanical experiments presented in this work were performed in the Materials Research Laboratory at NASA Langley Research Center. The tests were conducted on a vertically positioned electromechanical, screw-driven *MTS*[®] Alliance RT-1 test frame accessorised with a *MTS*[®] 1000 N load cell and a pair of *MTS*[®] 2000 N pneumatic grips equipped with 25.4 mm x 25.4 mm (1.0 in x 1.0 in) serrated grip faces. The grip pressure of the pneumatic grips was set to 80 kPa as to neither yield the specimen in the grip region or allow slipping of the material.

In addition, the characterization of the SMPs performed in this work required a complex, multi-step temperature profile and a controlled temperature rate. Consequently, the experimental setup included a *Thermcraft*[®] temperature chamber featuring forced convection heating and liquid nitrogen cooling with an integrated PID controller. The temperature range of the chamber is (-)73°C to 315°C - limits well beyond the necessary temperature range for the tests in this work. In addition, the temperature controller was linked to the software governing the mechanical movement of the test frame. This connection allowed the thermal and mechanical profiles to be interconnected and required less real-time control by the operator. The temperature was measured by a thermocouple placed near the gauge region of the SMP and the measured value was assumed to be representative of the temperature of the material in the gauge region. Figure 3a shows the entire experimental setup, and Fig. 3b presents a view of a specimen inside the pneumatic grips.

Due to the low elastic modulus of the shape memory polymer at high temperatures, a non-contact strain measurement technique was utilized to ensure that no interference of specimen motion occurred. Specifically, the displacement of the material was measured and recorded using the VIC 3D strain measurement technique. Developed by Correlated Solutions, Inc., the VIC 3D system records a picture of the specimen with the aforementioned painted pattern in the reference configuration and then takes a picture of the specimen throughout the experiment at a specified time interval. The system then calculates the displacement of each material point in the current configuration with respect to the reference configuration and subsequently calculates the full-field, two-dimensional strain measurements.



(a) Complete Testing Apparatus

(b) Interior of Furnace

Fig. 3. Experimental Setup

3. Test Matrix and Experimental Parameters

The purpose of the experimental effort in this study is to characterize the SMP material behavior, particularly the shape memory effect, and how it is affected by variations in the experimental parameters. In this work, two experimental parameters were changed - the value of the total applied deformation (extension) and the temperature rate (TR), where the temperature rate refers to the cooling and heating rate in steps 2 and 4 of Fig. 1, respectively. SMP specimens were deformed to values of extension of 10%, 25%, 50%, and 100% during the first step in Fig. 1. This range of extensions captures not only the relatively small deformation response (10% extension) but also the large deformation response up to 100% extension. Additionally, the

temperature rates were increased from 1°C/min to 5°C/min to determine the effects on the total amount of recoverable deformation. The matrix in Table I presents the tests performed on the shape memory polymers.

The experiments followed the thermomechanical cycle outlined in Fig. 1. First, the specimen was placed in the temperature chamber at room temperature. After placement of the specimen in the grips, the temperature was increased from room temperature to approximately 30 degrees above T_g while maintaining zero load on the specimen. As noted in the literature and verified by TMA experiments, the transition from the glass phase to the rubber phase occurs over a range of temperatures, rather than at an individual temperature T_g [6]. For the Veriflex[®] shape memory polymer, the T_g is calculated from the TMA results in Fig. 4 to be approximately 60°C, with complete transformation occurring near 85°C. As a result, the specimen is heated, at a constant temperature rate, to 90°C to ensure the specimen is completely in the rubber phase. The temperature value of 90°C was also observed by Atli et al. to be a sufficiently high temperature to observe negligible difference in material response in the rubber phase [21]. It is also observed that the transformation to the glass phase during cooling is complete at approximately 40°C.

After thermal equilibrium is achieved, the specimen is loaded at a strain rate of 0.025 (mm/mm)/min to the predetermined value of extension. This strain rate corresponds to a nominal displacement rate of 1.425 mm/min - a value within the standards posed by ASTM D638 which recommends a displacement rate in the range of 1 mm/min to 50 mm/min [29]. The deformation is then held constant and the specimen is cooled, at a constant temperature rate, to room temperature (25°C), thus ensuring complete transformation to the glass phase. The constraint disallowing thermal contraction results in a stress increase, which is subsequently unloaded to the predetermined recovery load after cooling is complete. In these experiments, the

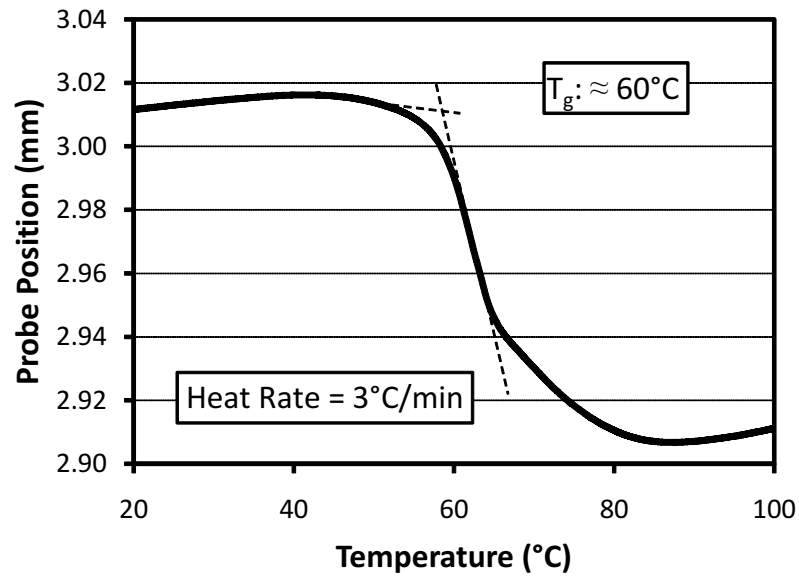


Fig. 4. Thermomechanical Analyzer Results Indicating a Glass Transition Temperature of 60°C

load is chosen to be zero, neglecting gravity. Finally, zero load is maintained on the specimen, and the temperature is again raised, at a constant temperature rate, to 90°C to induce shape recovery.

B. Results

Although an extensive set of tests was performed on SMP specimens, only a representative set of results is presented in this work. These results are intended to be sufficient to adequately portray the sensitivity of the material behavior with respect to changes in thermomechanical parameters such as the value of the total applied extension and temperature rate. The omitted results are denoted by the asterisk (*) in Table I.

Table I. Shape Memory Polymer Test Matrix. Tests with Full Results Not Presented Denoted by “*”

| Test Case | Applied Extension | Heating/Cooling Rate (°C/min) | Recovery Temperature (°C) | Recovery Stress (MPa) | Recovery Extension |
|--------------------------|-------------------|-------------------------------|---------------------------|-----------------------|--------------------|
| Constant Stress Recovery | 10% | 1*, 2, 3, 5* | $T = T_g + 30$ (~90°C) | $\sigma = 0$ | Output |
| | 25% | 1, 2, 3, 5 | $T = T_g + 30$ (~90°C) | $\sigma = 0$ | |
| | 50% | 2, 3*, 5* | $T = T_g + 30$ (~90°C) | $\sigma = 0$ | |
| | 100% | 2 | $T = T_g + 30$ (~90°C) | $\sigma = 0$ | |

1. 10% Applied Extension Experiment and Comparison to SME

Thermomechanical Cycle

To begin, consider the result presented in Fig. 5, in which a SMP specimen is deformed to an extension of 10%. The temperature rate for the experiment was 3°C/min. The experiment begins with the specimen at room temperature at which the SMP is below the glass transition temperature and consequently in the glass phase. Due to the fact that the thermomechanical cycle presented in Fig. 1 has the material in the rubber phase as the reference configuration, the first step is heating the specimen to 90°C at 3°C/min such that the reference configuration coincides with point ‘A’ in Fig. 1. During this heating process, zero load is maintained on the specimen, allowing the material to thermally expand without constraint. Upon the temperature passing the glass transition temperature T_g , and thus entering the rubber phase, a larger amount of thermal expansion is observed as a result the larger coefficient of thermal expansion of the material in the rubber phase. Consistent with the value calculated in the TMA results in Fig. 4, the glass transition temperature during heating is approximately 60°C during the initial heating.

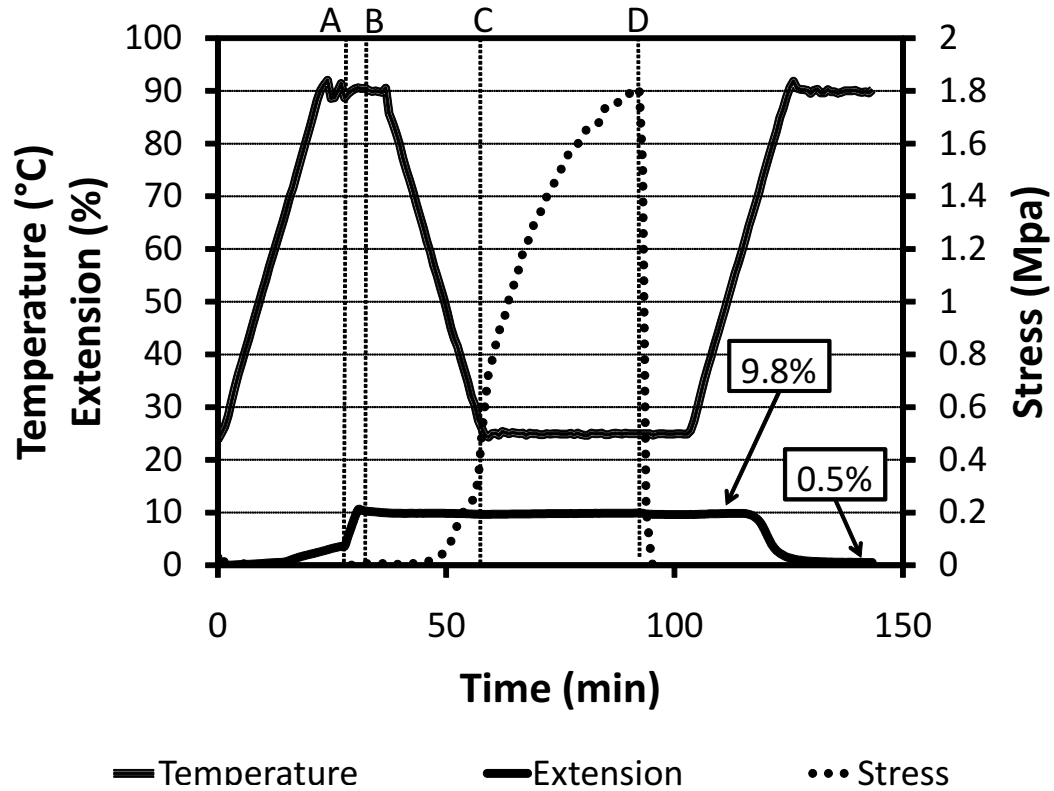


Fig. 5. Results from Experiment with 10% Applied Extension and a Temperature Rate of 3°C/min

After the temperature chamber has reached equilibrium at the end of the heating segment, denoted 'A' on the plot, the thermomechanical cycle follows the steps A->B->C->D outlined in Fig. 1. From A to B, the temperature is held constant at 90°C and the specimen is loaded at a strain rate of 0.025 (mm/mm)/min to the predetermined extension value of 10%.

From B to C, the deformation is held constant and the specimen is cooled to 25°C at a temperature rate of 3°C/min. During this cooling process, the material transitions from the rubber phase to the glass phase. Due to the constraint disallowing

thermal contraction during cooling, the stress increases with a larger stress increase noted due to further cooling below T_g as a result of the higher stiffness of the material in the glass phase. The qualitative trend of the stress increase during cooling to time C is consistent with that seen in literature by Liu et al. [5]. It is observed, however, that although the cooling has ceased at point C, the stress continues to increase. This increase is due to continued cooling of the system, particularly the pneumatic grips and extension rods. As the system continues to cool until thermal equilibrium at room temperature, the components of the experimental setup undergo thermal contraction which induces further deformation in the material that fails to be corrected by the PID control of the test frame. Figure 6 plots the stress increase as a function of the extension from the time C up to the time when the stress ceases to increase. This figure implies a linear stress-extension relationship during this time with the modulus (543 MPa) of the same order of magnitude as the calculated elastic modulus of the glass phase (1081 MPa).

A dwell period is used to allow the system to reach equilibrium, and then the load induced by the constrained cooling is removed - denoted by the time D. The elastic strain due to unloading is negligible compared to the total applied deformation in this work. After unloading, the furnace is opened, and the specimen is released from the bottom grip and allowed to hang freely from the top grip. This release of the bottom constraint ensures the specimen is allowed to recover under zero load conditions, neglecting gravity. Then, the furnace is closed, the specimen is again heated at a temperature rate of $3^\circ\text{C}/\text{min}$ to 90°C , and the nonlinear extension-temperature relationship is observed. The shape recovery of the material begins at the time when the temperature exceeds the glass transition temperature, which is again observed to be approximately 60°C . At the end of the heating segment, nearly all of the applied deformation has been recovered as the final, irrecoverable extension is 0.5%.

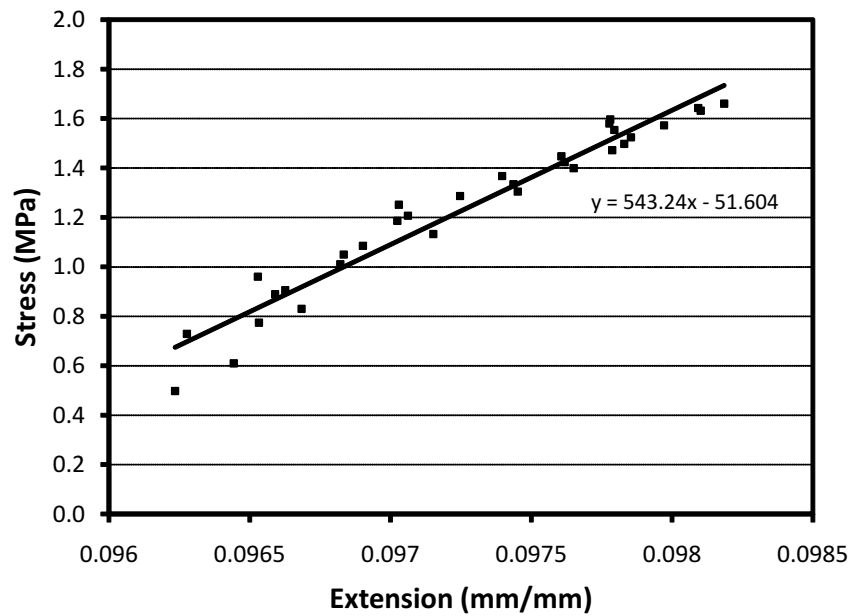
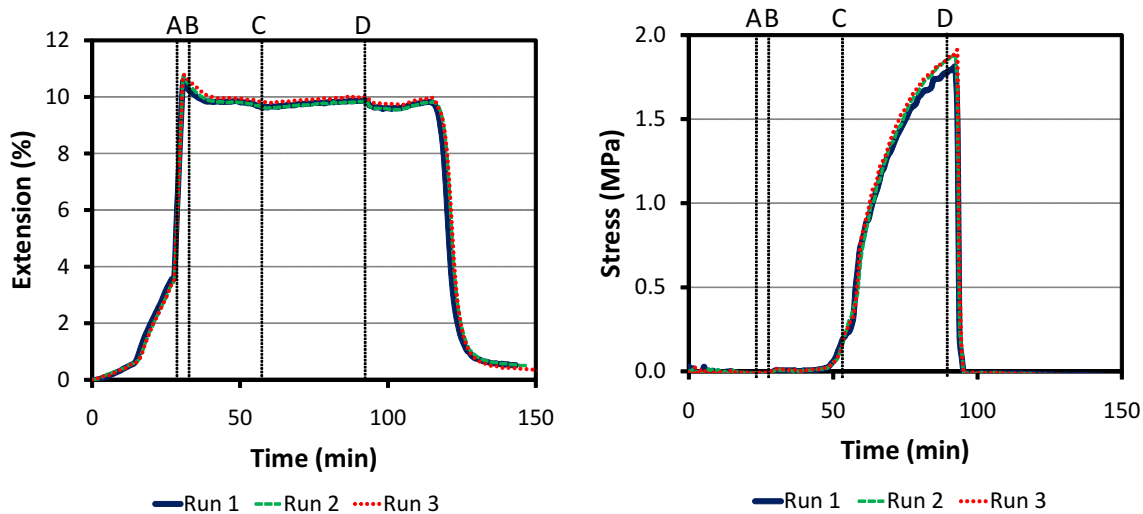


Fig. 6. Stress-Extension Relationship from the End of Specimen Cooling to the End of Observed Stress Increase

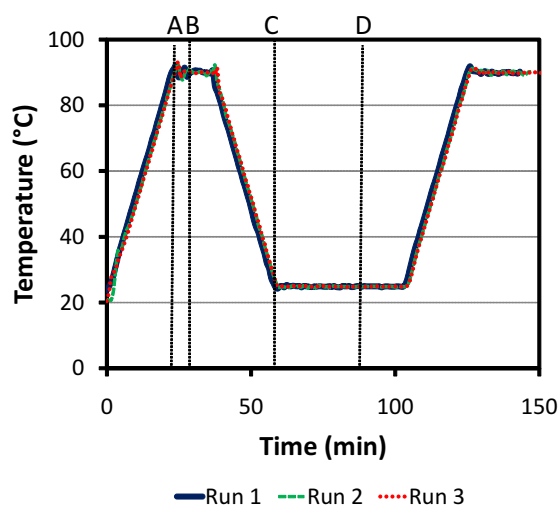
2. Repeatability of Experiments

Tests were performed with the same experimental parameters on two additional pristine specimens. In particular, the temperature rate was $3^{\circ}\text{C}/\text{min}$ and the total applied extension was 10%. Overlaying the results from these two tests with the data from the experiment in the previous section, Fig. 7a presents the extension profiles on the same time scale for all three experiments. In addition, Figs. 7b and 7c present the stress and temperature profiles, respectively.



(a) Extension

(b) Stress



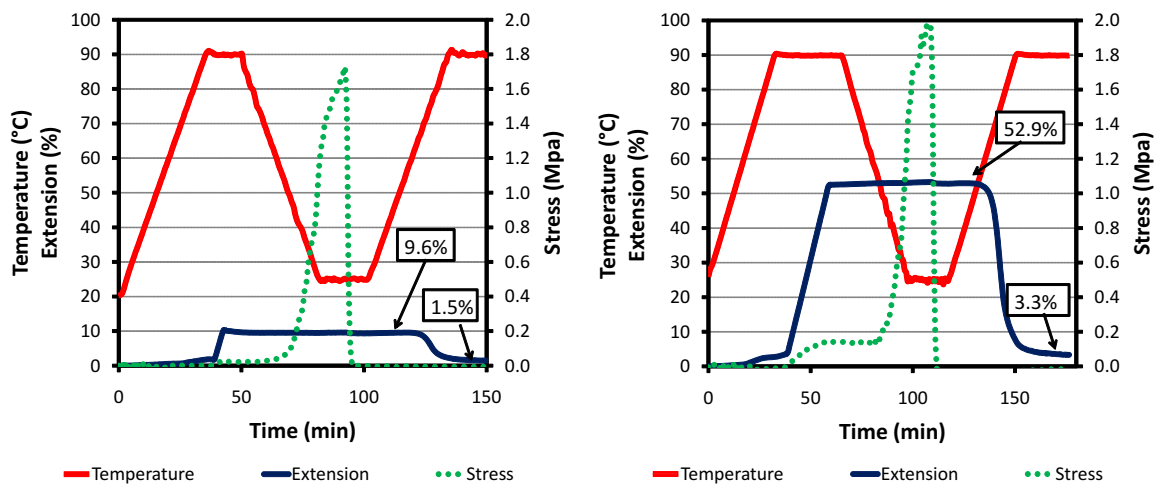
(c) Temperature

Fig. 7. Repeatability of Experiments Presented: 10% Applied Extension Experiments with a Temperature Rate of 3°C/min

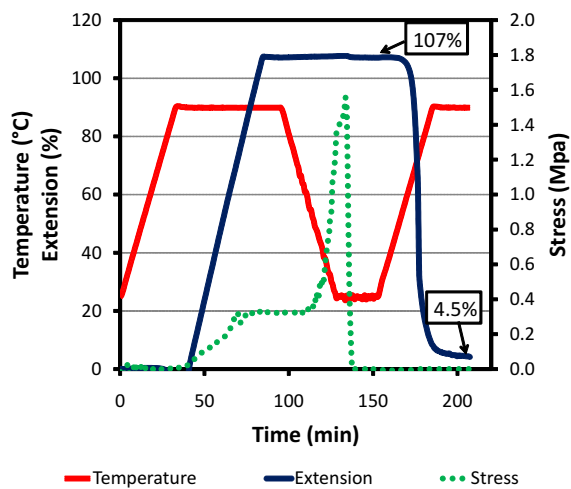
At the end of loading, the total extension of each specimen is between 9.8% and 10.0%, and the irrecoverable strain at the end of the experiment ranges from 0.3% to 0.5%. The glass transition temperature is approximately the same temperature for each experiment, as represented by the inflection points in the stretch curves during the initial and recovery heating processes. Furthermore, the stress profiles are nearly identical with a peak stress during cooling of approximately 1.75 MPa. These figures help confirm the repeatability of the thermomechanical experiments performed in this work when subjected to the same experimental parameters.

3. Influence of Increasing Applied Extension

Figures 8a - 8c present the results for experiments in which extensions of 10%, 50%, and 100% with a heating rate of 2°C/min are applied to pristine specimens. The three values of extension are chosen such that the results of the experiments with not only the smallest and largest values but also an intermediate value can be compared. The stress, extension, and temperature profiles are presented together as a function of time for each value of extension, and the steps in the thermomechanical profiles again correlate with the SME load path presented in Fig. 1. This section focuses on individual segments of the thermomechanical load path and discusses the differences observed in the material response due to increasing the value of the total applied extension.



(a) 10% Applied Extension, TR: 2°C/min (b) 50% Applied Extension, TR: 2°C/min



(c) 100% Applied Extension, TR: 2°C/min

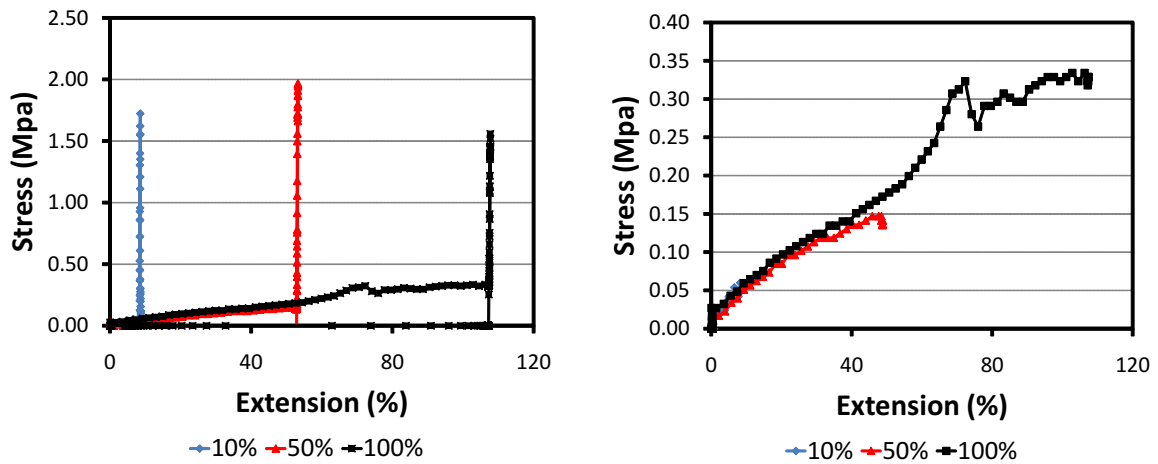
Fig. 8. 10%, 50%, and 100% Applied Extension Experiments with Temperature Rate of 2°C/min

a. Stress-Extension Relationship During Loading Above T_g

The stress-extension relationship for the 10%, 50%, and 100% extension experiments is presented in Fig. 9a with Fig. 9b focusing on the stress-extension relationship during loading. Analyzing the data, the stress-extension relationship appears linear for small values of extension. At values of extension greater than approximately 25-30%, however, the stress-extension relationship becomes nonlinear, denoted by the decreasing tangent modulus. Additionally, during loading to 100% extension, a local peak is observed in the stress at approximately 70% extension after which the stress-extension curve continues to decrease in slope. This peak may be related to polymer chain movements and alignments within the specimen, or the peak may be related to localized yielding in the paint on the surface of the specimen. Due to the fact that only one experiment was successfully performed for an extension value of 100%, additional experiments are necessary to determine the repeatability of the peak and to determine its cause.

b. Stress Increase Due to Constrained Cooling

The stress as a result of cooling at constant deformation is presented in Fig. 10 for all values of applied extension - 10%, 25%, 50%, and 100%. Not included in the previous discussion, the data from the 25% extension experiment is presented in this section to assist in establishing a correlation between increasing applied extension and the amount of stress increase upon cooling. In Fig. 10, the stress at the beginning of the cooling (90°C) is offset to zero for each case, such that only the increase in stress due to cooling is compared. The stress increases by a larger quantity upon further cooling below the glass transition temperature due to the higher stiffness of the material in the glass phase.



(a) Entire Thermomechanical Cycle

(b) Loading Portion

Fig. 9. Stress-Extension Results for Tensile Tests with Applied Strains of 10%, 50%, and 100%

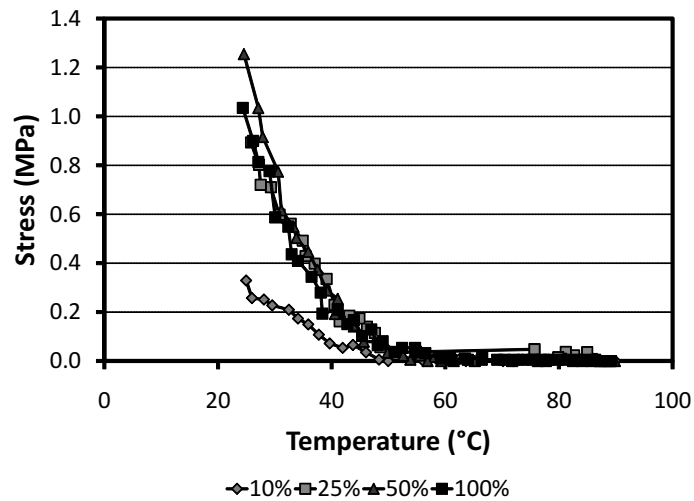


Fig. 10. Stress Increase vs. Temperature During Constrained Cooling for All Values of Applied Extension

It is observed that the change in the stress from the beginning of cooling to the end of cooling increases from the 10% test (0.3 MPa) to the 25% test (0.9 MPa) to the 50% test (1.3 MPa) and then decreases for the 100% experiment (1.1 MPa). Such a trend suggests a possibility that the stress increase is due not only to the constraint disallowing thermal contraction, but also due to another process related to the physical process of the phase transition. The fact that the stress increase is not as large for the 100% strain experiment may be a consequence of the local peak noted during the loading segment. Additional experiments are recommended to determine the stochastic variation in the stress increase for the 100% extension case.

c. Shape Recovery Behavior During Heating at Zero Load

The extension-temperature relationship for the 10%, 50%, and 100% extension experiments is presented in Fig. 11. In this figure, the results are presented for experiments with the same temperature rate of $2^{\circ}\text{C}/\text{min}$. The boundary condition on the specimen in each experiment is the load is zero in the axial direction, neglecting gravity, and is enforced by allowing the specimen to hang freely from the top grip with no constraint due to the bottom grip. In Fig. 11, the shape recovery begins at the same temperature for each specimen (approximately 60°C). It is also observed that the rate of change of the extension during recovery is greater with increasing values of applied extension, for which the 10% extension experiment displays a relatively gradual shape recovery and the 100% extension experiment exhibits a more rapid shape recovery. In other words, a larger amount of the applied extension is recovered during an equal amount of time to heat the specimen (equal temperature rate between experiments).

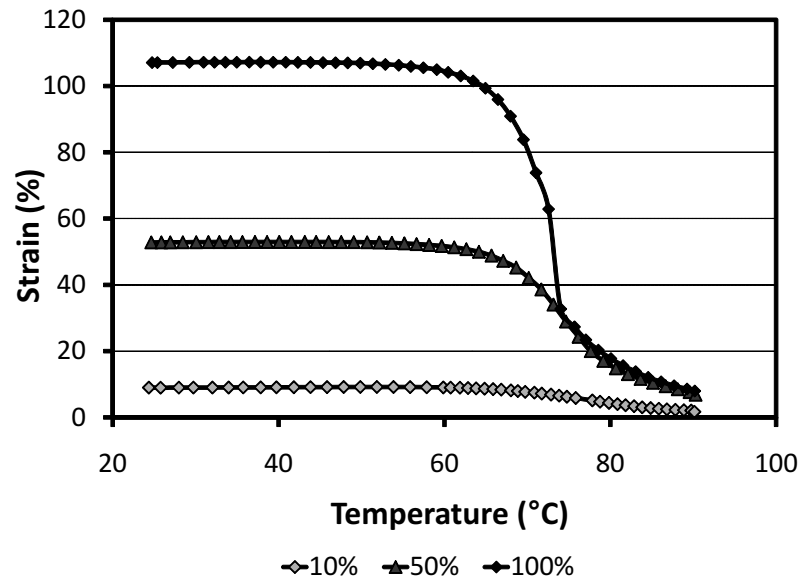


Fig. 11. Extension Recovery vs. Temperature for Tensile Tests with Applied Strains of 10%, 50%, and 100%

4. Influence of Experimental Parameters on the Total Amount of Recoverable Deformation

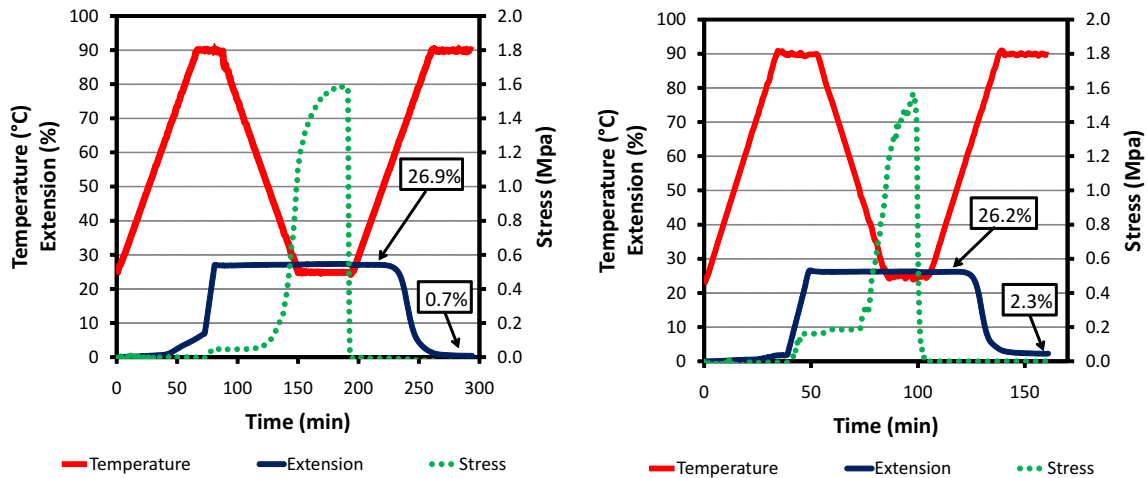
Figures 12a - 12c present a series of experimental results in which the value of the applied extension is held constant at 25% and the temperature rate is varied from 1°C/min to 5°C/min. Analysis of these figures, presented in Table II, indicates that a change in the temperature rate does not affect the amount of recoverable extension when calculated as a percentage of the total applied extension. In this table, a comparison is presented for the amount of recoverable deformation for the 25% applied extension experiments with temperature rates of 1°C/min, 3°C/min, and 5°C/min are presented. In each experiment, an extension of approximately 27% was applied to the specimen. At the end of the recovery process, the material has recovered

approximately 97% of the value of the applied extension (e.g., approximately 26% of the original 27% applied extension).

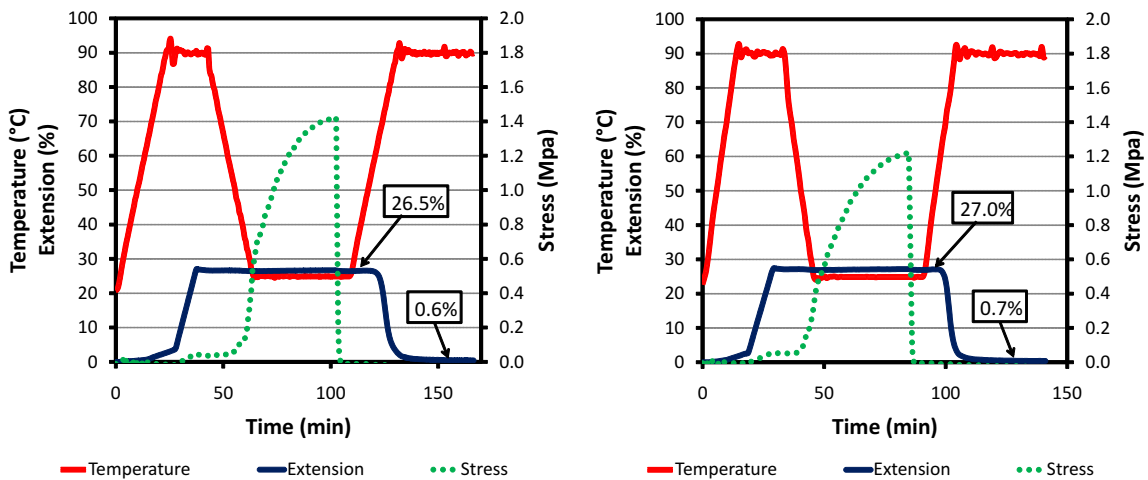
Table II. Effect of Increasing Temperature Rate on the Percentage of Recoverable Extension/Applied Extension

| Applied Extension | Temperature Rate | | |
|--------------------------|-------------------------|----------------|----------------|
| | 1°C/min | 3°C/min | 5°C/min |
| 25% | 97.4% | 97.8% | 97.4% |

Similar data was obtained as a result of testing SMP specimens for other values of applied extension and temperature rates, as noted in the test matrix in Table I. For all experiments, little variation was seen in the amount of recoverable extension as a percentage of the total applied extension. Figure 13 provides a comparison of the amount of recoverable deformation for all values of applied extension tested at different temperature rate values. In this figure, it is noted that the SMPs, independent of the temperature rate used during the thermomechanical cycle, recovered approximately 95% of the value of the total applied deformation. Additionally, because the irrecoverable deformation is a constant percentage for all values of temperature rate, it is concluded that the material does not undergo any significant viscoplastic (creep) deformation at this time scale. The irrecoverable deformation, however, may be a result of polymer chain entanglements or similar interactions which occur during the thermomechanical cycle. An investigation of the cyclic response of the material would provide insight as to whether this irrecoverable deformation plateaus or continues to increase with additional thermomechanical cycles.



(a) 25% Applied Extension, TR: 1°C/min (b) 25% Applied Extension, TR: 2°C/min



(c) 25% Applied Extension, TR: 3°C/min (d) 25% Applied Extension, TR: 5°C/min

Fig. 12. 25% Applied Extension Experiments with Temperature Rate Increased from 1°C/min to 5°C/min

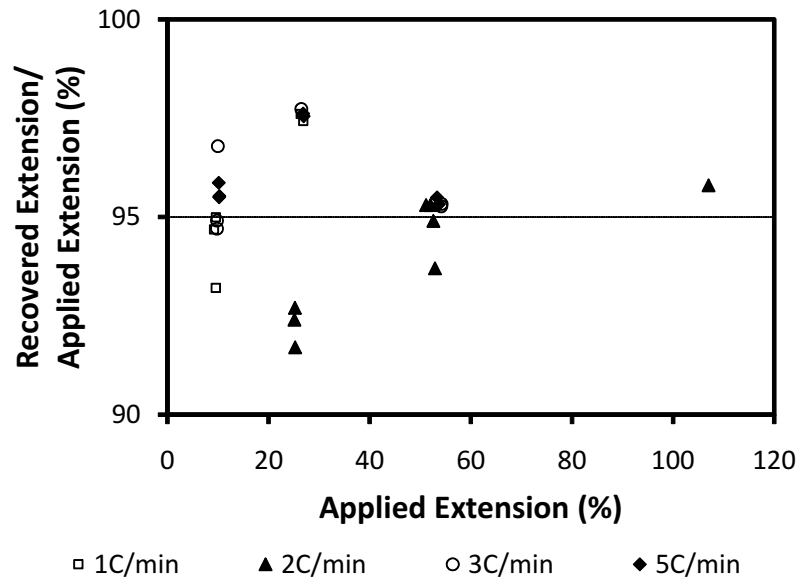


Fig. 13. Recoverable Extension as a Percentage of Applied Extension for All Experiments

C. Conclusions

An experimental investigation of the shape memory effect in a particular shape memory polymer was conducted. As part of the experimental efforts, a complex experimental apparatus was assembled at NASA Langley Research Center. The apparatus included a visual strain measurement system formally referred to as the VIC 3D system. SMP specimens were processed into dogbone specimens and the gauge area was painted with a white and black speckled pattern. The tests followed the SME thermomechanical cycle presented in Fig. 1, and focused strictly on the material response due to applied tensile deformations. Furthermore, the effects of increasing applied extension and temperature rate were evaluated.

Experiments with extensions of 10%, 25%, 50%, and 100% and temperature rates of 1°C/min to 5°C/min were performed on pristine shape memory polymer specimens, and the complete shape recovery profile was captured for all values of applied deformation. In analyzing the results, it was noted that the stress-extension relationship during loading is approximately linear for values of extension less than 25% after which the relationship becomes nonlinear as the value of the tangent modulus decreases. In addition, the amount of stress increase during constrained cooling is observed to increase as a function of increasing applied extension with the exception of the 100% extension case. This exception may be explained by the peak noted during loading at an extension of approximately 70%, where localized yielding of the surface paint or other polymer chain motions have occurred. Furthermore, the shape recovery was analyzed at zero load for all experiments. For a given temperature rate, the recovery not only begins at the same temperature but also finishes in the same amount of time. Finally, the temperature rate is shown to have negligible impact on the total amount of recoverable deformation as each specimen recovered approximately 95% of the value of the applied deformation.

CHAPTER III

MODEL CALIBRATION

A general introduction to shape memory polymers (SMPs) and the shape memory effect (SME) was provided in Chapter I. Additionally, Chapter I reviewed a series of models that have been proposed in attempts to describe the material response of SMPs. In Chapter II, a detailed experimental investigation of the thermomechanical behavior of a particular SMP was performed, and this chapter uses the data to calibrate two constitutive models developed to predict the material behavior. As a preliminary step to calibrating the general Chen and Lagoudas constitutive model, the calibration of the model as linearized for small deformations is performed. Subsequently, using a similar procedure for determining the calibration parameters, the general constitutive model is calibrated for large uniaxial deformations.

A. Description of the Chen and Lagoudas Constitutive Model

The model calibrated in this work is a constitutive model developed by Chen and Lagoudas [27]. This model is proposed on the basis of nonlinear thermoelasticity, and is thermodynamically formulated based on the Gibb's free energy function. Through assuming a thermoelastic material, the deformation of the material is assumed to be composed only of thermal and elastic contributions. As a result, the deformation gradient is assumed to be a function of the (first) Piola-Kirchoff stress \mathbf{S} and the absolute temperature θ .

The model is developed around the physical assumption that the shape memory polymer undergoes phase transformation through a series of nucleations. In other words, it is assumed that individual material particles transform from the frozen (glass) phase to the active (rubber) phase and vice versa until the entire material has

transformed into a single phase. As a result, the constitutive equations for particles in a single phase are first proposed. In proposing these equations, a deformation gradient $\hat{\mathbf{F}}_a$ is proposed for a particle with a reference configuration in the active phase that subsequently undergoes deformation while remaining purely in the active phase. Similarly, a deformation gradient $\hat{\mathbf{F}}_f$ is proposed for a particle with a reference configuration in the frozen phase and for which deformation occurs in the frozen phase. For a particle which has an active reference configuration, is frozen, and undergoes subsequent deformation in the frozen phase, the deformation gradient is assumed to be continuous at the glass transition temperature and the resulting deformation gradient is written in the form of $\hat{\mathbf{F}}_f \tilde{\mathbf{F}}$, where $\tilde{\mathbf{F}}$ is the term resulting from enforcing continuity at T_g [27]. A summary of the proposed deformation gradients for the various reference and deformed configurations is provided in Table III.

Table III. Deformation Gradients for Material Particles with Various Reference and Deformed Configurations

| Reference Configuration | Deformed Configuration | Deformation Gradient |
|-------------------------|------------------------|-------------------------------------------------------------|
| Active phase | Active phase | $\hat{\mathbf{F}}_a(\mathbf{S}, \theta)$ |
| Frozen phase | Frozen phase | $\hat{\mathbf{F}}_f(\mathbf{S}, \theta)$ |
| Active phase | Frozen phase | $\hat{\mathbf{F}}_f(\mathbf{S}, \theta) \tilde{\mathbf{F}}$ |

The shape memory polymer is then assumed to be a ‘composite’ of material particles in the active and frozen phases, and the constitutive equation describing the material behavior is presented in Eq. (3.1). This equation, derived from an integral over the volume of the individual particles, is observed to take the form

of a mixture, or composite, of the deformation gradients in the active and frozen phases, with an additional contribution from deformations in the active phase which are subsequently frozen. The term accounting for the portion of the material in the frozen phase is the frozen volume fraction $\phi(\theta)$ which is assumed to be only a function of temperature. Two assumptions are made in proposing the constitutive equation for the SMP material, specifically: (1), the deformation must be continuous during cooling, and (2) the deformation stored in the material during the freezing process is completely recovered upon subsequent heating through the same range of temperature values.

$$\begin{aligned} \mathbf{F}(\mathbf{t}) = & [1 - \phi(\theta(t))]\hat{\mathbf{F}}_a(\mathbf{S}(t), \theta(t)) \\ & + \int_0^t \hat{\mathbf{F}}_f(\mathbf{S}(t), \theta(t))\hat{\mathbf{F}}_f^{-1}(\mathbf{S}(\tau), \theta(\tau))\hat{\mathbf{F}}_a(\mathbf{S}(\tau), \theta(\tau))\phi'(\theta(\tau))\tilde{\theta}'(\tau)d\tau \end{aligned} \quad (3.1)$$

Another component of the proposed model is the idea of a ‘net cooling history,’ denoted in Eq. (3.1) by $\tilde{\theta}(\tau)$. This concept, a consequence of assumption (2), replaces a series of heating and cooling segments with a monotonically decreasing temperature profile, where τ is the last time at which the material experienced the temperature θ . In other words, it serves as a ‘memory’ term for recalling the state of the material when it previously experienced a particular temperature.

B. Calibration of the Constitutive Model as Linearized for Small Deformations

To compare with existing experimental data, Chen and Lagoudas linearized the general thermoelastic constitutive model, in particular Eq. (3.1), for small deformations [28]. The *highlights* of the derivation, exhausted in the literature by Chen and Lagoudas, will be presented first in this section. After the key equations are noted, the assumptions used to calibrate the model, the differences in the calibration method compared to that of Chen and Lagoudas, and the results of the calibration

and subsequent model predictions are presented.

1. Derivation of Linearized Model

In deriving the linearized constitutive model, the deformation of the material was assumed to be represented by the infinitesimal strain. This tensor, denoted \mathbf{E} , is related to the deformation gradient \mathbf{F} by Eq. (3.2), where \mathbf{I} is the identity tensor.

$$\mathbf{E} = \frac{1}{2}(\mathbf{F} + \mathbf{F}^T) - \mathbf{I} \quad (3.2)$$

Using this relationship, the deformation gradients \mathbf{F}_a and \mathbf{F}_f are expressed in terms of the infinitesimal strain tensors for the active and frozen phases, respectively, which are subsequently decomposed into the thermal and elastic contributions, as seen in Eq. (3.3).

$$\begin{aligned} \frac{1}{2}[\hat{\mathbf{F}}_a(\mathbf{S}, \theta) + \hat{\mathbf{F}}_a^T(\mathbf{S}, \theta)] - \mathbf{I} &= \hat{\mathbf{E}}_a(\mathbf{S}, \theta) = \mathbf{E}_a^t(\theta) + \mathbf{M}_a(\theta)[\mathbf{S}] \\ \frac{1}{2}[\hat{\mathbf{F}}_f(\mathbf{S}, \theta) + \hat{\mathbf{F}}_f^T(\mathbf{S}, \theta)] - \mathbf{I} &= \hat{\mathbf{E}}_f(\mathbf{S}, \theta) = \mathbf{E}_f^t(\theta) + \mathbf{M}_f(\theta)[\mathbf{S}] \end{aligned} \quad (3.3)$$

where \mathbf{M}_a and \mathbf{M}_f are the elastic compliance tensors in the active and frozen phases and \mathbf{E}_a^t and \mathbf{E}_f^t are the thermal strain tensors, respectively. Taking the first order approximation of Eq. (3.1) and using the assumption that the deformation gradient is close to the identity tensor for small deformations, the multiplicative deformation gradient terms in the integral of Eq. (3.1) are reduced to additive terms and Eq. (3.1) is simplified to Eq. (3.4)

$$\begin{aligned} \mathbf{F}(\mathbf{t}) &= [1 - \phi(\theta(t))]\hat{\mathbf{F}}_a(\mathbf{S}(t), \theta(t)) + \phi(\theta(t))\hat{\mathbf{F}}_f(\mathbf{S}(t), \theta(t)) \\ &\quad + \int_0^t [\hat{\mathbf{F}}_a(\mathbf{S}(t), \theta(t)) - \hat{\mathbf{F}}_f(\mathbf{S}(\tau), \theta(\tau))]\phi'(\theta(\tau))\tilde{\theta}'(\tau)d\tau \end{aligned} \quad (3.4)$$

Substituting the relationships in Eqs. (3.2) and (3.3) into Eq. (3.4), the constitutive equation written in terms of the infinitesimal strain is obtained in Eq. (3.5).

This equation becomes the foundation for calibrating the model for one-dimensional deformations.

$$\begin{aligned} \mathbf{E}(\mathbf{t}) = & [1 - \phi(\theta(t))][\hat{\mathbf{E}}_a^t(\theta(t)) + \mathbf{M}_a(\theta(t))[\mathbf{S}(t)]] + \phi(\theta(t))[\hat{\mathbf{E}}_f^t(\theta(t)) + \mathbf{M}_f(\theta(t))[\mathbf{S}(t)]] \\ & + \int_0^t [\hat{\mathbf{E}}_a^t(\theta(\tau)) + \mathbf{M}_a(\theta(\tau))[\mathbf{S}(\tau)] - \hat{\mathbf{E}}_f^t(\theta(\tau)) - \mathbf{M}_f(\theta(\tau))[\mathbf{S}(\tau)]] \phi'(\theta(\tau)) \tilde{\theta}'(\tau) d\tau \end{aligned} \quad (3.5)$$

The constitutive equation in Eq. (3.5) assumes the axial strain component can be fully described by the thermal and elastic contributions in both the active and the frozen phases, as well as the thermal and elastic deformations which are stored during the freezing process. The mixture of the active and frozen phases is accounted for via the frozen volume fraction $\phi(\theta)$.

2. Assumptions Made in Calibrating the Model

Several assumptions were made in calibrating the constitutive equation for the small deformation of SMPs presented in Eq. (3.5). First, it was assumed that SMP behaved as an isotropic, linear elastic material. The compliance tensors $\mathbf{M}_a(\theta)$ and $\mathbf{M}_f(\theta)$ are then represented by Eq. (3.6).

$$\begin{aligned} \mathbf{M}_a(\theta)[\mathbf{S}] &= \frac{1}{E_a(\theta)} [[1 + \nu_a(\theta)]\mathbf{S} - \nu_a(\theta)(tr\mathbf{S})\mathbf{I}] \\ \mathbf{M}_f(\theta)[\mathbf{S}] &= \frac{1}{E_f(\theta)} [[1 + \nu_f(\theta)]\mathbf{S} - \nu_f(\theta)(tr\mathbf{S})\mathbf{I}] \end{aligned} \quad (3.6)$$

where E_a , E_f , ν_a , and ν_f are the elastic moduli of the active and frozen phases and the Poisson's ratios of the active and frozen phases, respectively. The thermal strain tensors $\mathbf{E}_a^t(\theta)$ and $\mathbf{E}_f^t(\theta)$ can be written for isotropic materials in terms of a scalar thermal strain quantity as represented in Eq. (3.7).

$$\begin{aligned} \mathbf{E}_a^t(\theta) &= \varepsilon_a^t(\theta)\mathbf{I} \\ \mathbf{E}_f^t(\theta) &= \varepsilon_f^t(\theta)\mathbf{I} \end{aligned} \quad (3.7)$$

In calibrating the small deformation model, it is assumed that the first Piola-Kirchoff stress \mathbf{S} can be approximated by the Cauchy Stress σ . Such an assumption is generally reasonable for small deformations where it is assumed the cross-sectional area of the material changes negligibly as a result of the applied load. To predict the experimental results obtained in Chapter II, it is assumed that the SMP material is undergoing uniaxial tension. Consequently, the only non-zero component of the stress tensor is $\sigma_{11} = \sigma(t)$, and the infinitesimal strain tensor reduces to Eq. (3.8), where $\varepsilon(t)$ and $\varepsilon_l(t)$ are the axial and lateral strain components, respectively.

$$\mathbf{E}(t) = \begin{pmatrix} \varepsilon(t) & 0 & 0 \\ 0 & \varepsilon_l(t) & 0 \\ 0 & 0 & \varepsilon_l(t) \end{pmatrix} \quad (3.8)$$

Using the assumption on the stress state of the material in combination with Eqs. (3.5), (3.6), (3.7), and (3.8), the axial strain component can be written in its entirety in the form of Eq. (3.9).

$$\begin{aligned} \varepsilon(t) = & [1 - \phi(\theta(t))][\varepsilon_a^t(\theta(t)) + \frac{\sigma(t)}{E_a(\theta(t))}] + \phi(\theta(t))[\varepsilon_f^t(\theta(t)) + \frac{\sigma(t)}{E_f(\theta(t))}] \\ & + \int_0^t [\varepsilon_a^t(\theta(\tau)) - \varepsilon_f^t(\theta(\tau)) - \frac{\sigma(\tau)}{E_a(\theta(\tau))} + \frac{\sigma(\tau)}{E_f(\theta(\tau))}] \phi'(\theta(\tau)) \tilde{\theta}'(\tau) d\tau \end{aligned} \quad (3.9)$$

Assuming the material has a constant coefficient of thermal expansion (CTE) in each of the active and frozen phases, the thermal strain terms are rewritten in the form of Eq. (3.10).

$$\begin{aligned} \varepsilon_a^t(\theta(t)) &= \alpha_a \Delta\theta(t) \\ \varepsilon_f^t(\theta(t)) &= \alpha_f \Delta\theta(t) \end{aligned} \quad (3.10)$$

where α_a and α_f are the CTEs of the active and frozen phases, respectively, and $\Delta\theta(t)$ is the change in absolute temperature from the reference configuration. Hence, for a given stress profile $\sigma(t)$, the two coefficients of thermal expansion α_a and α_f ,

the elastic moduli of the active and frozen phases $E_a(\theta)$ and $E_f(\theta)$, and the frozen volume fraction $\phi(\theta)$ are the five calibration parameters required to fully calibrate the axial strain equation in Eq. (3.9) of an isotropic, linear elastic SMP undergoing small, uniaxial deformations.

3. Determination of Calibration Parameters from Experimental Data

Analyzing the results from the experimental investigation performed in Chapter II, it is noted that four of the five calibration parameters can be directly calculated from portions of the experimental results, and the fifth parameter can be realized as a normalization of a function obtained in the results. The experiments with the smallest value of applied extension(10%) in Chapter II are used to calibrate the small deformation model, where it has been assumed that the extension of the material obtained experimentally is approximately equal to the axial component of the infinitesimal strain in the constitutive model. As such, the coefficients of thermal expansion for the frozen and active phases are calculated from the extension-temperature curve during the initial heating. In this segment of the test, the load is maintained at zero, and the extension-temperature curve infers a linear relationship in each of the active and frozen phases which are separated by a phase transition region. Figure 14 presents the initial heating curve from a representative 10% applied extension experiment. From the slopes of the linear regions, $\alpha_a = 5.2 * 10^{-4}/^{\circ}C$ and $\alpha_f = 0.75 * 10^{-4}/^{\circ}C$.

Additionally, the material is assumed to be completely in the active phase when loading to the predetermined value of applied deformation. As a result, the elastic moduli for the active phase E_a is simply the slope of the stress-extension curve during loading. After the material is cooled to room temperature at a constant deformation, the load induced during the cooling process specimen is then unloaded. Assuming the material is purely in the frozen phase during this unloading process, the slope

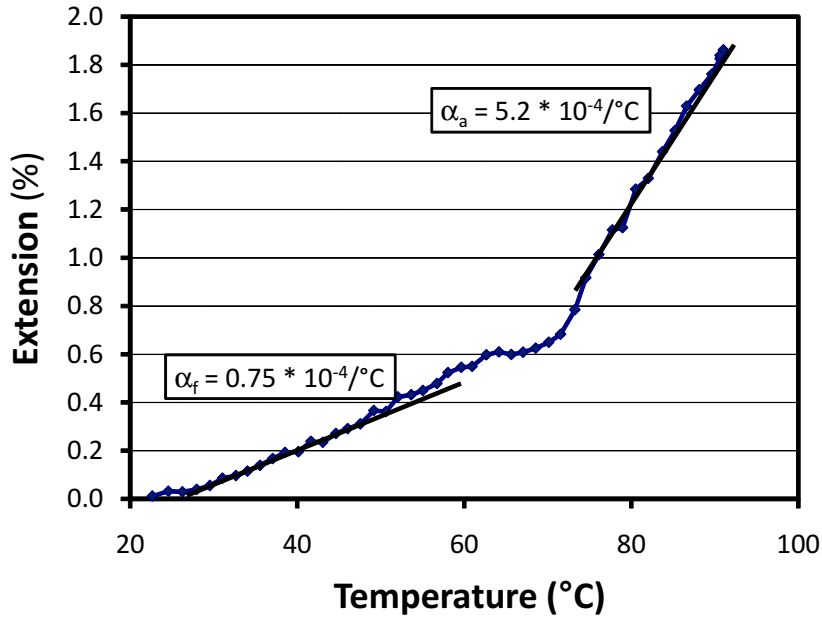
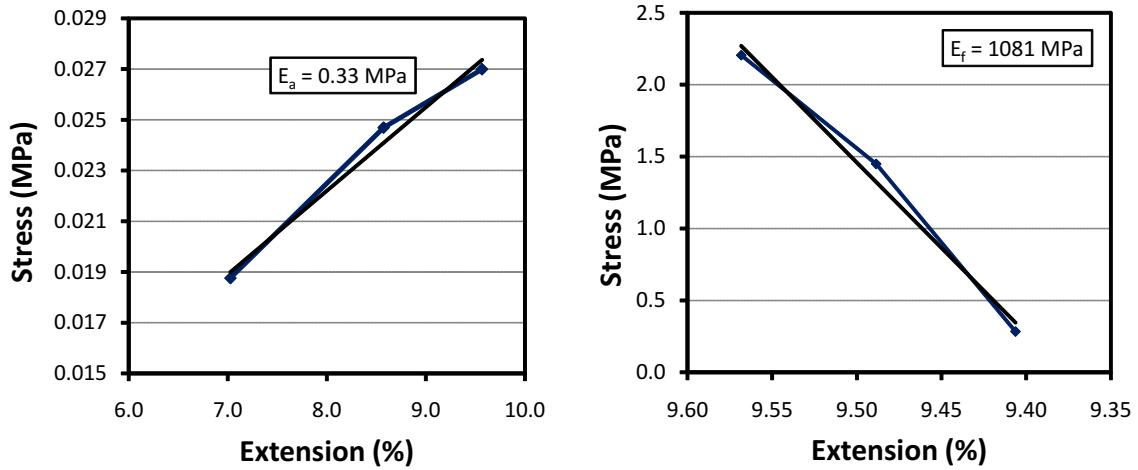


Fig. 14. Heating Curve Maintaining Zero Load

of the resultant stress-extension curve is the elastic moduli of the frozen phase E_f . Figures 15 (a) and (b) present the portions of the loading and unloading curves, respectively, from a representative 10% applied extension experiment, from which E_a and E_f are calculated to be 0.33 MPa and 1081 MPa, respectively. In this work, the elastic moduli is assumed to be independent of the temperature a material in either the active and frozen phases; thus, the functional dependence on temperature in the constitutive equations will be suppressed.

By obtaining α_a , α_f , E_a , and E_f , four of the necessary five calibration parameters are determined. The fifth calibration requirement, the frozen volume fraction $\phi(\theta)$, can be assumed to be related to the shape recovery profile during heating. When heating at zero stress, the elastic terms in Eq. (3.9) are zero. Further, by neglecting the thermal expansion, the only remaining term is the integral term. This term im-



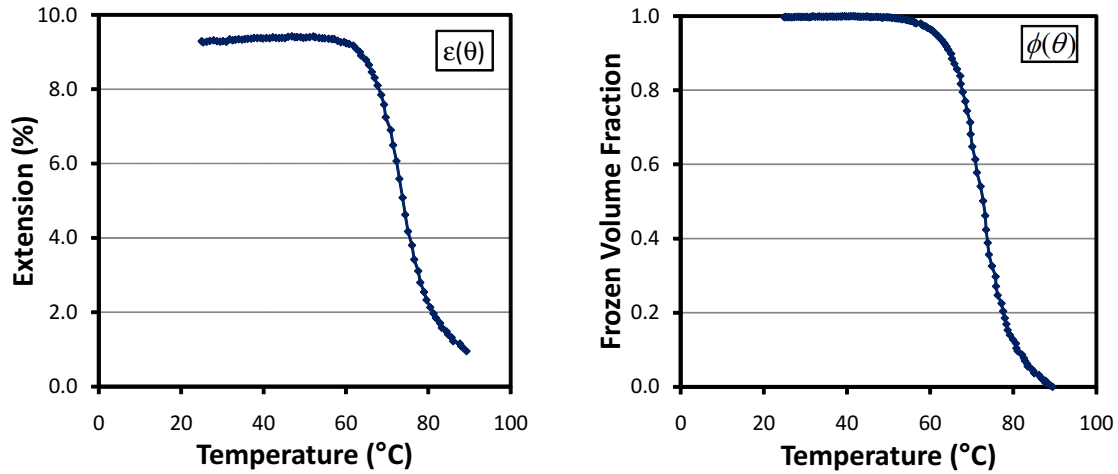
(a) Loading in Active Phase

(b) Unloading in Frozen Phase

Fig. 15. Elastic Moduli as Calculated from 10% Applied Extension Experimental Results

plies the shape recovery of the material during heating is dictated by the change in the frozen volume fraction at each temperature $\phi'(\theta)$. Specifically, the deformation which was 'frozen' upon cooling is 'restored' upon heating at a rate proportional to the change in the frozen volume fraction with respect to temperature. As a result, this work assumes the frozen volume fraction $\phi(\theta)$ is a normalization of the maximum recoverable extension during the recovery heating $\varepsilon(\theta)$. Figures 16 (a) and (b) present the shape recovery during heating and the resulting frozen volume fraction, respectively. Consistent with the assumption that all deformation which was 'frozen' is subsequently recovered upon heating, the frozen volume fraction is normalized to a scale of zero to one. A summary of the calibration requirements and the corresponding values as calculated from 10% experimental data is presented in Table IV.

This method used to obtain the calibration parameters differs from the method



(a) Extension Recovery During Heating at Zero Load

(b) Frozen Volume Fraction

Fig. 16. Frozen Volume Fraction as a Normalization of the Extension Recovery Profile

implemented in the literature by Chen and Lagoudas, for which it was assumed that the calibration functions could not be independently obtained for a given set of experimental results. As such, a series of mathematical manipulations were presented which in part reduced to the stress increase during cooling and the strain recovery during heating as combinations of the calibration requirements. Although the method used by Chen and Lagoudas presents an innovative way of combining parameters and using the experimental curves, it lacks a physical intuition of how the calibration parameters relate to physical quantities.

4. Axial Strain Constitutive Equation as Applied to SME Thermomechanical Load Path

The determination of the calibration requirements allows for the prediction of the material behavior as a result of general uniaxial strain-stress-temperature profiles.

Table IV. Calibration Parameters Derived from 10% Applied Extension Experimental Data

| Parameter | Value |
|--------------------------------------------------------------|---------------------------------------|
| Active phase coefficient of thermal expansion (α_a) | $5.2 \cdot 10^{-4}/^{\circ}\text{C}$ |
| Frozen phase coefficient of thermal expansion (α_f) | $0.75 \cdot 10^{-4}/^{\circ}\text{C}$ |
| Active phase elastic modulus (E_a) | 0.33 MPa |
| Frozen phase elastic modulus (E_f) | 1081 MPa |
| Frozen volume fraction ($\phi(\theta)$) | $f(\epsilon(\theta))$ |

The focus of this work, however, is to predict and compare the response due to the specific thermomechanical load path described in Chapters I and II. As a result, this section reduces Eq. (3.9) to a series of equations for each step in the load path which can be easily implemented in MATLAB[®].

Revisiting Eq. (3.9) and considering the first step of the thermomechanical path, the integral term of the equation can be eliminated. This term is eliminated due to the fact that the temperature is held constant during loading, and thus $\tilde{\theta}'(\tau) = 0$. In addition, the thermal strain terms are equal to zero as no change in temperature is occurring. The equation for the first step is then written as Eq. (3.11), which can be interpreted as a rule of mixtures formulation for the elastic strains due to the contributions from the fraction of the material in the active and frozen phases, respectively. In implementing this equation, the stress profile calculated assuming linear elastic loading for the predetermined strain value is provided as input. Then,

the values of strain are predicted as output for the range of stress values from zero to the calculated final stress.

$$\varepsilon(t) = [1 - \phi(\theta(t))] \frac{\sigma(t)}{E_a} + \phi(\theta(t)) \frac{\sigma(t)}{E_f} \quad (3.11)$$

In the second step, the temperature is assumed to decrease in a monotone manner, and Eq. (3.9) is rewritten in terms of temperature in Eq. (3.12).

$$\begin{aligned} \varepsilon(\theta) = & [1 - \phi(\theta)] \left[\varepsilon_a^t(\theta) + \frac{\sigma(\theta)}{E_a} \right] + \phi(\theta) \left[\varepsilon_f^t(\theta) + \frac{\sigma(\theta)}{E_f} \right] \\ & + \int_{\theta_0}^{\theta} \left[\varepsilon_a^t(\zeta) - \varepsilon_f^t(\zeta) - \frac{\sigma(\zeta)}{E_a} + \frac{\sigma(\zeta)}{E_f} \right] \phi'(\zeta) d\zeta \end{aligned} \quad (3.12)$$

where the integral variable ζ represents the intermediate temperatures during cooling. In this step, the deformation is held constant and the material is cooled to below the glass transition temperature to ‘freeze’ the material in its temporary shape. The deformation (strain) to be held constant is provided as input and the stress increase as a function of temperature is the output. Differentiating Eq. (3.12) with respect to temperature and invoking the fundamental theorem of calculus on the integral term, the equation can be rewritten as an ordinary differential equation for stress as a function of temperature in Eq. (3.13).

$$0 = [1 - \phi(\theta)] \alpha_a + \phi(\theta) \alpha_f + \left[\frac{1 - \phi(\theta)}{E_a} + \frac{\phi(\theta)}{E_f} \right] \frac{d\sigma(\theta)}{d\theta} \quad (3.13)$$

where the relationships for the thermal strains $\varepsilon_a^t(\theta) = \alpha_a(\theta - \theta_0)$ and $\varepsilon_f^t(\theta) = \alpha_f(\theta - \theta_0)$ have been used and θ_0 represents the temperature at the beginning of the cooling phase. Rearranging Eq. (3.13) for the derivative of stress with respect to temperature $\dot{\sigma}(\theta)$ results in Eq. (3.14).

$$\frac{d\sigma(\theta)}{d\theta} = -\frac{[1 - \phi(\theta)]\alpha_a + \phi(\theta)\alpha_f}{\left[\frac{1-\phi(\theta)}{E_a} + \frac{\phi(\theta)}{E_f}\right]} \quad (3.14)$$

The result obtained in Eq. (3.14) is an ordinary differential equation for which all of the terms on the right hand side are known calibration parameters, and the stress at the end of loading in step 1 is in the initial condition.

In the third step of the thermomechanical load path, the temperature is held constant at $T < T_g$, and the material is unloaded to a predetermined recovery stress. In this work, this stress was chosen to be equal to zero. As a consequence of the constant temperature during this step, the integral term in Eq. (3.9) is reduced to include only the contribution from cooling in the second step. As a result, Eq. (3.9) reduces to the form presented in Eq. (3.15), where $\theta(t) = \theta_2$ and θ_2 is a constant temperature in the frozen phase.

$$\begin{aligned} \varepsilon(t) = & [1 - \phi(\theta_2)][\varepsilon_a^t(\theta_2) + \frac{\sigma(t)}{E_a}] + \phi(\theta_2)[\varepsilon_f^t(\theta_2) + \frac{\sigma(t)}{E_f}] \\ & + \int_{\theta_0}^{\theta_2} [\varepsilon_a^t(\zeta) - \varepsilon_f^t(\zeta) - \frac{\sigma(\zeta)}{E_a} + \frac{\sigma(\zeta)}{E_f}] \phi'(\zeta) d\zeta \end{aligned} \quad (3.15)$$

where the integral term in Eq. (3.15) is replaced using the relationship in Eq. (3.16) for the strain at the end of the cooling segment. Consequently, Eq. (3.15) is simplified to Eq. (3.17).

$$\begin{aligned} \varepsilon_{pre} = \varepsilon(\theta_2) = & [1 - \phi(\theta_2)][\varepsilon_a^t(\theta_2) + \frac{\sigma(\theta_2)}{E_a}] + \phi(\theta_2)[\varepsilon_f^t(\theta_2) + \frac{\sigma(\theta_2)}{E_f}] \\ & + \int_{\theta_0}^{\theta_2} [\varepsilon_a^t(\zeta) - \varepsilon_f^t(\zeta) - \frac{\sigma(\zeta)}{E_a} + \frac{\sigma(\zeta)}{E_f}] \phi'(\zeta) d\zeta \end{aligned} \quad (3.16)$$

$$\varepsilon(t) = \varepsilon_{pre} + \left[\frac{1 - \phi(\theta_2)}{E_a} + \frac{\phi(\theta_2)}{E_f}\right][\sigma(t) - \sigma(\theta_2)] \quad (3.17)$$

where ε_{pre} is the predetermined applied strain to which the material was loaded in the first step of the thermomechanical path. The strain in the third step of the load path

in Eq. (3.17) is again interpreted as a rule of mixtures, with the contribution due to the frozen phase defined by the frozen volume fraction evaluated at the temperature at which unloading occurs.

During the fourth and final step, the load is maintained at a value of zero, and the temperature is raised to $T > T_g$ to induce shape recovery in the material. With the applied stress $\sigma(t) = 0$, Eq. (3.9) reduces to Eq. (3.18).

$$\begin{aligned} \varepsilon(t) = & [1 - \phi(\theta(t))]\varepsilon_a^t(\theta(t)) + \phi(\theta(t))\varepsilon_f^t(\theta(t)) \\ & + \int_0^t [\varepsilon_a^t(\theta(\tau)) - \varepsilon_f^t(\theta(\tau)) + \frac{\sigma(\tau)}{E_a} - \frac{\sigma(\tau)}{E_f}]\phi'(\theta(\tau))\tilde{\theta}'(\tau)d\tau \end{aligned} \quad (3.18)$$

Recalling the assumption that the temperature is constant in the first and third steps, the contributions to the integral term for these steps are zero, and Eq. (3.18) is rewritten as Eq. (3.19) for a monotonically increasing temperature profile.

$$\begin{aligned} \varepsilon(\theta) = & [1 - \phi(\theta)]\varepsilon_a^t(\theta) + \phi(\theta)\varepsilon_f^t(\theta) \\ & + \int_{\theta_0}^{\theta} [\varepsilon_a^t(\zeta) - \varepsilon_f^t(\zeta) + \frac{\acute{\sigma}(\zeta)}{E_a} - \frac{\acute{\sigma}(\zeta)}{E_f}]\phi'(\zeta)d\zeta \end{aligned} \quad (3.19)$$

where the strain as a function of temperature $\varepsilon(\theta)$ is the unknown quantity, and the values of the stress at the intermediate temperatures ζ are known from the output during the second step (cooling at constant deformation), and $\acute{\sigma}(\theta)$ is the value of the stress of the material when last at the temperature ζ . Differentiating Eq. (3.19) with respect to temperature eliminates the integral term and results in an ordinary differential equation for the function $\varepsilon(\theta)$ in Eq. (3.20). The measure of stress $\acute{\sigma}(\theta)$ is recalled the cooling process in second step, and the initial condition for the differential equation is the strain at the end of unloading.

$$\frac{d\varepsilon(\theta)}{d\theta} = [1 - \phi(\theta)]\alpha_a + \phi(\theta)\alpha_f + \left[\frac{1}{E_a} - \frac{1}{E_f}\right]\phi'(\theta)\acute{\sigma}(\theta) \quad (3.20)$$

The following four equations summarize the main equations, specifically Eqs. (3.11), (3.14), (3.17), and (3.20), obtained for each step of the load path in question, respectively.

$$\begin{aligned}\varepsilon(t) &= [1 - \phi(\theta(t))]\frac{\sigma(t)}{E_a} + \phi(\theta(t))\frac{\sigma(t)}{E_f} \\ \frac{d\dot{\sigma}(\theta)}{d\theta} &= -\frac{[1 - \phi(\theta)]\alpha_a + \phi(\theta)\alpha_f}{[\frac{1-\phi(\theta)}{E_a} + \frac{\phi(\theta)}{E_f}]} \\ \varepsilon(t) &= \varepsilon_{pre} + [\frac{1 - \phi(\theta_2)}{E_a} + \frac{\phi(\theta_2)}{E_f}][\sigma(t) - \sigma(\theta_2)] \\ \frac{d\varepsilon(\theta)}{d\theta} &= [1 - \phi(\theta)]\alpha_a + \phi(\theta)\alpha_f + [\frac{1}{E_a} - \frac{1}{E_f}]\phi'(\theta)\dot{\sigma}(\theta)\end{aligned}$$

5. Prediction of Experimental Load Path and Discussion

Using the values of the calibration parameters previously obtained in Table IV, Eqs. (3.11), (3.14), (3.17), and (3.20) are numerically implemented in MATLAB[®], and predictions are made for different values of applied strain in one-dimensional loading. The files used to implement the constitutive model linearized for small, uniaxial deformations are available in Appendix A.

The constitutive model is first used to predict the shape memory effect in 1-D of the SMP for 10% applied tensile strain. Figure 17 presents, in a similar fashion to Fig. 1 in Chapter I, the strain-stress-temperature profile for the entire thermomechanical load path. This figure compares the prediction with the actual experimental data. As used for all such plots, the solid lines represents the model prediction, and the discrete points represent actual experimental data obtained in Chapter II. Examining this figure, the model prediction matches well with the experimental data.

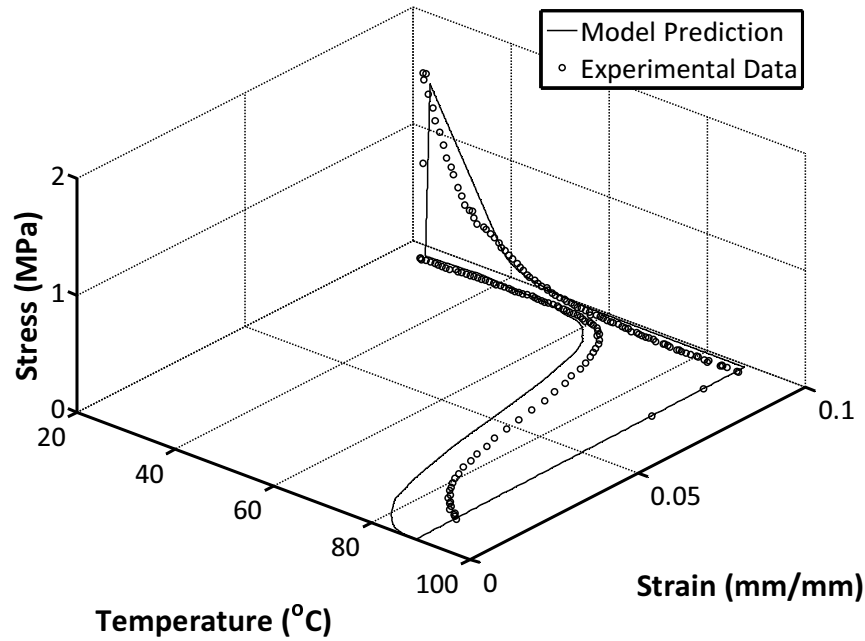


Fig. 17. Strain-Stress-Temperature Prediction for SME with 10% Applied Tensile Strain

Figure 18 focuses on the stress-strain behavior for the complete load path. The model prediction again agrees well with the experimental data. In particular, the assumption of a linear elastic response is observed to be reasonable for this material undergoing this value of deformation, and the peak value of the stress during constrained cooling is near that observed experimentally.

In addition, Fig. 19 presents the stress-temperature data. A stress increase is observed at the maximum temperature due to loading the material to the predetermined strain value. Upon cooling at a constant deformation, a second stress increase is observed. The model prediction agrees well with the experimental data for the stress increase. In particular, comparing model prediction and the experimental data, the slopes of the stress-temperature curves are nearly identical for temperatures outside of the transition region.

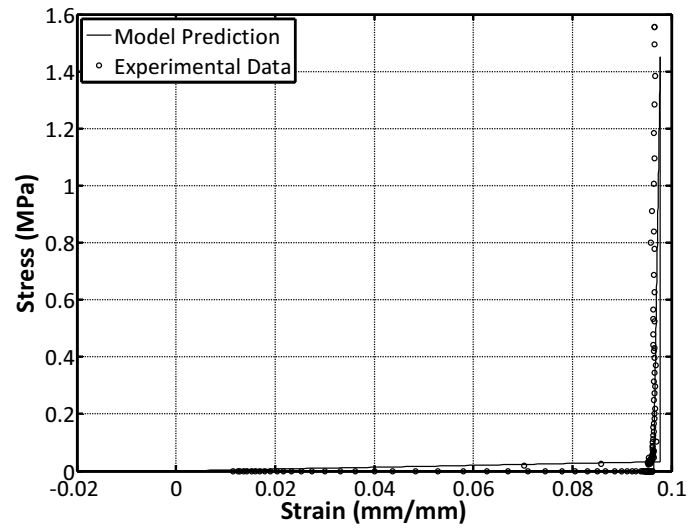


Fig. 18. Stress-Strain Prediction for SME with 10% Applied Tensile Strain

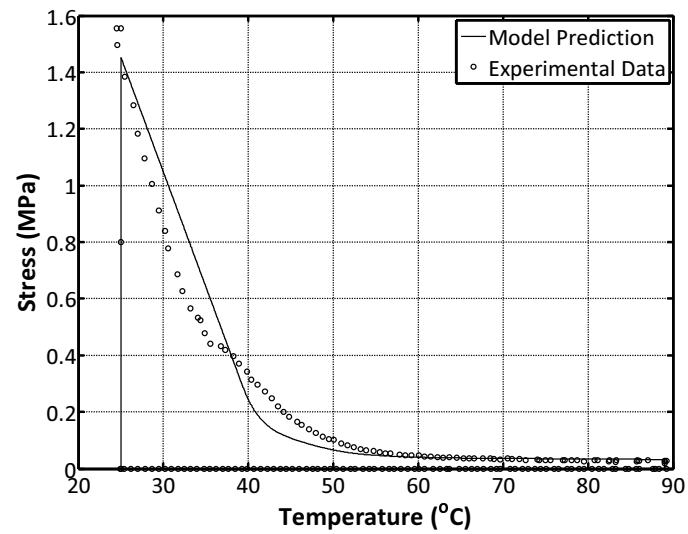


Fig. 19. Stress-Temperature Prediction for SME with 10% Applied Tensile Strain

A difference in the slope of the stress-temperature relationship, however, is noted in the transition region. This difference, as well as the difference in the final stress value during this cooling process, may be attributed to the constraint of the test frame, as discussed in Chapter II, which imposed slight elastic deformation on the specimen while attempting to maintain a constant value of deformation. Also, the model does not account for differences in the glass transition behavior due to thermal cycling at non-zero values of stress.

Figure 20 presents the strain-temperature data for the 10% applied strain experiment. Of particular importance in this figure is the strain recovery upon heating the material at zero stress. It is observed that the model prediction agrees well qualitatively with the data produced experimentally. Specifically, the strain recovery begins at approximately the same temperature, and occurs in a similar nonlinear strain vs. temperature manner. These observations, however, were expected as the frozen volume fraction was assumed to be a normalization of this strain recovery behavior. On the other hand, the model prediction does not account for the irrecoverable strain at the end of heating. This difference is due to the assumption made during model development that all of the deformation ‘frozen’ in the material is recovered upon subsequent heating. Furthermore, the value of the stress during cooling consistently takes a higher value for the predicted stress. Because the predicted value of stress is then used to calculate the amount of strain recovered during heating, a larger value of strain is ‘stored’ in the material and subsequently recovered upon heating.

In addition to predicting the 10% applied strain experiment, the model was used to predict the material response for the 25%, 50%, and 100% applied strain cases. Although 10% borders on the limit of what is generally considered a ‘small deformation,’ the other three values are well out of the range of what is classically accepted as a small deformation. As such, the assumptions of the infinitesimal strain

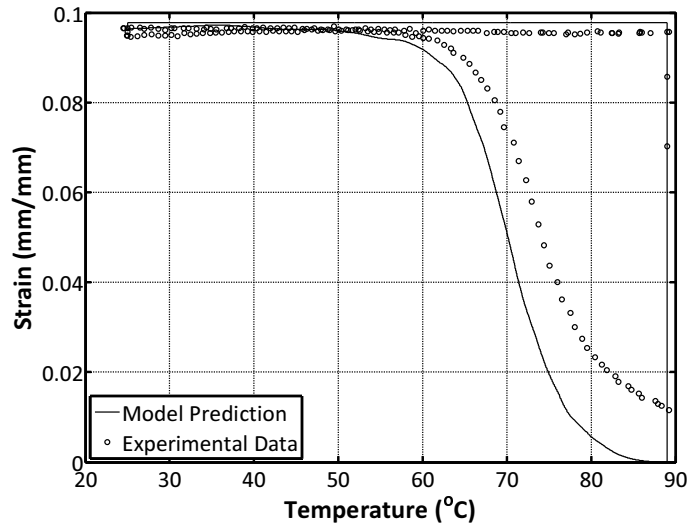


Fig. 20. Strain-Temperature Prediction for SME with 10% Applied Tensile Strain

tensor and the Cauchy stress tensor are no longer valid as representative measures of the state of the material. It is noted that the model prediction of the 25%, 50%, and 100% applied strain cases presents an empirical prediction of the material response and the experimental ‘strain’ used for comparison is actually the extension of the material.

Figure 21 presents the three-dimensional strain-stress-temperature predictions for all considered values of applied strain, including the 10% case previously considered. From this figure, the model prediction agrees empirically with the experimental data. In addition, Figs. 22 and 23 present the stress-strain and stress-temperature relationships for the entire experimental path, respectively. As noted in Chapter II, the stress-strain relationship becomes nonlinear when loading to larger values of applied strain in the active phase. The calibration of the small deformation model, however, assumes a linear elastic material such that the nonlinear deviation, although relatively small, is not captured for the larger values of applied strain. In addition, the

stress-temperature prediction in Fig. 23 shows good qualitative agreement with experimental data. The sources of error discussed in the 10% case, such as the constraint of the experimental apparatus, the non-zero stress during glass transformation, etc., still exist for the prediction of the 25%, 50% and 100% cases and likely contribute to the differences between the predictions and the experimental data.

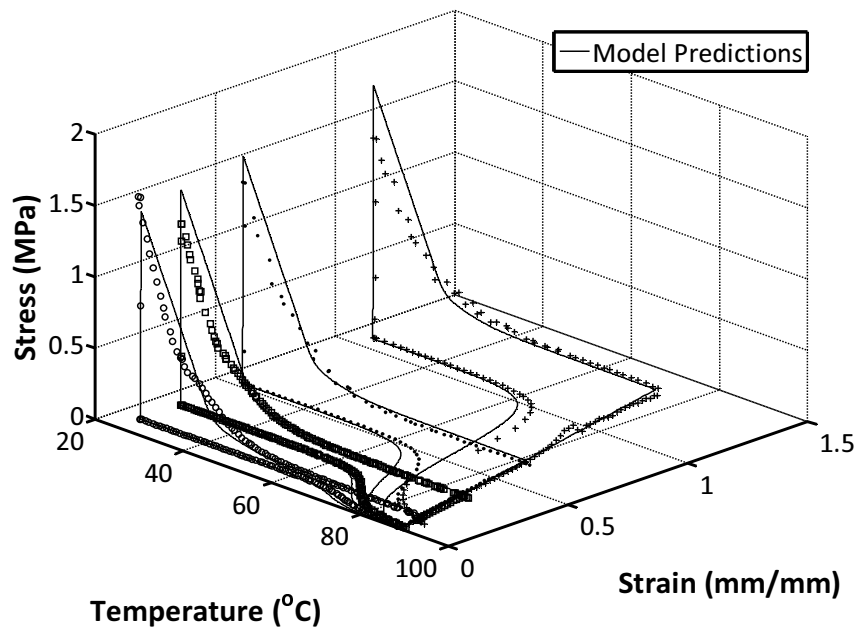


Fig. 21. Strain-Stress-Temperature Prediction for 10%, 25%, 50%, and 100% Applied Tensile Strain

Finally, Fig. 24 presents the strain-temperature predictions for each of the four cases. In this figure, the strain recovery behavior at zero load is considered. It is noted that the model predicts the strain recovery to follow a similar qualitative nonlinear strain vs. temperature profile and finish upon heating through the same range of temperatures. Due to the fact that the model does not capture irrecoverable strain and thermal expansion is neglected for this step, the model prediction again does not completely match the experimental results.

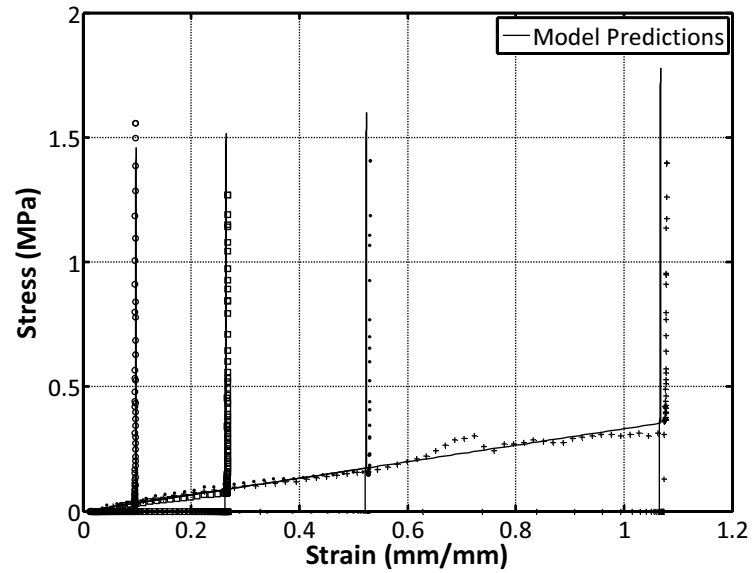


Fig. 22. Stress-Strain Prediction for 10%, 25%, 50%, and 100% Applied Tensile Strain

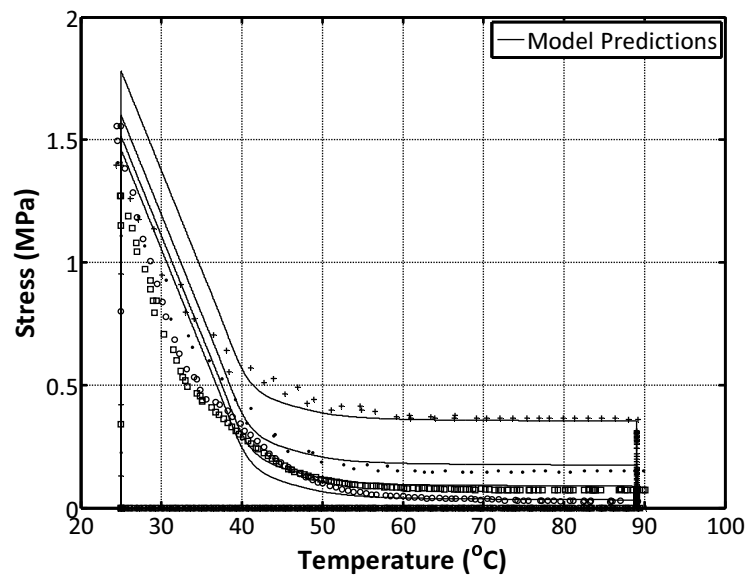


Fig. 23. Stress-Temperature Prediction for 10%, 25%, 50%, and 100% Applied Tensile Strain

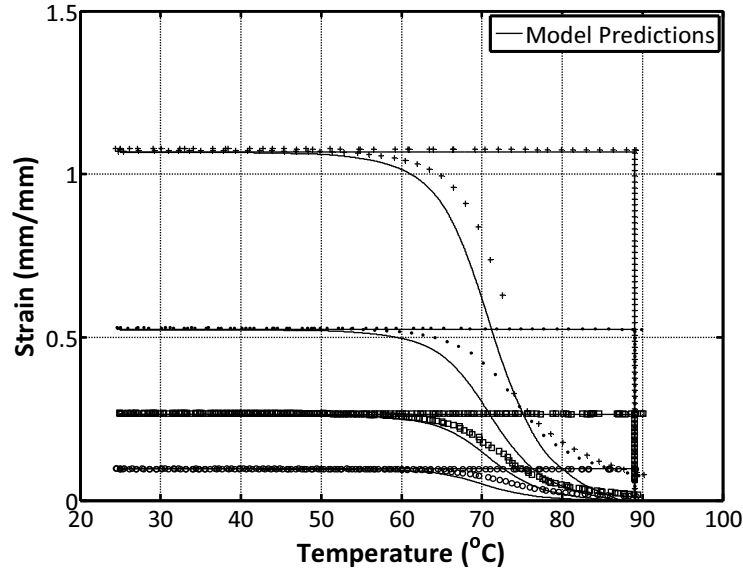


Fig. 24. Strain-Temperature Prediction for 10%, 25%, 50%, and 100% Applied Tensile Strain

C. Calibration of the Constitutive Model for Large Deformations

After being used to calibrate the linearized Chen and Lagoudas model for small, uniaxial deformations of SMPs, the experimental data was then used to calibrate the original Chen and Lagoudas model which accounts for general deformation gradients that are capable of handling large deformations. The calibration of this model provides a means to predict the large deformation response of SMPs observed experimentally on a more accurate and consistent basis. The method used to reduce the constitutive equations to a useable form will be the method proposed by Chen and Lagoudas [27]. After presenting the necessary equations and assumptions, the results of the model calibration and predictions will be presented.

In calibrating the model for the large deformations of SMPs, Eq. (3.1) is recalled

and presented again as Eq. (3.21). This equation represents the constitutive equation for a SMP undergoing general deformations and includes contributions due to deformations in the active and frozen phases as well as deformations occurring in the active phase which are subsequently stored upon cooling to the frozen phase.

$$\begin{aligned} \mathbf{F}(\mathbf{t}) = & [1 - \phi(\theta(t))] \hat{\mathbf{F}}_a(\mathbf{S}(t), \theta(t)) \\ & + \int_0^t \hat{\mathbf{F}}_f(\mathbf{S}(t), \theta(t)) \hat{\mathbf{F}}_f^{-1}(\mathbf{S}(\tau), \theta(\tau)) \hat{\mathbf{F}}_a(\mathbf{S}(\tau), \theta(\tau)) \phi'(\theta(\tau)) \tilde{\theta}'(\tau) d\tau \end{aligned} \quad (3.21)$$

1. Assumption of a Neo-Hookean Material

To reduce the constitutive equation in Eq. (3.21) to a form consisting of measurable quantities, such as stress, etc., assumptions must be made corresponding to the material behavior. In this work, following the method proposed by Chen and Lagoudas, the material is assumed to behave as a neo-Hookean material. A neo-Hookean model is frequently used for the modeling of rubber-like materials which are incompressible when deformed. This assumption is deemed reasonable for SMPs due to the rubber-like material response when in the active phase - the phase in which relatively large deformations are typically considered.

The constitutive equation for a neo-Hookean material as related to a general deformation gradient is presented in Eq. (3.22), where \mathbf{S} is the first Piola-Kirchoff stress, p is the hydrostatic pressure required to maintain incompressibility, $\mu(\theta)$ is the shear modulus, and $\nu(\theta)$ is the ratio of the volume at a current temperature to the volume at the reference temperature [27, 30]. In this work, the shear modulus $\mu(\theta)$ as a function of temperature is not obtained for the entire temperature range of the experiment but instead at two discrete temperatures, specifically the loading and the unloading temperatures. In addition, it is assumed that the volume ratio $\nu(\theta)$ is unity for deformations occurring to a material at a constant temperature in either

the active or the frozen phase. It is shown later that the functional dependence of the shear modulus on temperature (and thus, the stretch of the material) can be related to terms obtained in the calibration of the constitutive model for small deformations.

$$\begin{aligned}\mathbf{S} &= -p\mathbf{F}^{-T} + \mu(\theta)\mathbf{F} \\ \det\mathbf{F} &= \nu(\theta)\end{aligned}\tag{3.22}$$

To relate measurable experimental quantities to the constitutive equation proposed in Eq. (3.21), the tensors \mathbf{S} and \mathbf{F} are decomposed via the polar decomposition theorem as shown in Eq. (3.23), where \mathbf{Q} and \mathbf{R} are proper orthogonal tensors (rotation tensors) and \mathbf{T} and \mathbf{U} are positive definite, symmetric tensors.

$$\begin{aligned}\mathbf{S} &= \mathbf{Q}\mathbf{T} \\ \mathbf{F} &= \mathbf{R}\mathbf{U}\end{aligned}\tag{3.23}$$

Substituting Eq. (3.23) into Eq. (3.22) results in the equation shown in Eq. (3.24).

$$\begin{aligned}\mathbf{Q}\mathbf{T} &= -p\mathbf{R}\mathbf{U}^{-T} + \mu(\theta)\mathbf{R}\mathbf{U} \\ \det\mathbf{R}\mathbf{U} &= \det\mathbf{R}\det\mathbf{U} = \det\mathbf{U} = \nu(\theta)\end{aligned}\tag{3.24}$$

Assuming $\mathbf{Q} = \mathbf{R}$ such that the stress is aligned with the imposed deformation, Eq. (3.24) reduces to the form of Eq. (3.25).

$$\begin{aligned}\mathbf{T} &= -p\mathbf{U}^{-T} + \mu(\theta)\mathbf{U} \\ \det\mathbf{U} &= \nu(\theta)\end{aligned}\tag{3.25}$$

where Eq. (3.25) implies that \mathbf{T} and \mathbf{U} have the same eigenvectors. It is then possible to use the spectral decomposition to decompose the tensors \mathbf{T} and \mathbf{U} into the form of Eq. (3.26), where s_i and λ_i are the principal stresses and stretches, respectively.

$$\begin{aligned}\mathbf{T} &= \sum_{i=1}^3 s_i \mathbf{e}_i \otimes \mathbf{e}_i \\ \mathbf{U} &= \sum_{i=1}^3 \lambda_i \mathbf{e}_i \otimes \mathbf{e}_i\end{aligned}\tag{3.26}$$

Substituting the spectral decomposition presented in Eq. (3.26) into the tensorial equation presented in Eq. (3.25) results in Eq. (3.27).

$$\begin{aligned}s_i &= -p\lambda_i^{-1} + \mu(\theta)\lambda_i, & i = 1, 2, 3 \\ \lambda_1\lambda_2\lambda_3 &= \nu(\theta)\end{aligned}\tag{3.27}$$

The equations presented in Eq. (3.27) relate the first Piola-Kirchoff stress to the stretch in a neo-Hookean material. This relationship is subsequently used in conjunction with Eq. (3.21) to develop an equation for the axial stretch in a material undergoing uniaxial deformations.

2. Constitutive Equation as Applied to SME with Uniaxial Tension

The experiments in Chapter II applied a uniaxial tension to a series of shape memory polymer specimens. To model the material response due to this type of deformation, this section will derive from Eqs. (3.21) and (3.27) the constitutive equation for the axial stretch of a material undergoing such a uniaxial stress state. To begin, the only nonzero stress component for uniaxial tension is $s_1 = s(t)$ while $s_2 = s_3 = 0$, where $s(t)$ is the stress profile for a given experiment. Substituting this relationship into Eq. (3.27) and eliminating the hydrostatic pressure p yields the relationship in Eq. (3.28) for the components of the stretch tensor.

$$\begin{aligned}\lambda_1 &= \lambda \\ \lambda_2 &= \lambda_3 = \sqrt{\frac{\nu(\theta)}{\lambda}}\end{aligned}\tag{3.28}$$

where λ is the stretch in the direction of the applied stress, which is quantified by Eq. (3.29), and it is recalled that $\mu(\theta)$, $\nu(\theta)$, and s are the shear modulus, volume ratio, and Piola-Kirchoff stress, respectively.

$$\mu(\theta)\left(\lambda - \frac{\nu(\theta)}{\lambda^2}\right) = s \quad (3.29)$$

Furthermore, by assuming $\mathbf{R} = \mathbf{I}$ (no rotation) in the polar decomposition presented in Eq. (3.23), the deformation gradient \mathbf{F} is represented by a diagonal matrix in Eq. (3.30) whose values are equal to the principal values of the right stretch tensor \mathbf{U} .

$$\mathbf{F} = \begin{pmatrix} \lambda & 0 & 0 \\ 0 & \sqrt{\frac{\nu(\theta)}{\lambda}} & 0 \\ 0 & 0 & \sqrt{\frac{\nu(\theta)}{\lambda}} \end{pmatrix} \quad (3.30)$$

Through defining an equation of the form of Eq. (3.29) for each the active and the frozen phase in the form of Eq. (3.31), it is possible to construct the active and frozen phase deformation gradients \mathbf{F}_a and \mathbf{F}_f as shown in Eq. (3.32).

$$\begin{aligned} \mu_a(\theta)\left(\lambda_a - \frac{\nu_a(\theta)}{\lambda_a^2}\right) &= s \\ \mu_f(\theta)\left(\lambda_f - \frac{\nu_f(\theta)}{\lambda_f^2}\right) &= s \end{aligned} \quad (3.31)$$

$$\begin{aligned} \mathbf{F}_a &= \begin{pmatrix} \lambda_a & 0 & 0 \\ 0 & \sqrt{\frac{\nu_a(\theta)}{\lambda_a}} & 0 \\ 0 & 0 & \sqrt{\frac{\nu_a(\theta)}{\lambda_a}} \end{pmatrix} \\ \mathbf{F}_f &= \begin{pmatrix} \lambda_f & 0 & 0 \\ 0 & \sqrt{\frac{\nu_f(\theta)}{\lambda_f}} & 0 \\ 0 & 0 & \sqrt{\frac{\nu_f(\theta)}{\lambda_f}} \end{pmatrix} \end{aligned} \quad (3.32)$$

These deformation gradients are substituted into Eq. (3.21), and the constitutive equation for the axial component of the deformation gradient is reduced to an equation for the axial stretch of the material as shown in Eq. (3.33).

$$\begin{aligned} \lambda(t) = & [1 - \phi(\theta(t))] \lambda_a(s(t), \theta(t)) \\ & + \int_0^t \frac{\lambda_f(s(t), \theta(t)) \lambda_a(s(\tau), \theta(\tau))}{\lambda_f(s(\tau), \theta(\tau))} \phi'(\theta(\tau)) \tilde{\theta}'(\tau) d\tau \end{aligned} \quad (3.33)$$

Assuming the stretches in each phase take the form of Eq. (3.31), then five functions need to be calibrated to fully describe the axial stretch of a material undergoing uniaxial tension as presented by Eq. (3.33). Those five functions are $\phi(\theta)$, $\mu_a(\theta)$, $\mu_f(\theta)$, $\nu_a(\theta)$, and $\nu_f(\theta)$, or the frozen volume fraction, the shear moduli in the active and frozen phases, and the volume ratios in the active and frozen phases, respectively.

3. Determination of Calibration Parameters

In comparing the calibration functions with the results of the experimental investigation performed in Chapter II, it is noted that all of the five calibration functions can be either be directly related to or considered to be a function of measurable experimental quantities.

In particular, the values of the volume ratios ν_a and ν_f can be deduced from measurements of the deformations in the axial and transverse directions during uniaxial tension or from constraints due to assuming a neo-Hookean material. The experimental investigation presented in Chapter II includes data from loading the material at a high temperature and a low temperature, during which the Poisson's ratio is measured experimentally in the active and frozen phases, respectively. Figures 25 (a) and (b) present the Poisson's ratio for small values of axial extension occurring in the active and frozen phases, respectively. From these figures, the Poisson's ratio is shown to be 0.4 for $T = 25^\circ C$ in the frozen phase and 0.5 for $T = 90^\circ C$ in the active phase.

Recalling the assumption of a neo-Hookean material for the behavior of a material in

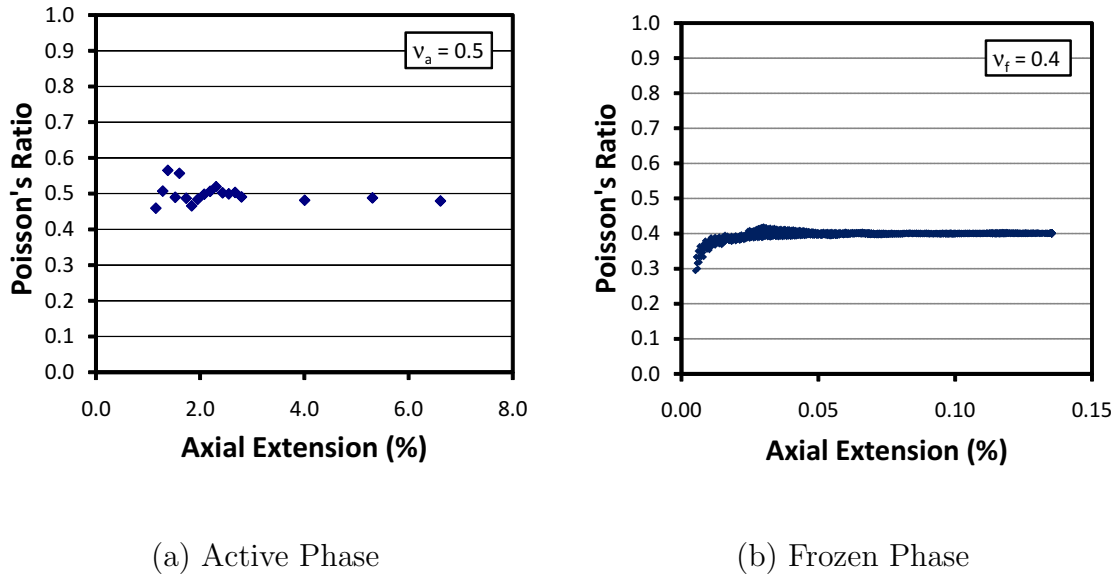


Fig. 25. Poisson's Ratios for Shape Memory Polymer

each phase, however, implies an incompressibility constraint for a material deformed at a constant temperature. As such, the values of the volume ratios ν_a and ν_f are taken to be unity for deformations occurring at high and low temperatures during loading and unloading, respectively. While the Poisson's ratio for the active phase is consistent with that of an incompressible material, the ratio for the frozen phase is not equal to the value of 0.5 dictated by the incompressibility assumption. Noting that relatively large deformations for the particular thermomechanical cycle generally occur in the active phase, and allowing for simplicity of the model calibration, the assumption that a material behaves like a neo-Hookean material in both the active and frozen phases is maintained.

It is noted that no information on the relationship of the parameters with respect to a change in temperature is obtained or assumed, as dictated by the constitutive

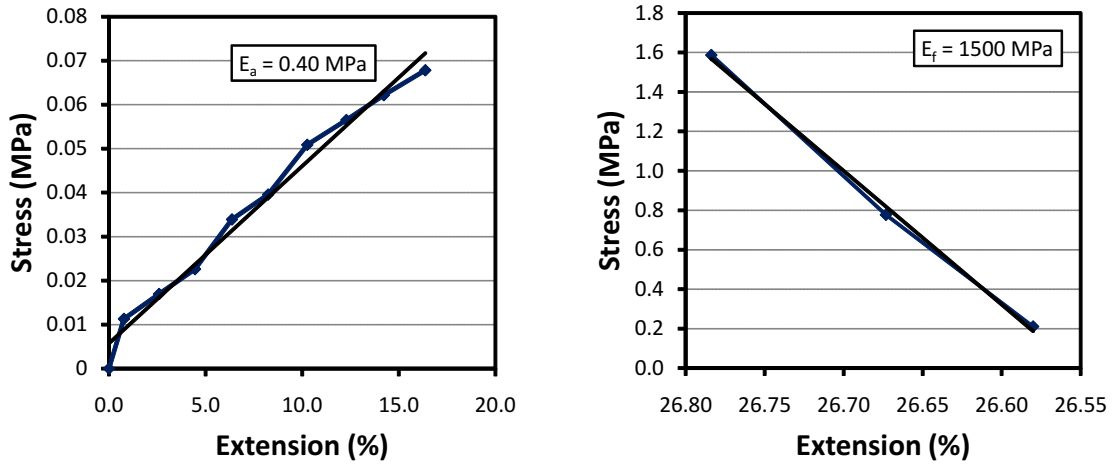
model. The function dependence of these parameters will be addressed later, with the stretch values as a function of temperature related to quantities previously obtained in calibrating the small deformation model.

Furthermore, by assuming the SMP in question is an isotropic material, the shear modulus in each phase can be related to the elastic modulus and the Poisson's ratios through Eq. (3.34) at the discrete temperatures for which $E(\theta)$ and $\nu(\theta)$ are available.

$$\begin{aligned}\mu_a(\theta) &= \frac{E_a}{2(1 + \nu_a(\theta))} \\ \mu_f(\theta) &= \frac{E_f}{2(1 + \nu_f(\theta))}\end{aligned}\tag{3.34}$$

where E_a and E_f are the elastic moduli in each phase, and $\nu_a(\theta)$ and $\nu_f(\theta)$ are the Poisson's ratios which are assumed to be 0.5 as previously discussed for the active and frozen phases, respectively. For the large deformation model, values of the tensile modulus are calculated from the 25% extension experiments, which corresponds to a stretch equal to 1.25, and are averaged with the previously presented values from the 10% extension experiments. Similar to the small deformation calibration, the elastic moduli for each phase are calculated from the loading in the active phase and unloading in the frozen phase, which are presented in Figs. 26 (a) and (b) respectively.

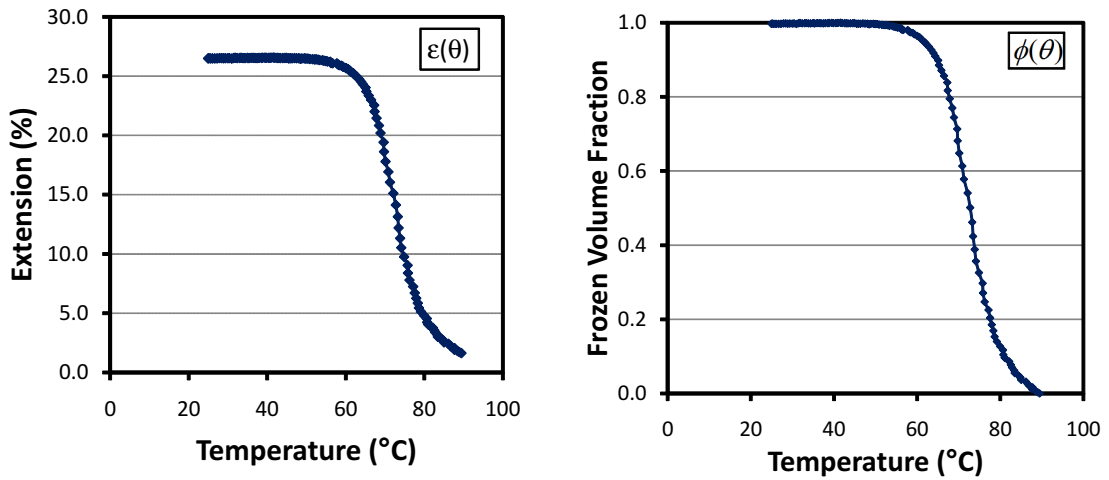
The frozen volume fraction is again assumed to be a function of the shape recovery profile upon heating at zero load. Specifically, the frozen volume fraction $\phi(\theta)$ is assumed to be the extension recovery profile $\varepsilon(\theta)$ normalized by the maximum amount of recoverable deformation. Figure 27 (a) presents the shape recovery profile for the experiment with an extension of 25%, and Fig. 27 (b) presents the function for the frozen volume fraction. Due to the fact that the material is assumed to be completely in the frozen and active phases at beginning and end of heating, respectively, the frozen volume fraction is normalized such that the upper and lower bounds of the function are 1 and 0, respectively.



(a) Loading in Active Phase

(b) Unloading in Frozen Phase

Fig. 26. Elastic Moduli as Calculated from 25% Applied Extension Results



(a) Strain Recovery During Heating at Zero Load

(b) Frozen Volume Fraction

Fig. 27. Frozen Volume Fraction as a Normalization of the Extension Recovery Profile

After determining the function for $\phi(\theta)$, all of the necessary calibration requirements have been assumed and/or calculated. It is noted that, although the parameters were calibrated using *extension* data, the numbers are consistent for use with the model which is developed in terms of *stretch* which is equal to the extension plus one (undeformed state implies stretch = 1), and thus represents a uniform shift in the data that does not affect the slopes or normalization. A summary of the calibration requirements and the corresponding values is presented in Table V.

Table V. Necessary Calibration Parameters for the Large Deformation Constitutive Model

| Parameter | Value |
|-----------------------------------------------------------------|-----------------------|
| Active phase volume ratio ($\nu_a(\theta=90^\circ\text{C})$) | 1 |
| Frozen phase volume ratio ($\nu_f(\theta=25^\circ\text{C})$) | 1 |
| Active phase shear modulus ($\mu_a(\theta=90^\circ\text{C})$) | 0.12 MPa |
| Frozen phase shear modulus ($\mu_f(\theta=25^\circ\text{C})$) | 433 MPa |
| Frozen volume fraction ($\phi(\theta)$) | $f(\epsilon(\theta))$ |

It is noted that the shear modulus $\mu(\theta)$ encompasses the elastic modulus E presented in calibrating the small deformation model. In addition, the volume ratios ν are assumed to be unity for deformations occurring at a constant temperature, but the temperature dependence of ν encompasses the thermal expansion coefficients in the small deformation model. As a result, the calibration requirements for the large deformation model are simply functions of the calibration requirements for the

small deformation model. The difference originates from the different form of the constitutive equations posed for each model.

4. Reduction of Large Deformation Model for Small Deformations

The large deformation model has been posed, through the neo-Hookean assumption, in terms of stretches, shear moduli, and volume ratios. As such, each of the active and frozen phases were assumed to have the material response described through Eq. (3.35).

$$\begin{aligned}\mu(\theta)\left(\lambda - \frac{\nu(\theta)}{\lambda^2}\right) &= s \\ \frac{\mu(\theta)}{\lambda^2}(\lambda^3 - \nu(\theta)) &= s\end{aligned}\tag{3.35}$$

Where, due to the incompressibility assumption, the shear modulus is rewritten through Eq. (3.36)

$$\mu(\theta) = \frac{E(\theta)}{2(1 + \nu)} = \frac{E(\theta)}{3}\tag{3.36}$$

In reducing the equation for small, uniaxial deformations, it is assumed that the axial stretch component can be written in terms of the axial component of the infinitesimal strain tensor through Eq. 3.37.

$$\lambda = (1 + \varepsilon)\tag{3.37}$$

In addition, it is noted that the volume ratio can be written in terms of the coefficients of thermal expansion (recall the assumption that mechanical deformations do not change the volume). As such, the volume ratio for an isotropic material with an unit reference volume is written as Eq. (3.38), where the higher order terms have been neglected.

$$\nu(\theta) = (1 + \alpha\Delta\theta)^3 \approx (1 + 3\alpha\Delta\theta)\tag{3.38}$$

Using Eq. (3.37) and neglecting the higher order terms of ε for small deforma-

tions, Eq. (3.35) reduces to Eq. (3.39).

$$\begin{aligned}\frac{E(\theta)}{3\lambda^2}((1 + \varepsilon)^3 - (1 + 3\alpha\Delta\theta)) &= s \\ \frac{E(\theta)}{3\lambda^2}(1 + 3\varepsilon - (1 + 3\alpha\Delta\theta)) &= s \\ \frac{E(\theta)}{3\lambda^2}(3\varepsilon - 3\alpha\Delta\theta) &= s\end{aligned}\tag{3.39}$$

Invoking another assumption that λ is close to 1 for small deformations, and thus λ^2 is near 1, Eq. (3.39) reduces to Eq. (3.40).

$$E(\theta)(\varepsilon - \alpha\Delta\theta) = s\tag{3.40}$$

Recalling the assumption that the first Piola-Kirchhoff stress can be approximated by the Cauchy stress for small deformations, Eq. (3.40) reduces to the familiar linear thermoelastic relationship for isotropic materials, where ε represents the elastic strain component and $\alpha\Delta\theta$ represents the thermal strain.

$$E(\theta)(\varepsilon - \alpha\Delta\theta) = \sigma\tag{3.41}$$

The reduction of the model reinforces the notion that the small deformation model and large deformation model are equivalent, particularly for small deformations. The large deformation model, in a simplistic approach, is essentially the small deformation model without the nonlinear strain terms neglected. As such, the small deformation model is incapable of capturing the nonlinear stress-strain relationship in loading to large deformations. This notion was previously presented in the large deformation predictions produced using the small deformation model. An additional observation is that the calibration requirements of the two models in Table IV and Table V are not independent as the shear moduli and volume ratios can be rewritten in terms of the elastic moduli and coefficients of thermal expansion as previously discussed.

5. Axial Stretch Equation as Applied to the SME Thermomechanical Load Path

After all of the calibration parameters required to describe the axial stretch of a SMP are determined, the equations for each step of the shape memory effect thermomechanical load path are simplified from Eq. (3.33). These equations are presented in such a manner as to be convenient for one-dimensional numerical implementation in MATLAB[®].

In the first step of the thermomechanical load path, the material is at a constant temperature in the active phase and is loaded to the predetermined value of deformation (stretch). Applying these conditions to the axial stretch equation derived in Eq. (3.33), the integral term of the equation is eliminated due to the fact that the constant temperature infers $\tilde{\theta}'(\tau) = 0$. Furthermore, the assumption that the material is completely in the active phase during loading infers the frozen volume fraction $\phi(\theta) = 0$. Consequently, the axial stretch equation in Eq. (3.33) reduces to Eq. (3.42) which, as expected, equates the axial stretch of the material to the value of the axial stretch due to loading purely in the active phase.

$$\lambda(t) = \lambda_a(s(t), \theta(t)) \quad (3.42)$$

In the second step, the temperature is assumed to be monotone decreasing during the cooling step, and the net cooling history $\tilde{\theta}(\tau)$ reduces to $\theta(\tau)$, where $\theta(\tau)$ is the cooling profile measured during the experiment. Using the assumption of constant deformation in this step in addition to the integral term equal to zero for $0 \leq t \leq t_1$, the axial stretch equation reduces to Eq. (3.43).

$$\begin{aligned} \lambda(t) = \lambda_1 = & [1 - \phi(\theta(t))] \lambda_a(s(t), \theta(t)) \\ & + \int_{t_1}^t \frac{\lambda_f(s(t), \theta(t)) \lambda_a(s(\tau), \theta(\tau))}{\lambda_f(s(\tau), \theta(\tau))} \phi'(\theta(\tau)) \theta'(\tau) d\tau \end{aligned} \quad (3.43)$$

where the stress as a function of temperature $\dot{s}(\theta)$ is the unknown quantity. Differentiating Eq. (3.43) is thus differentiated with respect to time results in Eq. (3.44) with the left hand side is equal to zero due to the constant stretch during this step.

$$0 = [1 - \phi(\theta(t))] \frac{d}{dt} \lambda_a(s(t), \theta(t)) + \frac{d}{dt} [\lambda_f(s(t), \theta(t))] \lambda_f^{-1}(s(t), \theta(t)) [\lambda_1 - [1 - \phi(\theta(t))] \lambda_a(s(t), \theta(t))] \quad (3.44)$$

Expanding the time derivatives and treating the stress s as a function of the temperature θ , eliminates the functional dependence on time from Eq. (3.44) and reduces the equation to Eq. (3.45).

$$0 = [1 - \phi(\theta)] \left\{ \frac{\partial}{\partial s} \lambda_a(s, \theta) \left[\frac{ds}{d\theta} \right] + \frac{\partial}{\partial \theta} \lambda_a(s, \theta) \right\} + \left\{ \frac{\partial}{\partial s} \lambda_f(s, \theta) \left[\frac{ds}{d\theta} \right] + \frac{\partial}{\partial \theta} \lambda_f(s, \theta) \right\} \lambda_f^{-1}(s, \theta) [\lambda_1 - [1 - \phi(\theta)] \lambda_a(s, \theta)] \quad (3.45)$$

which is an ordinary differential equation for the stress as a function of temperature. To solve this equation, the quantities $\frac{\partial}{\partial s} \lambda_a(s, \theta)$, $\frac{\partial}{\partial s} \lambda_f(s, \theta)$, $\frac{\partial}{\partial \theta} \lambda_a(s, \theta)$, and $\frac{\partial}{\partial \theta} \lambda_f(s, \theta)$ must be known. These parameters represent the change in axial stretches due to changes in stress and temperature, respectively. Although explicit analytical functions could be obtained for the change in axial stretch with respect to temperature ($\frac{\partial}{\partial s} \lambda_a(s, \theta)$ and $\frac{\partial}{\partial s} \lambda_f(s, \theta)$) from Eq. (3.29), measurements performed in this work do not explicitly provide the change in the volume ratio and shear modulus with respect to temperature. Consequently, these quantities are assumed to reduce to the coefficients of thermal expansion calibrated as part of the small deformation model.

$$\begin{aligned} \frac{\partial}{\partial \theta} \lambda_a(s, \theta) &= \alpha_a = 5.2 * 10^{-4} / ^\circ C \\ \frac{\partial}{\partial \theta} \lambda_f(s, \theta) &= \alpha_f = 0.75 * 10^{-4} / ^\circ C \end{aligned} \quad (3.46)$$

Furthermore, rather than working with the cubic function for the stretch-stress relationship, the terms $\frac{\partial}{\partial s}\lambda_a(s, \theta)$ and $\frac{\partial}{\partial s}\lambda_f(s, \theta)$ are approached in a different manner. First, it is assumed that little deformation occurs in the frozen phase, and thus the stretch can be approximated by a linear relationship with respect to temperature and is related to the elastic modulus in the frozen phase E_f previously calibrated. In addition, the stretch-stress relationship in the active phase is approximated by an exponential function to capture the nonlinear behavior for large deformations. The resulting approximations for the derivatives of the stretch λ with respect to the temperature θ are presented in Eq. (3.47).

$$\begin{aligned}\frac{\partial}{\partial s}\lambda_a(s, \theta) &= 2.5e - 006 * e^{2.5e-006*s}[MPa^{-1}] \\ \frac{\partial}{\partial s}\lambda_f(s, \theta) &= \frac{1}{E_f} = 7.69e - 10[MPa^{-1}]\end{aligned}\tag{3.47}$$

In the third step of the thermomechanical load path, the stress generated due to the constrained cooling process is released. During this step, the temperature is held constant at a value θ_2 such that the contribution in Eq. (3.9) to the integral term from $t_2 \leq t \leq t_3$ is zero, and the axial stretch equation reduces to Eq. (3.48).

$$\begin{aligned}\lambda(t) &= [1 - \phi(\theta(t_2))]\lambda_a(s(t), \theta_2) \\ &+ \int_{t_1}^{t_2} \frac{\lambda_f(s(t), \theta_2)\lambda_a(s(\tau), \theta(\tau))}{\lambda_f(s(\tau), \theta(\tau))} \phi'(\theta(\tau))\theta'(\tau)d\tau\end{aligned}\tag{3.48}$$

Using the equations derived during the second step of the experimental path, the integral term in Eq. (3.48) is replaced and the equation is rewritten in the form of Eq. (3.49).

$$\begin{aligned}\lambda(t) &= [1 - \phi(\theta(t_2))]\lambda_a(s(t), \theta_2) \\ &+ \lambda_f(s(t), \theta_2)\lambda_f^{-1}(s_2, \theta_2)[\lambda_1 - [1 - \phi(\theta_2)\lambda_a(s_2, \theta_2)]]\end{aligned}\tag{3.49}$$

where s_2 is the stress at the end of the constrained cooling and λ_1 is the constant

value of the axial stretch maintained during the cooling step. Assuming the material is completely in the frozen phase at the low temperature infers $\phi(\theta_2) = 1$, and Eq. (3.49) reduces to Eq. (3.50).

$$\lambda(t) = \lambda_f(s(t), \theta_2) \lambda_f^{-1}(s_2, \theta_2) \lambda_1 \quad (3.50)$$

The fourth and final step involves heating the material while maintaining a constant load. In this work, the load is zero, neglecting gravity. Assuming the temperature is monotone increasing during this step, the axial stretch equation in Eq. (3.33) is rewritten as Eq. (3.51).

$$\begin{aligned} \lambda(\theta) = & [1 - \phi(\theta)] \lambda_a(0, \theta) \\ & + \int_{\theta_0}^{\theta} \frac{\lambda_f(0, \zeta) \lambda_a(s(\zeta), \zeta)}{\lambda_f(s(\zeta), \zeta)} \phi'(\zeta) d\zeta \end{aligned} \quad (3.51)$$

where the integral variable ζ is used to represent the intermediate temperatures during heating, and θ_0 is the original temperature of the material at which the material was in the reference configuration. The stretch as a function of temperature during the final heating is the unknown quantity in this equation. As such, Eq. (3.51) is differentiated with respect to temperature to eliminate the integral term, resulting in Eq. (3.52).

$$\frac{d\lambda}{d\theta} = -\phi'(\theta) \lambda_a(0, \theta) + [1 - \phi(\theta)] \frac{d\lambda_a}{d\theta} + \lambda_f(0, \theta) \lambda_f^{-1}(\acute{s}(\theta)) \lambda_a(\acute{s}(\theta)) \phi'(\theta) \quad (3.52)$$

Equation (3.52) defines an ordinary differential equation for the stretch of the material as a function of temperature $\acute{\lambda}(\theta)$ where $\acute{s}(\theta)$ is the stress of the material when it last experienced the temperature θ . In other words, for this load path, $\acute{s}(\theta)$ is the stress of the material at temperature θ during the constrained cooling, and $\lambda_f^{-1}(\acute{s}(\theta))$ and $\lambda_a(\acute{s}(\theta))$ are the values of the axial stretches in each phase as

evaluated at this stress. To simplify Eq. (3.52), it is assumed that the stretches due to thermal expansion $\lambda_a(0, \theta)$ and $\lambda_f(0, \theta)$ are approximately equal to one (small values of extension), and that the derivative of the stretch in the active phase with respect to temperature $\frac{d\lambda_a}{d\theta}$ is again assumed to be the thermal expansion coefficient of the active phase α_a . Using these assumptions, Eq. (3.52) reduces to Eq. (3.53).

$$\frac{d\lambda}{d\theta} = -\phi'(\theta) + [1 - \phi(\theta)]\alpha_a + \lambda_f^{-1}(\acute{s}(\theta))\lambda_a(\acute{s}(\theta))\phi'(\theta) \quad (3.53)$$

The derivation of Eq. (3.53) completes the set of equations needed to predict the shape memory effect observed in the experimental investigation of Chapter II. These equations, namely Eqs. (3.42), (3.45), (3.50), and (3.53), are summarized in the following four equations.

$$\begin{aligned} \lambda(t) &= \lambda_a(s(t), \theta(t)) \\ 0 &= [1 - \phi(\theta)]\left\{\frac{\partial}{\partial s}\lambda_a(s, \theta)\left[\frac{ds}{d\theta}\right] + \frac{\partial}{\partial \theta}\lambda_a(s, \theta)\right\} \\ &\quad + \left\{\frac{\partial}{\partial s}\lambda_f(s, \theta)\left[\frac{ds}{d\theta}\right] + \frac{\partial}{\partial \theta}\lambda_f(s, \theta)\right\}\lambda_f^{-1}(s, \theta)\lambda_1 - [1 - \phi(\theta)]\lambda_a(s, \theta) \\ \lambda(t) &= \lambda_f(s(t), \theta_2)\lambda_f^{-1}(s_2, \theta_2)\lambda_1 \\ \frac{d\lambda}{d\theta} &= -\phi'(\theta) + [1 - \phi(\theta)]\alpha_a + \lambda_f^{-1}(\acute{s}(\theta))\lambda_a(\acute{s}(\theta))\phi'(\theta) \end{aligned}$$

Numerically implementing these equations in MATLAB[®] and using the values of the calibration parameters presented in Table V, predictions are made for different values of applied stretch. The files used to implement the constitutive equations are provided in Appendix B.

6. Prediction of Experimental Load Path and Discussion

After calibrating the necessary parameters to implement Eqs. (3.42), (3.45), (3.50), and (3.53) for the shape memory effect thermomechanical cycle, the model was used to predict the material response for the shape memory effect with 10% extension. The results were compared to the model prediction of the small deformation model in Fig. 28. A slight difference is seen in the shape recovery segment of the thermomechanical load path. This difference is due to the slight variations in the frozen volume fraction, as the function for the two models was calibrated from experiments with different values of applied deformation. Overall, the model predictions are nearly identical for small values of applied deformation. This comparison is expected as a neo-Hookean model is generally considered an adaptation of linear elastic material response for large deformations.

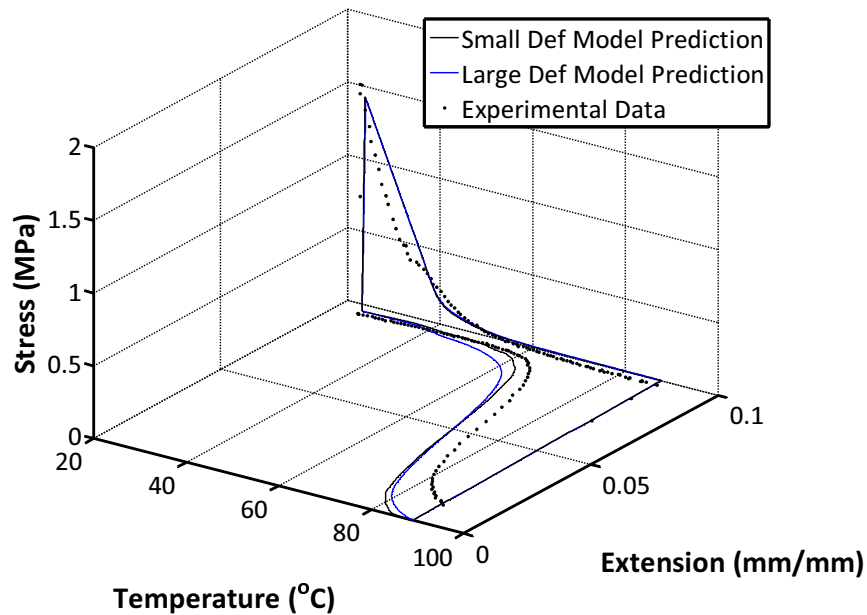


Fig. 28. Comparison of Stretch-Stress-Temperature Predictions for SME with 10% Applied Tensile Extension

In addition to the 10% extension case, the model was used to predict the SME response for a SMP assumed to behave as a neo-Hookean material for axial stretch values of 1.25, 1.5, and 2.0. These stretch values can be directly related to the experiments performed in Chapter II with respective extensions of 25%, 50%, and 100%. In particular, the stretch of a material is defined as the ratio of the current length of the material to the original length, or is one (1) plus the value of the extension.

The constitutive model is first used to predict the shape memory effect in one-dimension for a material subjected to a value of stretch equal to 1.25. Figure 29 presents the stretch-stress-temperature profile for the entire thermomechanical load path. Similar to the predictions obtained from implementing the model for small deformations, the three-dimensional plot in the figure is analogous to the thermomechanical cycle presented in Fig. 1. In this figure, the model prediction matches well with that of the experimental data, and the following figures focus on particular relationships of the state of the material to provide more insight as to the accuracy of the comparison. In this figure and all such figures, the solid lines again represents the model predictions while the discrete points represent actual experimental data obtained in Chapter II.

Figure 30 presents the stress-stretch data for the case of stretch equal to 1.25. The model prediction matches well with the experimental data, and the prediction captures the nonlinear stress-stretch relationship at relatively larger values of applied stretch. This nonlinearity is both observed experimentally and expected to be captured by the model prediction due to the nonlinear equations for the stress in terms of the stretch presented in Eq. (3.29). Furthermore, Fig. 30 shows good agreement for the stress increase during cooling while maintaining a constant value of stretch.

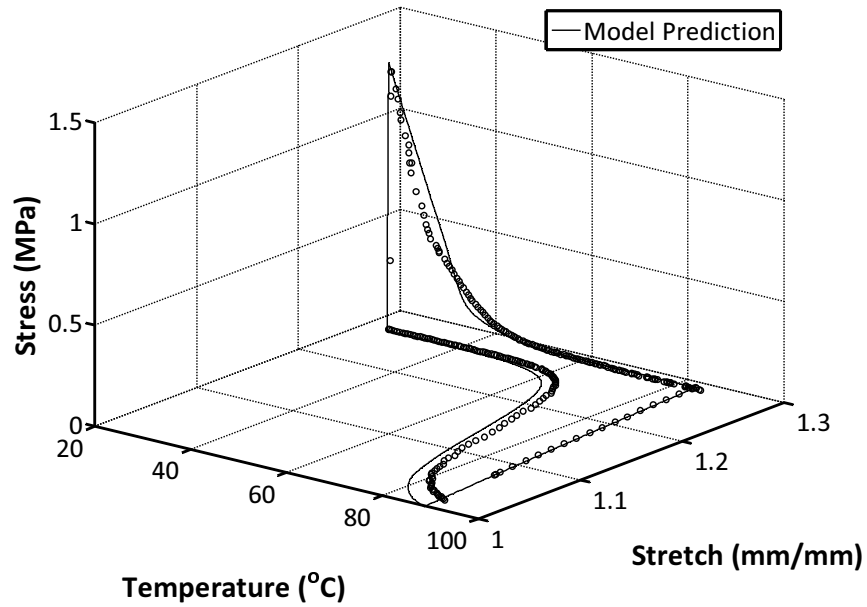


Fig. 29. Stretch-Stress-Temperature Prediction for SME with Stretch Equal to 1.25

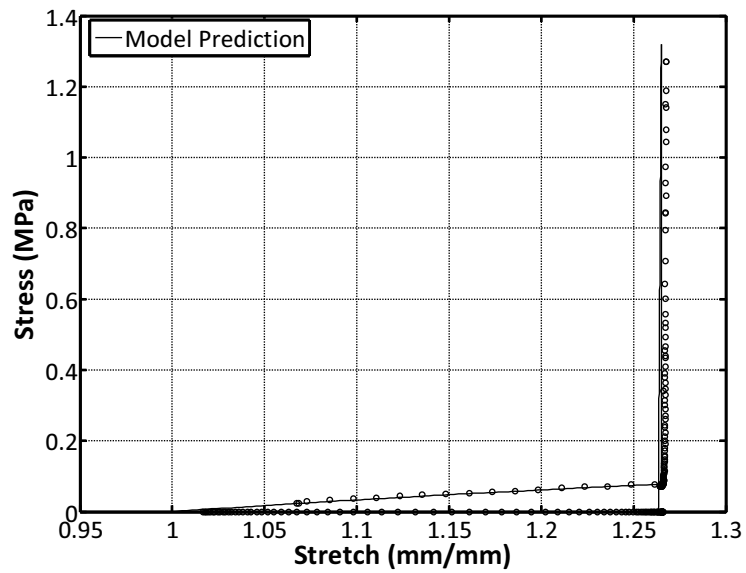


Fig. 30. Stress-Stretch Prediction for SME with Stretch Equal to 1.25

Figure 31 presents the stress-temperature results for the model prediction and the corresponding experimental data. From this figure, it is observed that in general, the prediction matches well with experimental data both qualitatively and quantitatively. Specifically, the stress increase due to the constrained cooling has good agreement. A key observation is that the onset of the glass transition predicted by the model matches well with the experimental data as denoted by the more rapid increase in stress during the constrained cooling process. In addition, the final stress at the end of cooling is nearly identical for the model prediction compared to that observed in the experimental data. The stress profiles, however, are not identical in part due to the effects of the kinematic constraint on the material which is possibly affecting the glass transition behavior which is calibrated from the strain recovery profile at zero load. Nonetheless, the model prediction matches well with the experimental data during this step of the thermomechanical load path.

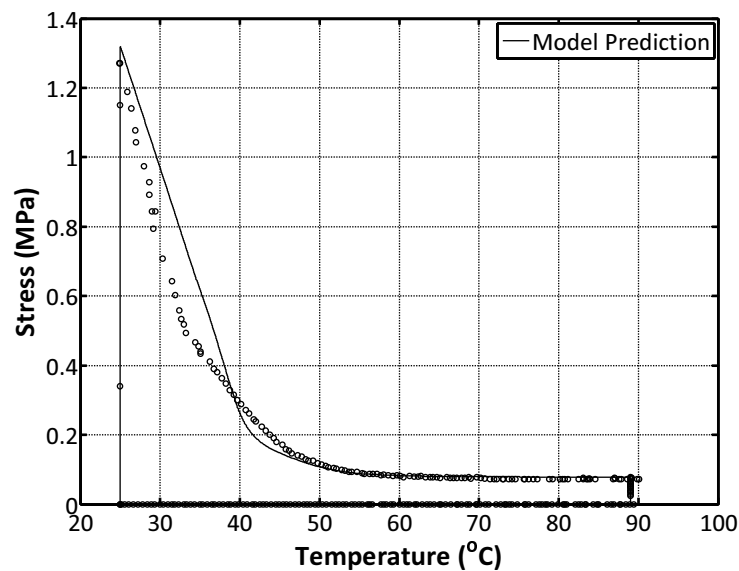


Fig. 31. Stress-Temperature Prediction for SME with Stretch Equal to 1.25

The final figure for the 1.25 stretch case is the stretch-temperature plot presented in Fig. 32. Although half of the thermomechanical load path involves constant temperature segments which contribute little to the comparison, a key component in this figure is the shape recovery profile upon heating at zero load. It is again observed that the model prediction has reasonable agreement with the experimental data. In particular, the qualitative nonlinear stretch recovery profile with respect to temperature is observed, and the shape recovery begins at approximately the same temperature for both the prediction and the experimental data. This agreement is expected as the frozen volume fraction, the parameter which ‘dictates’ the shape recovery during heating, is calibrated from this experimentally-obtained stretch recovery profile. There is a difference in the final value of the stretch, however, due to the fact that the model is developed on the assumption that all ‘frozen’ deformation is recovered upon subsequent heating through the same temperature range and consequently does not account for the experimentally observed irrecoverable deformation. Additionally, similar to the predictions of the linearized model, the values of stretch obtain a value less than 1.0 (undeformed state) near the end of recovery. This observation is due to ‘extra’ deformation stored during cooling as a result of the stress predicted by the model lying above that of the experimental data. Thus, when the stress from this step is recalled during heating, the model predicts a larger amount of recovery.

In addition to predicting the material response for the case with stretch equal to 1.25, the model was used to predict the material response when the stretch was increased to values of 1.5 and 2.0 for which the corresponding extensions were 50% and 100%, respectively. Unlike the predictions for these values of extensions by the linearized model, the predictions made by the large deformation model for the corresponding values of stretch present more than just an empirical prediction. Specifically, the calculated stretches are theoretically consistent in representing entire deformation

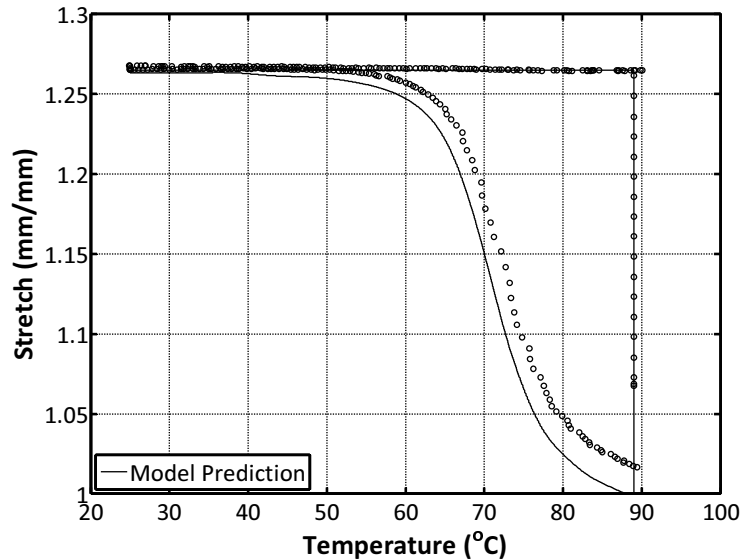


Fig. 32. Stretch-Temperature Prediction for SME with Stretch Equal to 1.25

of the body undergoing uniaxial tension. For instance, if desired (but not performed in this work), the axial component of the Green strain or other finite deformation measure could be calculated from the value of the axial stretch.

Figures 33 and 34 presents the complete, three-dimensional stretch-stress-temperature profiles for the cases with stretch equal to 1.5 and 2.0, respectively, with the experimental data plotted for purposes of comparison. It is again observed that the model prediction has reasonable agreement with the experimental data for both values of applied extension, and the following figures focus on particular relationships in the data to present a more thorough comparison.

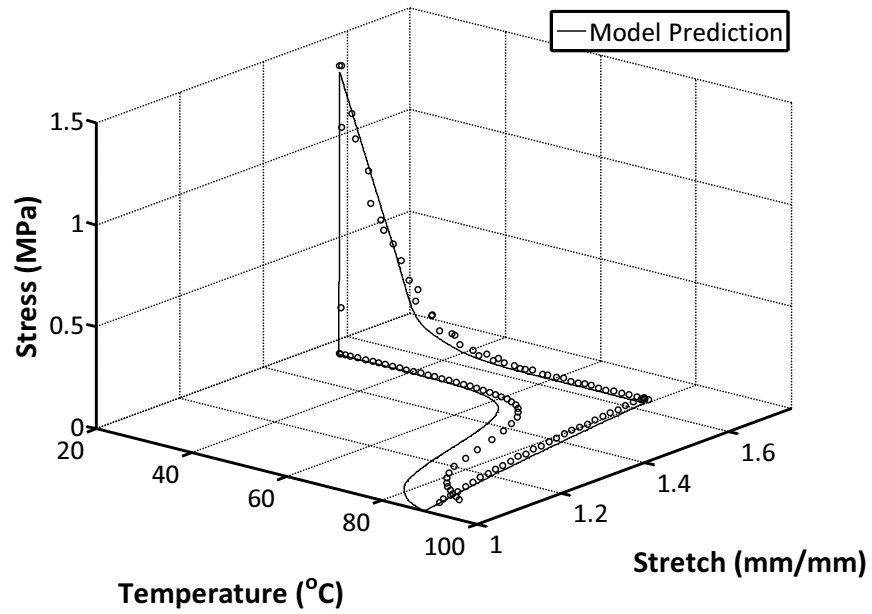


Fig. 33. Stretch-Stress-Temperature Prediction for SME with Stretch Equal to 1.5

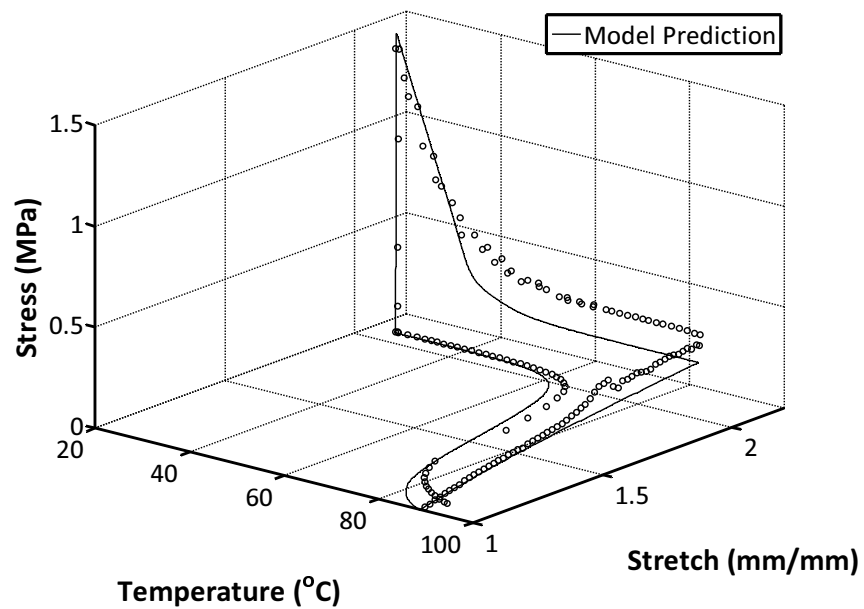


Fig. 34. Stretch-Stress-Temperature Prediction for SME with Stretch Equal to 2.0

Figure 35 presents the stress-stretch prediction for the two load cases. Examining Fig. 35, reasonable agreement is seen for the stress profiles with increasing stretch. One feature not captured by the model is the local stress peak observed at a stretch of approximately 1.7 in the experiment when loading to the stretch value of 2.0. This local peak results in an upward shift in the stress which is also not captured by the model prediction. On the other hand, the nonlinear trend of the stress-stretch profile during loading is captured qualitatively well by the model predictions. It is important to note that even very small fluctuations (even 10kPa) in the value of the calibrated elastic modulus, and thus the shear modulus, of the active phase can result in significant shifts in the model prediction. This strong dependence on the moduli of the material in the active phase likely contributes to the slight differences between the model prediction and the experimental data, for which individual specimens may exhibit slightly different material properties.

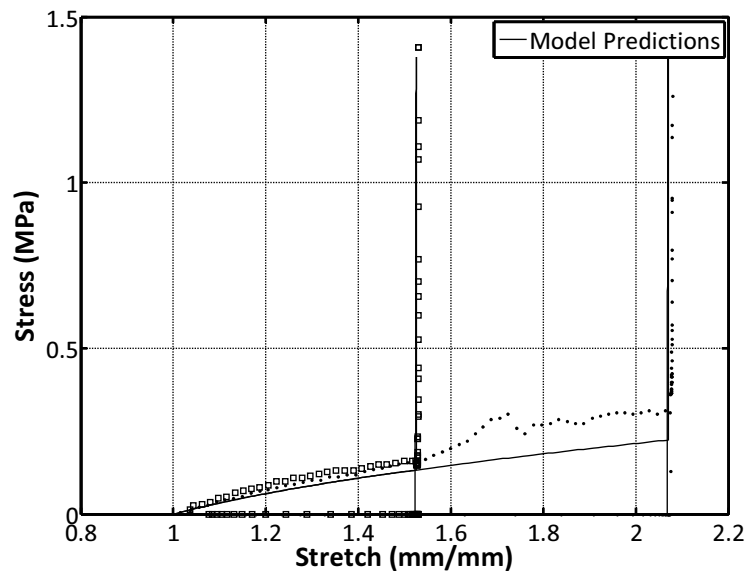


Fig. 35. Stress-Stretch Prediction for SME with Stretch Equal to 1.5 and 2.0

Figure 36 presents the stress-temperature prediction compared to the experimental results for the two load cases. The stress-temperature profile predicted by the model for an axial stretch value equal to 1.5 not only closely follows the profile observed in the experimental data, but the predicted final value is also very near that observed experimentally. The load case where the stretch is equal to 2.0 also exhibits good qualitative agreement but not as good of quantitative agreement. In particular, the stress increase predicted by the model is larger than that observed in the data. This discrepancy may be attributed to the discussion in Chapter II where some inelastic phenomena may be present in the material as related to the peak observed during loading, and these inelastic effects may have affected the ability of the material to sustain as high of stresses upon cooling.

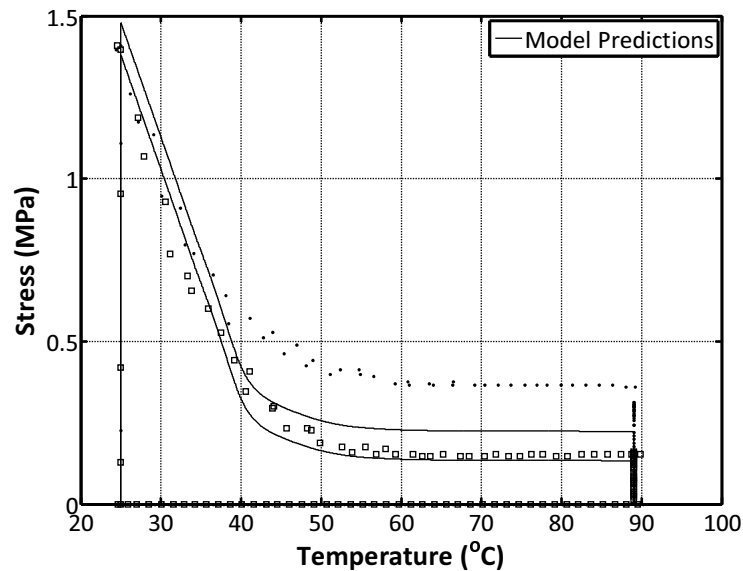


Fig. 36. Stress-Temperature Prediction for SME with Stretch Equal to 1.5 and 2.0

Finally, Fig. 37 provides the stretch-temperature prediction for the two load cases. The key component in this such figure is the shape recovery upon heating

at zero load, depicted by the qualitative nonlinear stretch-temperature profile. The model prediction shows good agreement with experimental data, but does not capture the irrecoverable deformation which remains in the material at the end of heating. Additionally, the stretch obtains a value less than 1.0 during recovery for the same reason as the case with stretch equal to 1.25, where additional deformation is recovered due to the discrepancies in the stress prediction during cooling. Furthermore, it is observed that similar to the experimental observations in Chapter II, the rate of strain recovery due to a constant temperature rate increases with increasing values of deformation.

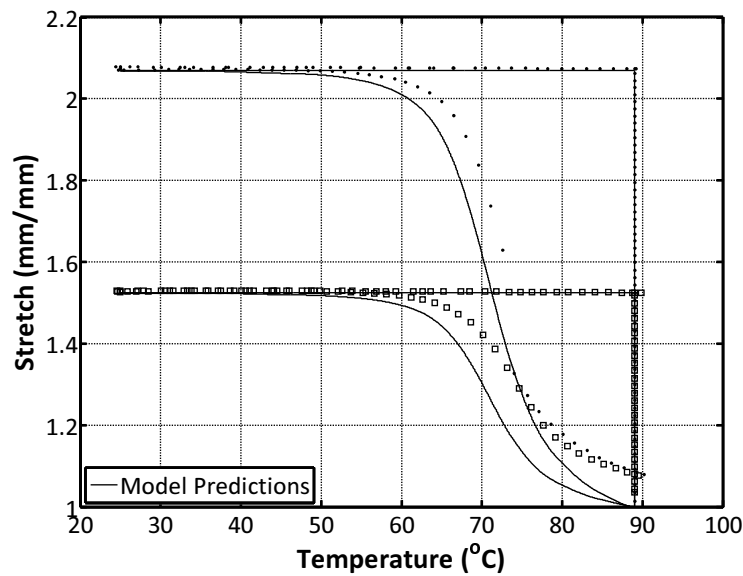


Fig. 37. Stretch-Temperature Prediction for SME with Stretch Equal to 1.5 and 2.0

D. Conclusions

In this work, the experimental data obtained in Chapter II was used to calibrate two constitutive models aimed at describing the shape memory effect in shape memory

polymers. The models, proposed by Chen and Lagoudas, were the general, large deformation model as well as the small deformation model obtained through linearizing of the large deformation model. The one-dimensional constitutive equations were then numerically implemented in MATLAB[®] for the shape memory effect thermo-mechanical cycle presented in Fig. 1.

The small deformation model assumed infinitesimal strains, Cauchy stress, and an isotropic, linear elastic material. The integral term in Eq. (3.1) containing deformation gradients multiplied together was reduced via a first order approximation to an additive decomposition of the deformations due to the active and frozen phases, and the deformation in the active phase subsequently frozen upon cooling. This work calibrated the model in one-dimension for the axial component of the infinitesimal strain tensor. The resulting calibration requirements, namely the frozen volume fraction, the elastic moduli the active and frozen phases, and the thermal expansion coefficients in the active and frozen phases, were calculated from the experimental data obtained in Chapter II and summarized in Table IV. The data from the 10% applied strain (extension) experiment was used to calibrate the material properties, and the model was subsequently used to predict the shape memory effect for 10%, 25%, 50%, and 100% applied strain. While the model predicted reasonable agreement for the thermomechanical load path for each value of applied strain, it was noted that the predictions for larger values of applied strain were essentially empirical predictions for the extension of the material because materials undergoing relatively larger values of applied extension can no longer have the state of the material accurately represented by the infinitesimal strain tensor.

In addition, the large deformation model was calibrated using the experimental data obtained in Chapter II, and the material was assumed to behave as an isotropic, neo-Hookean material in that it was assumed that the material was incompressible for

any deformations occurring at a constant temperature. Using this neo-Hookean assumption, the constitutive equation proposed by Chen and Lagoudas in Eq. (3.1) was reduced to a one-dimensional constitutive equation for the axial stretch of the SMP. The resulting constitutive equation again needed five calibration functions which were assumed to be functions of temperature, namely the frozen volume fraction, the shear moduli in the active and frozen phases, and the volume ratios in the active and frozen phases. The data from the experiments with stretch equal to 1.25 (25% extension) was used to calibrate the constitutive equations but only provided the shear moduli and volume ratios for the material at two discrete temperatures - namely the high and low temperatures at which loading and unloading occurred, respectively. As a result, assumptions were made that for each phase, the derivative of the stretch (a function of the shear moduli and volume ratio) with respect to temperature was approximated as the coefficient of thermal expansion previously calibrated for the small deformation model. After calibrating the necessary functions, the model was used to predict the stretch-stress-temperature profiles for uniaxial stretches of 1.25, 1.5, and 2.0. The model predictions agreed well with the experimental data, but failed to capture the irrecoverable deformations at the end of the recovery heating as well as the stress peak during load to a stretch of 2.0. The first difference is due to the assumption made during model development that the material recovers all of the deformation which is frozen upon subsequent heating, and the second difference may be due to yielding or other inelastic phenomena occurring in the material.

In conclusion, the constitutive models developed by Chen and Lagoudas were successfully calibrated with and used to predict the experimental data obtained in Chapter II. The model predictions agreed well with the corresponding experimental data, and present the first attempt to calibrate a large deformation model for shape memory polymers. The model predictions not only help validate the development of

the model, but also the experimental procedures used in characterizing the SMPs.

CHAPTER IV

CONCLUSIONS

In this work, a thermomechanical experimental investigation of the shape memory effect in a particular shape memory polymer was conducted. Tests were performed on the VeriflexTM shape memory polymer developed by Cornerstone Research Group, Inc., and followed the thermomechanical cycle for the SME in shape memory polymers presented in Fig. 1 focusing strictly on the material response due to tensile deformations. This experimental investigation involved the use of a complex experimental apparatus at NASA Langley Research Center that included an optical strain measurement technique named the VIC 3-D system that was capable of capturing large deformations and subsequently calculating the full-field strain measurements in two dimensions.

Experiments with tensile extensions of 10%, 25%, 50%, and 100% and temperature rates of 1°C/min to 5°C/min were performed on pristine shape memory polymer specimens. The material was observed to recover approximately 95% of the applied deformation under zero load recovery conditions during the first actuation cycle. In addition, the amount of recoverable deformation was negligibly influenced by variations in the temperature rate used during the experiment. The results produced in this experimental investigation also represent one of the first known efforts to capture the complete shape recovery profile for dogbone specimens undergoing large deformations.

In addition, two constitutive models were reduced to a form for the axial deformation component during uniaxial tension, and then calibrated with and used to predict the response of the material observed experimentally. The models, proposed by Chen and Lagoudas, were the general large deformation model as well as the

small deformation model obtained through linearizing of the large deformation model. The one-dimensional constitutive equations were then numerically implemented in MATLAB[®] to predict the SME of the Veriflex[®] SMP.

The calibration of the small deformation model assumed infinitesimal strains, approximation of the Piola-Kirchoff stress as the Cauchy stress, and an isotropic, linear elastic material. The calibration requirements, namely the frozen volume fraction, the elastic moduli in each phase, and the thermal expansion coefficients in each phase, were calculated from the 10% extension experimental data. The model was then used to predict the shape memory effect for extensions of 10%, 25%, 50%, and 100%. Although the model predicted reasonable agreement for the thermomechanical load path for each value of applied strain, it is noted that the predictions for larger values of applied strain were essentially empirical predictions of the extension of the material as materials undergoing such large values of deformation can no longer have the state of the material accurately represented by the infinitesimal strain tensor and the Cauchy stress tensor.

The large deformation model was then calibrated in one-dimension using the experimental data obtained in Chapter II. In this work, the material was assumed to behave as an isotropic, neo-Hookean material. Using this assumption, the three-dimensional constitutive equation proposed by Chen and Lagoudas was reduced to a one-dimensional constitutive equation for the axial stretch in the SMP. The resulting constitutive equation needed five calibration functions, namely the frozen volume fraction, the shear moduli in each phase, and the volume ratios in each phase, all of which were assumed to be functions of temperature. These functions were either calibrated from the experimental data with stretch equal to 1.25 (25% applied extension) or assumptions were made as to the value of terms when sufficient experimental data was not available. After calibrating the required functions, the model was used to predict

the stretch-stress-temperature profiles for large deformations including stretch values of 1.25, 1.5, and 2.0 which corresponded to the experimental data for extensions of 25%, 50%, and 100%. The model predictions agreed well with the experimental data and also captured the nonlinear stress-stretch behavior which was not captured by the small deformation model.

In both the small deformation and large deformation models, the predictions matched well with the experimental data, but did not capture the irrecoverable deformations at the end of the recovery heating. This difference is due to the assumption made during model development that the material recovers all of the ‘frozen’ deformation upon subsequent heating. In fact, the models predict too much shape recovery due to the inaccuracies of the stress prediction during cooling which is used to dictate the stored (and hence, recovered) deformation.

In summary, a complex thermomechanical characterization on a particular shape memory polymer was performed which represented one of the first known efforts to capture the complete shape recovery profile for dogbone specimens. Using this data, two constitutive models proposed by Chen and Lagoudas were successfully calibrated with and used to predict the experimental data obtained in Chapter II. The model predictions agreed well with the corresponding experimental data, and present the first attempt to calibrate the large deformation model proposed by Chen and Lagoudas for shape memory polymers. Good agreement between the model predictions and the experimental results not only help validate the development of the model but also the experimental procedures used in characterizing the SMPs. This work helps provide a foundation for future numerical implementation in a finite element software, such as ABAQUS[®], to aid in designing applications using SMPs and predicting the material response due to complex thermomechanical loading on non-trivial structures.

REFERENCES

- [1] K. Otsuka, C. Wayman, Shape Memory Materials, Cambridge University Press, New York, NY, 1999.
- [2] A. Srinivasan, D. McFarland, Smart Structures: Analysis and Design, Cambridge University Press, Cambridge, 2001.
- [3] D. J. Hartl, D. C. Lagoudas, Aerospace applications of shape memory alloys, *Journal of Aerospace Engineering* 221 (2007) 535–552.
- [4] K. Gall, M. Mikulas, N. Munshi, F. Beavers, M. Tupper, Carbon fiber reinforced shape memory polymer composites, *Journal of Intelligent Material Systems and Structures* 11 (2000) 877–886.
- [5] Y. Liu, K. Gall, M. Dunn, A. Greenberg, J. Diani, Thermomechanics of shape memory polymers: Uniaxial experiments and constitutive modeling, *International Journal of Plasticity* 22 (2006) 279–313.
- [6] A. Lendlein, S. Kelch, Shape-memory polymers, *Angew. Chem. Int. Ed.* 41 (2002) 2034–2057.
- [7] H. Tobushi, T. Hashimoto, S. Hayashi, E. Yamada, Thermomechanical constitutive modeling in shape memory polymer of polyurethane series, *Journal of Intelligent Material Systems and Structures* 8 (1997) 711–718.
- [8] H. Tobushi, T. Hashimoto, N. Ito, S. Hayashi, E. Yamada, Shape fixity and shape recovery in a film of shape memory polymer of polyurethane series, *Journal of Intelligent Material Systems and Structures* 9 (1998) 127–136.

- [9] C. Liu, H. Qin, P. T. Mather, Review of progress in shape-memory polymers, *Journal of Materials Chemistry* 17 (2007) 1543–1558.
- [10] V. A. Beloshenko, V. N. Varyukhin, Y. V. Voznyak, The shape memory effect in polymers, *Russian Chemical Reviews* 74 (2005) 265–283.
- [11] D. Ratna, J. Karger-Kocsis, Recent advances in shape memory polymers and composites: A review, *Journal of Materials Science* 43 (2008) 254–269.
- [12] P. A. Toensmeir, Radical departure, *Aviation Week and Space Technology* 5 (2005) 72–73.
- [13] K. Gall, M. Dunn, Y. Liu, D. Finch, M. Lake, N. Munshi, Shape memory polymer nanocomposites, *Acta Materialia* 50 (2002) 5115–5126.
- [14] T. Ohki, Q. Ni, N. Ohsako, M. Iwamoto, Mechanical and shape memory behavior of composites with shape memory polymer, *Composites: Part A* 35 (2004) 1065–1073.
- [15] Z. G. Wei, R. Sandstrom, S. Miyazaki, Shape-memory materials and hybrid composites. Part I: Shape-memory materials, *Journal of Materials Science* 33 (1998) 3743–3762.
- [16] Z. G. Wei, R. Sandstrom, S. Miyazaki, Shape memory materials and hybrid composites. Part II: Shape-memory hybrid composites, *Journal of Materials Science* 33 (1998) 3763–3783.
- [17] J. Manzo, E. Garcia, Methodology for design of an active rigidity joint, *Journal of Intelligent Material Systems and Structures* 20 (2009) 311–327.

- [18] G. McKnight, C. Henry, Variable stiffness materials for reconfigurable surface applications, in: Proceedings of SPIE 2005 Smart Structures and Materials, Vol. 5761, 2005, pp. 5761S1–8.
- [19] C. Henry, G. McKnight, Cellular variable stiffness materials for ultra-large reversible deformations in reconfigurable structures, in: Proceedings of SPIE 2006 Smart Structures and Materials, Vol. 6170, 2006, pp. 6170S1–12.
- [20] G. Baer, T. Wilson, D. Matthews, D. Maitland, Shape-memory behavior of thermally stimulated polyurethane for medical applications, *Journal of Applied Polymer Science* 103 (2006) 3882–3892.
- [21] B. Atli, F. Gandhi, G. Karst, Thermomechanical characterization of shape memory polymers, in: Y. Bar-Cohen (Ed.), Proceedings of SPIE 2007 Electroactive Polymer Actuators and Devices, Vol. 6524, 2007, pp. 6524S1–10.
- [22] H. Tobushi, K. Okumura, S. Hayashi, N. Ito, Thermomechanical constitutive model of shape memory polymer, *Mechanics of Materials* 33 (2001) 545–554.
- [23] A. Bhattacharyya, H. Tobushi, Analysis of the isothermal mechanical response of a shape memory polymer rheological model, *Polymer Engineering Science* 40 (2000) 2498–2510.
- [24] S. Hong, W. Yu, J. Youk, Thermomechanical deformation analysis of shape memory polymers using viscoelasticity, in: Proceedings of ESAFORM 10th Annual Conference on Material Forming, Vol. 907, 2007, pp. 853–860.
- [25] A. Srinivasa, P. Gosh, A simple, Gibbs potential based multinetwork model for shape memory polymers, *Smart Devices: Modeling of Material Systems, An International Workshop 08* (2008) 58–74.

- [26] I. J. Rao, Constitutive modeling of crystallizable shape memory polymers, in: Proceedings of SPE-ANTEC, Vol. 60, 2002, pp. 1936–1940.
- [27] Y. Chen, D. Lagoudas, A constitutive theory for shape memory polymers. Part I: Large deformations, *Journal of the Mechanics and Physics of Solids* 56 (2008) 1752–1765.
- [28] Y. Chen, D. Lagoudas, A constitutive theory for shape memory polymers. Part II: A linearized model for small deformations, *Journal of the Mechanics and Physics of Solids* 56 (2008) 1766–1778.
- [29] ASTM Standard D638, Standard test method for tensile properties of plastics, ASTM International (2003) 1–15, doi:10.1520/D0638-08.
URL www.astm.org
- [30] M. E. Gurtin, *An Introduction to Continuum Mechanics*, Academic Press, New York, NY, 1981.

APPENDIX A

MATLAB FILES FOR ONE-DIMENSIONAL NUMERICAL IMPLEMENTATION
OF SMALL DEFORMATION MODEL

```

%%%%%%%%%%%%%%%%%%%%%%%%%%%%%%%%%%%%%%%%%%%%%%%%%%%%%%%%%%%%%%%%%%%%%%%% MAIN SOURCE CODE %%%%%%%%%%%%%%%%%%%%%%%%%%%%%%%%%%%%%%%%%%%%%%%%%%%%%%%%%%%%%%%%%%%%%%%%%

%%%%%%%% Brent Volk
%%%%%%%% Calibration of Shape Memory Polymer
%%%%%%%% Model developed by Dr. Chen & Dr. Lagoudas

%%%%%%%% SMP Thermomechanical cycle includes:
%%%%%%%% (1) Apply strain to material in rubber phase
%%%%%%%% (2) Hold strain constant and cool material to below Tg
%%%%%%%% (3) Unload specimen
%%%%%%%% (4) Heat specimen under zero load for shape recovery

%%%%%%%% Clearing the workspace
clc;
clear;

%%%%%%%% SETTING THE GLOBAL VARIABLES (allows use by all functions)
%%%%%%%% Variables include: Elastic moduli, coefficients of thermal expansion,
%%%%%%%% frozen volume fraction, and the temperature and stress during cooling
%%%%%%%% which are used to "recover" the strain upon heating
global E_a
global E_f
global alpha_a
global alpha_f
global CALIBRATIONPHI
global CALIBRATIONTEMP
global Temperature_during_cooling
global Stress_during_cooling

%%%%%%%% Setting the values of the calibration requirements
E_a = 0.33e006;
E_f = 1081e006;
alpha_a = 5.2e-004;
alpha_f = 0.75e-004;
[CALIBRATIONPHI CALIBRATIONTEMP] = Calibrationdata_25perc;

```



```

%%%%% Setting test parameters, including maximum and minimum temperatures,
%%%%% and stress under which the material is allowed to recover
Temperature_maximum = 362;
Temperature_minimum = 298;
Cooling_increment = -1;
Heating_increment = 1;
RecoveryStress = 0;

%%%%% Setting the value of the desired applied strain, and inputting the
%%%%% corresponding experimental data for comparison

Applied_Strain = 0.098;
[ActualLoadingStress ActualLoadingTemperature ActualLoadingStrain ...
 ActualCoolingStress ActualCoolingTemperature ActualCoolingStrain ...
 ActualUnloadingStress ActualUnloadingStrain ActualUnloadingTemperature ...
 ActualRecoveryStrain ActualRecoveryTemperature ActualRecoveryStress] = ...
ReducedActualdata10Perc_2;

% Applied_Strain = 0.265;
% [ActualLoadingStress ActualLoadingTemperature ActualLoadingStrain ...
% ActualCoolingStress ActualCoolingTemperature ActualCoolingStrain ...
% ActualUnloadingStress ActualUnloadingStrain ActualUnloadingTemperature ...
% ActualRecoveryStrain ActualRecoveryTemperature ActualRecoveryStress] = ...
% ReducedActualdata25Perc;

% Applied_Strain = 0.525;
% [ActualLoadingStress ActualLoadingTemperature ActualLoadingStrain ...
% ActualCoolingStress ActualCoolingTemperature ActualCoolingStrain ...
% ActualUnloadingStress ActualUnloadingStrain ActualUnloadingTemperature ...
% ActualRecoveryStrain ActualRecoveryTemperature ActualRecoveryStress] = ...
% ReducedActualdata50Perc;

% Applied_Strain = 1.07;
% [ActualLoadingStress ActualLoadingTemperature ActualLoadingStrain ...
% ActualCoolingStress ActualCoolingTemperature ActualCoolingStrain ...
% ActualUnloadingStress ActualUnloadingStrain ActualUnloadingTemperature ...
% ActualRecoveryStrain ActualRecoveryTemperature ActualRecoveryStress] = ...
% ReducedActualdata100Perc;

%%%%% STEP 1 - Apply deformation to material while in rubber phase

%%%%% Predicting the final stress for the desired applied strain.
%%%%% The final stress is calculated assuming linear elastic behavior.

```

```

Final_Stress = E_a*Applied_Strain;
Stress_during_loading = linspace(0, Final_Stress);

%%%%% Setting the temperature during loading to the maximum temperature.
Temperature_during_loading = Temperature_maximum.*...
    (ones(size(Stress_during_loading)));

%%%%% Initializing the strain vector during loading
Strain_during_loading = zeros(size(Stress_during_loading));

%%%%% Calculating the strain during loading.
for i = 1:length(Stress_during_loading)
    curr_phi = GetPhi(Temperature_during_loading(i));
    Strain_during_loading(i) = (1-curr_phi)*(Stress_during_loading(i)/E_a)...
        + curr_phi*(Stress_during_loading(i) / E_f);
end

%%%%% STEP 2 - Cool material to below Tg while maintaining deformation

%%%%% Setting the temperature during cooling from the max temperature to
%%%%% the minimum temperature at an arbitrary cooling increment.
Decreasing_Temperature = ...
    (Temperature_maximum:Cooling_increment:Temperature_minimum);

%%%%% Solving the ODE for stress as a function of temperature. The function
%%%%% arguments are the desired cooling temperature span as well as the
%%%%% starting stress(initial condition). The starting stress is taken
%%%%% to be the stress value at the end of the loading segment.
[Temperature_during_cooling Stress_during_cooling] = ...
    ode23('Cooling_ode_withBrentdata', Decreasing_Temperature, ...
    Stress_during_loading(length(Stress_during_loading)));

%%%%% The strain during cooling is taken to be a constant, with a value of
%%%%% that at the end of the loading in Step 1.
Strain_during_cooling=Strain_during_loading(length(Strain_during_loading))...
    .*(ones(size(Temperature_during_cooling)));

%%%%% STEP 3 - Unload the material at a constant temperature
%%%%% in the glass phase (T < Tg)

%%%%% Setting the stress during unloading from the stress at the end of
%%%%% cooling to the desired recovery stress.

```

```

Stress_during_unloading = linspace(Stress_during_cooling...
    (length(Stress_during_cooling)),RecoveryStress);

%%%%% Setting the temperature during unloading to the minimum temperature.
Temperature_during_unloading = Temperature_minimum.*...
    (ones(size(Stress_during_unloading)));

%%%%% Determining the frozen volume fraction at the desired unloading temp.
unload_phi = GetPhi(Temperature_minimum);

%%%%% Calculating the values of strain during the unloading process.
Strain_during_unloading=Strain_during_cooling(length(Strain_during_cooling))...
    + ((1-unload_phi)/E_a + unload_phi/E_f)*(Stress_during_unloading - ...
    Stress_during_cooling(length(Stress_during_cooling)));

%%%%% STEP 4 - Heat the material to T < Tg to allow strain recovery.
%%%%% Assumes material recovers completely upon heating.

%%%%% Setting the temperature during heating from the min temperature to
%%%%% the maximum temperature at an arbitrary cooling increment.
Increasing_Temperature = ...
    Temperature_minimum:Heating_increment:Temperature_maximum;

%%%%% Solving the ODE for strain recovery as a function of temperature.
%%%%% The function arguments are the desired heating temperature span as
%%%%% well as the strain at the end of unloading (initial
%%%%% condition).
[Temperature_during_recovery    Strain_during_recovery] = ...
    ode23('Heating_ode_withBrentdata', Increasing_Temperature, ...
    Strain_during_unloading(length(Strain_during_unloading)));

%%%%% The stress during recovery is taken to be a constant, with a value of
%%%%% the desired recovery stress previously defined.
Stress_during_recovery = RecoveryStress.*...
    (ones(size(Temperature_during_recovery)));

%%%%% Creating plots
%%%%% Setting the parameters of the figures
set(0,'defaultaxesfontsize',20);
set(0,'defaultaxesfontname','calibri');

```

```

%%%%% Plotting the Stress vs. Temperature
figure(1);
plot(Temperature_during_loading, Stress_during_loading, 'k', ...
     ActualLoadingTemperature, ActualLoadingStress, 'ko', ...
     Temperature_during_cooling, Stress_during_cooling, 'k', ...
     ActualCoolingTemperature, ActualCoolingStress,'ko', ...
     Temperature_during_unloading, Stress_during_unloading, 'k', ...
     ActualUnloadingTemperature, ActualUnloadingStress,'ko', ...
     Temperature_during_recovery, Stress_during_recovery,'k', ...
     ActualRecoveryTemperature, ActualRecoveryStress,'ko', 'LineWidth',2);
hold on

xlabel('Temperature (K)', 'fontsize',24, 'FontName','arial')
ylabel('Stress (Pa)', 'fontsize',24, 'FontName','arial')
legend('Model Prediction', 'Experimental Data')
grid on

%%%%% Plotting the Strain vs. Temperature
figure(2);
plot(Temperature_during_loading, Strain_during_loading, 'k', ...
     ActualLoadingTemperature, ActualLoadingStrain, 'ko', ...
     Temperature_during_cooling, Strain_during_cooling, 'k', ...
     ActualCoolingTemperature, ActualCoolingStrain,'ko', ...
     Temperature_during_unloading, Strain_during_unloading, 'k', ...
     ActualUnloadingTemperature, ActualUnloadingStrain,'ko', ...
     Temperature_during_recovery, Strain_during_recovery,'k', ...
     ActualRecoveryTemperature, ActualRecoveryStrain,'ko', 'LineWidth',2);
hold on

xlabel('Temperature (K)', 'fontsize',24, 'FontName','arial')
ylabel('Strain (mm/mm)', 'fontsize',24, 'FontName','arial')
legend('Model Prediction', 'Experimental Data')
grid on

%%%%% Plotting the Stress vs. Strain
figure(3);
plot(Strain_during_loading, Stress_during_loading, 'k', ...
     ActualLoadingStrain, ActualLoadingStress, 'ko', ...
     Strain_during_cooling, Stress_during_cooling, 'k', ...
     ActualCoolingStrain, ActualCoolingStress,'ko', ...
     Strain_during_unloading, Stress_during_unloading, 'k', ...
     ActualUnloadingStrain, ActualUnloadingStress,'ko', ...
     Strain_during_recovery, Stress_during_recovery,'k', ...

```

```

        ActualRecoveryStrain, ActualRecoveryStress,'ko', 'LineWidth',2);
hold on

xlabel('Strain (mm/mm)', 'fontsize',24, 'FontName','arial')
ylabel('Stress (Pa)', 'fontsize',24, 'FontName','arial')
legend('Model Prediction', 'Experimental Data')
grid on

%%%%% Plotting the Stress-Strain-Temperature Profile in 3-D
figure(4);
plot3(Temperature_during_loading, Strain_during_loading,...
      Stress_during_loading, 'k', ...
      ActualLoadingTemperature, ActualLoadingStrain,...
      ActualLoadingStress, 'ko', ...
      Temperature_during_cooling, Strain_during_cooling,...
      Stress_during_cooling, 'k', ...
      ActualCoolingTemperature, ActualCoolingStrain, ...
      ActualCoolingStress,'ko', ...
      Temperature_during_unloading, Strain_during_unloading,...
      Stress_during_unloading, 'k', ...
      ActualUnloadingTemperature, ActualUnloadingStrain, ...
      ActualUnloadingStress, 'ko', ...
      Temperature_during_recovery, Strain_during_recovery,...
      Stress_during_recovery, 'k', ...
      ActualRecoveryTemperature, ActualRecoveryStrain, ...
      ActualRecoveryStress, 'ko', 'LineWidth',2);
hold on

xlabel('Temperature (K)', 'fontsize',24, 'FontName','arial')
ylabel('Strain (mm/mm)', 'fontsize',24, 'FontName','arial')
zlabel('Stress (Pa)', 'fontsize',24, 'FontName','arial')
legend('Model Prediction', 'Experimental Data')
grid on

```

```

%%%%%%%%%%%%%%%%%%%%%%%%%%%%%%%%%%%%%%%%%%%%%%%%%%%%%%%%%%%%%%%%%%%%%%%% COOLING ODE CODE %%%%%%%%%%%%%%%%%%%%%%%%%%%%%%%%%%%%%%%%%%%%%%%%%%%%%%%%%%%%%%%%%%%%%%%%%

%%%%%%%% Function to solve for the stress increase with respect to a change
%%%%%%%% in temperature while maintaining constant deformation
function dydT = Cooling_ode_withBrentdata (T2, y)

%%%%%%%% Initializing the global variables (material properties).
global E_a
global E_f
global alpha_a
global alpha_f

%%%%%%%% Getting the frozen volume fraction for each increment of temperature.
curr_phi = GetPhi(T2);

%%%%%%%% Setting the expression of the ODE for the stress w.r.t. temperature.
dydT = -((1-curr_phi)*alpha_a + curr_phi*alpha_f) / ...
        ((1-curr_phi)/E_a + curr_phi/E_f);

```

```

%%%%%%%%%%%%%%%%%%%%%%%%%%%%%%%%%%%%%%%%%%%%%%%%%%%%%%%%%%%%%%%%%%%%%%%%%% HEATING ODE CODE %%%%%%%%%%%%%%%%%%%%%%%%%%%%%%%%%%%%%%%%%%%%%%%%%%%%%%%%%%%%%%%%%%%%%%%%%%%

%%%%%%%% Function to obtain the ODE for the strain recovery with respect
%%%%%%%% to a change in temperature while maintaining constant stress
function dydT = Heating_ode_withBrentdata (T4, y)

%%%%%%%% Initializing the global variables (material properties).
global alpha_a
global alpha_f
global E_a
global E_f
global CALIBRATIONPHI
global CALIBRATIONTEMP

%%%%%%%% Initializing the temperature and stress the material experienced
%%%%%%%% during constrained cooling.
global Temperature_during_cooling
global Stress_during_cooling

%%%%%%%% Getting the frozen volume fraction for each increment of temperature.
heat_phi = GetPhi(T4);

%%%%%%%% Numerically differentiating the frozen volume fraction w.r.t.
%%%%%%%% temperature.
dp = diff(CALIBRATIONPHI);
dp(length(dp)+1) = dp(length(dp));
dT = diff(CALIBRATIONTEMP);
dT(length(dT)+1) = dT(length(dT));
dpdT = dp./dT;

%%%%%%%% Interpolating for the derivative of the frozen volume fraction at the
%%%%%%%% current temperature the stress of the material when last at the
%%%%%%%% current temperature.
dphi = interp1(CALIBRATIONTEMP, dpdT, T4);
Stress = interp1(Temperature_during_cooling, Stress_during_cooling, T4);

%%%%%%%% Setting the expression of the ODE for the strain w.r.t. temperature.
dydT = (1-heat_phi)*alpha_a + heat_phi*alpha_f + ...
        (1/E_a + 1/E_f)*dphi*Stress;

```

APPENDIX B

MATLAB FILES FOR ONE-DIMENSIONAL NUMERICAL IMPLEMENTATION
OF LARGE DEFORMATION MODEL

```

%%%%%%%%%%%%%%%%%%%%%%%%%%%%%%%%%%%%%%%%%%%%%%%%%%%%%%%%%%%%%%%%%%%%%%%% MAIN SOURCE CODE %%%%%%%%%%%%%%%%%%%%%%%%%%%%%%%%%%%%%%%%%%%%%%%%%%%%%%%%%%%%%%%%%%%%%%%%%

%%%%%% Brent Volk
%%%%%% Calibration of Shape Memory Polymer
%%%%%% Large Deformation Model developed by Dr. Chen & Dr. Lagoudas

%%%%%% SMP Thermomechanical cycle includes:
%%%%%% (1) Apply strain to material in rubber phase
%%%%%% (2) Hold strain constant and cool material to below Tg
%%%%%% (3) Unload specimen
%%%%%% (4) Heat specimen under zero load for shape recovery

%%%%%% Clearing the workspace
clc;
clear;

%%%%%% SETTING THE GLOBAL VARIABLES (allows use by all functions)
%%%%%% Variables include: elastic moduli, coefficients of thermal expansion,
%%%%%% shear moduli, Poissons ratios, volume ratios
%%%%%% frozen volume fraction, the equations used to calculate the
%%%%%% stretches in each phase, and values of the state of the material
%%%%%% during certain portions of the experiment (allows for shape
%%%%%% "recovery).
global E_a
global E_f

global alpha_a
global alpha_f

global Rubber_shearmod
global Glass_shearmod

global Rubber_poissons
global Glass_poissons

```



```

global Rubber_vf
global Glass_vf

global CALIBRATIONPHI
global CALIBRATIONTEMP

global lambda_a
global lambda_f

global Stretch_1
global Stress_during_cooling
global Temperature_during_cooling

%%%% Setting the values of the calibration requirements
E_a = 0.365e006;
E_f = 1081e006;
alpha_a = 1.3e-004;
alpha_f = 0.65e-004;

Rubber_modulus = E_a;
Rubber_poissons = 0.5;
Rubber_vf = 1;
Rubber_shearmod = Rubber_modulus/(2*(1+Rubber_poissons));

Glass_modulus = E_f;
Glass_poissons = 0.5;
Glass_vf = 1;
Glass_shearmod = Glass_modulus/(2*(1+Glass_poissons));

[CALIBRATIONPHI CALIBRATIONTEMP] = Calibrationdata_25perc;

%%%% Setting test parameters, including maximum and minimum temperatures,
%%%% and stress under which the material is allowed to recover
Temperature_maximum = 362;
Temperature_minimum = 298;
Cooling_increment = -1;
Heating_increment = 1;
RecoveryStress = 0;

%%%% Setting the value of the desired applied strain, and inputting the
%%%% corresponding experimental data for comparison

Applied_Extension = 0.265;
[ActualLoadingStress ActualLoadingTemperature ActualLoadingStrain ...
 ActualCoolingStress ActualCoolingTemperature ActualCoolingStrain ...

```

```

ActualUnloadingStress ActualUnloadingStrain ActualUnloadingTemperature ...
ActualRecoveryStrain ActualRecoveryTemperature ActualRecoveryStress] = ...
ReducedActualdata25Perc;

% Applied_Extension = 0.525;
% [ActualLoadingStress ActualLoadingTemperature ActualLoadingStrain ...
% ActualCoolingStress ActualCoolingTemperature ActualCoolingStrain ...
% ActualUnloadingStress ActualUnloadingStrain ActualUnloadingTemperature ...
% ActualRecoveryStrain ActualRecoveryTemperature ActualRecoveryStress] = ...
% ReducedActualdata50Perc;

% Applied_Extension = 1.07;
% [ActualLoadingStress ActualLoadingTemperature ActualLoadingStrain ...
% ActualCoolingStress ActualCoolingTemperature ActualCoolingStrain ...
% ActualUnloadingStress ActualUnloadingStrain ActualUnloadingTemperature ...
% ActualRecoveryStrain ActualRecoveryTemperature ActualRecoveryStress] = ...
% ReducedActualdata100Perc;

ActualLoadingStretch = ActualLoadingStrain + 1;
ActualCoolingStretch = ActualCoolingStrain + 1;
ActualUnloadingStretch = ActualUnloadingStrain + 1;
ActualRecoveryStretch = ActualRecoveryStrain + 1;

%%%%%Creating the symbolic equations for the stretches (deformation
%%%%%gradients) in the active and frozen phases.
syms s la ma va lf mf vf

eq1 = sym('ma*(la - va/la^2) - s');
lambda_a = solve(eq1, la);
lambda_a = lambda_a(1);

eq2 = sym('mf*(lf - vf/lf^2) - s');
lambda_f = solve(eq2, lf);
lambda_f = lambda_f(1);

%%%%% STEP 1 - Apply deformation (stretch) to material while in active phase

%%%%% Setting the stretch vector from 1 (underformed) to the desired
%%%%% deformation previously defined.
Stretch_during_loading = linspace(1,(1+Applied_Extension));

%%%%% Setting the temperature during loading to the maximum temperature.
Temperature_during_loading = Temperature_maximum.*...

```

```

        (ones(size(Stretch_during_loading)));

    %%%% Initializing the stress vector during loading
    Stress_during_loading = zeros(1,length(Stretch_during_loading));

    %%%% Calculating the stress during loading corresponding to the values
    %%%% of stretch.
    for i = 1:1:length(Stretch_during_loading)
        Stress_during_loading(i) = Rubber_shearmod*(Stretch_during_loading(i) ...
            - Rubber_vf/(Stretch_during_loading(i)^2));
    end

    %%%% Storing the value of the stretch at the end of the loading process.
    Stretch_1 = Stretch_during_loading(length(Stretch_during_loading));

    %%%%STEP 2 - Cool material to below Tg while maintaining deformation

    %%%% Setting the temperature during cooling from the max temperature to
    %%%% the minimum temperature at an arbitrary cooling increment.
    Decreasing_Temperature = ...
        (Temperature_maximum:Cooling_increment:Temperature_minimum);

    %%%% Solving the ODE for stress as a function of temperature. The function
    %%%% arguments are the desired cooling temperature span as well as the
    %%%% starting stress(initial condition). The starting stress is taken
    %%%% to be the stress value at the end of the loading segment.
    [Temperature_during_cooling Stress_during_cooling] = ...
        ode23('Cooling_ode_withBrentdata', Decreasing_Temperature, ...
            Stress_during_loading(length(Stress_during_loading)));

    %%%% The stretch during cooling is taken to be a constant, with a value of
    %%%% that at the end of the loading in Step 1.
    Stretch_during_cooling = Stretch_1.*(ones(size(Temperature_during_cooling)));

    %%%% Storing the value of the stress and temperature at the end of
    %%%% the cooling process.
    S_2 = Stress_during_cooling(length(Stress_during_cooling));
    T_2 = Temperature_during_cooling(length(Temperature_during_cooling));

    %%%% STEP 3 - Unload the material at a constant temperature
    %%%% in the glass phase (T < Tg)

```

```

%%%%%%%% Setting the stress during unloading from the stress at the end of
%%%%%%%% cooling to the desired recovery stress.
Stress_during_unloading = linspace(S_2, RecoveryStress);

%%%%%%%% Setting the temperature during unloading to the minimum temperature.
Temperature_during_unloading = T_2.*(ones(size(Stress_during_unloading)));

%%%%%%%% Calculating the values of the stretch in each phase at the end of
%%%%%%%% the cooling process
lf_2 = subs(lambda_f, {mf, vf, s}, {Glass_shearmod, Glass_vf, S_2});
la_2 = subs(lambda_a, {ma, va, s}, {Rubber_shearmod, Rubber_vf, S_2});

%%%%%%%% Initializing the stretch vector during unloading
Stretch_during_unloading = zeros(1, length(Stress_during_unloading));

%%%%%%%% Calculating the stretch during unloading.
for i = 1:length(Stress_during_unloading)
%%%%%%%% Determining the frozen volume fraction at the desired unloading temp.
    curr_phi = GetPhi(Temperature_during_unloading(i));

%%%%%%%% Calculating the stretch of the material if purely in either phase.
    curr_la = subs(lambda_a, {ma, va, s}, {Rubber_shearmod, Rubber_vf, ...
        Stress_during_unloading(i)});
    curr_lf = subs(lambda_f, {mf, vf, s}, {Glass_shearmod, Glass_vf, ...
        Stress_during_unloading(i)});

%%%%%%%% Calculating the stretch of the material as related by the frozen
%%%%%%%% volume fraction
    Stretch_during_unloading(i) = (1-curr_phi)*curr_la + curr_lf*(1/lf_2)*...
        (Stretch_1 - (1-curr_phi)*la_2);
end

%%%%%%%% STEP 4 - Heat the material to T < Tg to allow shape recovery.
%%%%%%%% Assumes material recovers completely upon heating.

%%%%%%%% Setting the temperature during heating from the min temperature to
%%%%%%%% the maximum temperature at an arbitrary cooling increment.
Increasing_Temperature = ...
    Temperature_minimum:Heating_increment:Temperature_maximum;

%%%%%%%% Solving the ODE for stretch recovery as a function of temperature.
%%%%%%%% The function arguments are the desired heating temperature span as

```

```

%%%%% well as the stretch at the end of unloading (initial
%%%%% condition).
[Temperature_during_recovery  Stretch_during_recovery] = ...
    ode23('Heating_ode_withBrentdata', Increasing_Temperature, ...
        Stretch_during_unloading(length(Stretch_during_unloading)));

%%%%% The stress during recovery is taken to be a constant, with a value of
%%%%% the desired recovery stress previously defined.
Stress_during_recovery = RecoveryStress.*...
    (ones(size(Temperature_during_recovery)));

%%%%% Creating plots
%%%%% Setting the parameters of the figures
set(0,'defaultaxesfontsize',20);
set(0,'defaultaxesfontname','calibri');

%%%%% Plotting the Stress vs. Temperature
figure(1);
plot(Temperature_during_loading, Stress_during_loading, 'k', ...
    ActualLoadingTemperature, ActualLoadingStress, 'ko', ...
    Temperature_during_cooling, Stress_during_cooling, 'k', ...
    ActualCoolingTemperature, ActualCoolingStress, 'ko', ...
    Temperature_during_unloading, Stress_during_unloading, 'k', ...
    ActualUnloadingTemperature, ActualUnloadingStress, 'ko', ...
    Temperature_during_recovery, Stress_during_recovery, 'k', ...
    ActualRecoveryTemperature, ActualRecoveryStress, 'ko', 'LineWidth',2);
hold on

xlabel('Temperature (K)', 'fontsize',24, 'FontName','arial')
ylabel('Stress (Pa)', 'fontsize',24, 'FontName','arial')
legend('Model Prediction', 'Experimental Data')
grid on

%%%%% Plotting the Stretch vs. Temperature
figure(2);
plot(Temperature_during_loading, Stretch_during_loading, 'k', ...
    ActualLoadingTemperature, ActualLoadingStretch, 'ko', ...
    Temperature_during_cooling, Stretch_during_cooling, 'k', ...
    ActualCoolingTemperature, ActualCoolingStretch, 'ko', ...
    Temperature_during_unloading, Stretch_during_unloading, 'k', ...
    ActualUnloadingTemperature, ActualUnloadingStretch, 'ko', ...
    Temperature_during_recovery, Stretch_during_recovery, 'k', ...

```

```

    ActualRecoveryTemperature, ActualRecoveryStretch,'ko', 'LineWidth',2);
hold on

```

```

xlabel('Temperature (K)', 'fontsize',24, 'FontName','arial')
ylabel('Stretch (mm/mm)', 'fontsize',24, 'FontName','arial')
legend('Model Prediction', 'Experimental Data')
grid on

```

```

%%%%% Plotting the Stress vs. Stretch

```

```

figure(3);
plot(Stretch_during_loading, Stress_during_loading, 'k', ...
     ActualLoadingStretch, ActualLoadingStress, 'ko', ...
     Stretch_during_cooling, Stress_during_cooling, 'k', ...
     ActualCoolingStretch, ActualCoolingStress,'ko', ...
     Stretch_during_unloading, Stress_during_unloading, 'k', ...
     ActualUnloadingStretch, ActualUnloadingStress,'ko', ...
     Stretch_during_recovery, Stress_during_recovery,'k', ...
     ActualRecoveryStretch, ActualRecoveryStress,'ko', 'LineWidth',2);
hold on

```

```

xlabel('Stretch (mm/mm)', 'fontsize',24, 'FontName','arial')
ylabel('Stress (Pa)', 'fontsize',24, 'FontName','arial')
legend('Model Prediction', 'Experimental Data')
grid on

```

```

%%%%% Plotting the Stress-Stretch-Temperature Profile in 3-D

```

```

figure(4);
plot3(Temperature_during_loading, Stretch_during_loading,...
     Stress_during_loading, 'k', ...
     ActualLoadingTemperature, ActualLoadingStretch,...
     ActualLoadingStress, 'ko', ...
     Temperature_during_cooling, Stretch_during_cooling,...
     Stress_during_cooling, 'k', ...
     ActualCoolingTemperature, ActualCoolingStretch, ...
     ActualCoolingStress,'ko', ...
     Temperature_during_unloading, Stretch_during_unloading,...
     Stress_during_unloading, 'k', ...
     ActualUnloadingTemperature, ActualUnloadingStretch, ...
     ActualUnloadingStress, 'ko', ...
     Temperature_during_recovery, Stretch_during_recovery,...
     Stress_during_recovery, 'k', ...
     ActualRecoveryTemperature, ActualRecoveryStretch, ...
     ActualRecoveryStress, 'ko', 'LineWidth',2);

```

```
hold on
```

```
xlabel('Temperature (K)', 'fontsize', 24, 'FontName', 'arial')  
ylabel('Stretch (mm/mm)', 'fontsize', 24, 'FontName', 'arial')  
zlabel('Stress (Pa)', 'fontsize', 24, 'FontName', 'arial')  
legend('Model Prediction', 'Experimental Data')  
grid on
```

```

%%%%%%%%%%%%%%%%%%%%%%%%%%%%%%%%%%%%%%%%%%%%%%%%%%%%%%%%%%%%%%%%%%%%%%%% COOLING ODE CODE %%%%%%%%%%%%%%%%%%%%%%%%%%%%%%%%%%%%%%%%%%%%%%%%%%%%%%%%%%%%%%%%%%%%%%%%%

%%%%%%%% Function to solve for the stress increase with respect to a change
%%%%%%%% in temperature while maintaining constant deformation
function dydT = Cooling_ode_withBrentdata (T2, y)

%%%%%%%% Initializing the global variables: material properties and
%%%%%%%% equations for the stretch in each phase.
global E_f

global alpha_a
global alpha_f

global Rubber_shearmod
global Glass_shearmod

global Rubber_vf
global Glass_vf

global lambda_a
global lambda_f

%%%%%%%% Recalling the stretch at the end of the loading segment
global Stretch_1

syms s ma va mf vf

%%%%%%%% Getting the frozen volume fraction for each increment of temperature.
curr_phi = GetPhi(T2);

%%%%%%%% Setting the change in stretch w.r.t. change in temperature to be
%%%%%%%% the coefficients of thermal expansion.
dla_dtemp = alpha_a;
dlf_dtemp = alpha_f;

%%%%%%%% Setting the value for the change in stretch w.r.t. a change in
%%%%%%%% stress. Frozen phase is assumed to be the inverse of the elastic
%%%%%%%% moduli and the active phase is taken to be a curve fit of the loading
%%%%%%%% curve in the active phase.
dlf_ds = 1/E_f;
dla_ds = 2.5e-006*exp(2.5e-006*y);

%%%%%%%% Calculating the stretch in each material phase.
la = subs(lambda_a, {ma, va, s}, {Rubber_shearmod, Rubber_vf, y});

```



```
lf = subs(lambda_f, {mf, vf, s}, {Glass_shearmod, Glass_vf, y});

%%%%% Setting the expression of the ODE for the stress w.r.t. temperature.
dydT = ((1-curr_phi)*dla_dtemp + dlf_dtemp*(1/lf)*(Stretch_1 - ...
(1-curr_phi)*la))/(-(1-curr_phi)*dla_ds - dlf_ds*(1/lf)*...
(Stretch_1-(1-curr_phi)*la));
```

```

%%%%%%%%%%%%%%%%%%%%%%%%%%%%%%%%%%%%%%%%%%%%%%%%%%%%%%%%%%%%%%%%%%%%%%%%%% HEATING ODE CODE %%%%%%%%%%%%%%%%%%%%%%%%%%%%%%%%%%%%%%%%%%%%%%%%%%%%%%%%%%%%%%%%%%%%%%%%%%%

%%%%%%%% Function to obtain the ODE for the stretch recovery with respect
%%%%%%%% to a change in temperature while maintaining constant stress
function dydT = Heating_ode_withBrentdata (T4, y)

%%%%%%%% Initializing the global variables: material properties and the
%%%%%%%% equations to solve for the stretch in each phase.

global alpha_a

global Rubber_vf
global Glass_vf

global Rubber_shearmod
global Glass_shearmod

global CALIBRATIONPHI
global CALIBRATIONTEMP

global lambda_a
global lambda_f

%%%%%%%% Recalling the values of the temperature and stress the material
%%%%%%%% experienced during cooling
global Temperature_during_cooling
global Stress_during_cooling

syms s ma va mf vf

%%%%%%%% Getting the frozen volume fraction for each increment of temperature.
heat_phi = GetPhi(T4);

%%%%%%%% Numerically differentiating the frozen volume fraction w.r.t.
%%%%%%%% temperature.
dp = diff(CALIBRATIONPHI);
dp(length(dp)+1) = dp(length(dp));
dT = diff(CALIBRATIONTEMP);
dT(length(dT)+1) = dT(length(dT));
dpdT = dp./dT;

%%%%%%%% Interpolating for the derivative of the frozen volume fraction at the
%%%%%%%% current temperature the stress of the material when last at the
%%%%%%%% current temperature.

```

```
dphi = interp1(CALIBRATIONTEMP, dpdT, T4);
Stress = interp1(Temperature_during_cooling, Stress_during_cooling, T4);

%%%%% Caclulating the stretch of the material in each phase due to the
%%%%% stress of the material when last at the current temperature (during
%%%%% cooling).
la = subs(lambda_a, {ma, va, s}, {Rubber_shearmod, Rubber_vf, Stress});
lf = subs(lambda_f, {mf, vf, s}, {Glass_shearmod, Glass_vf, Stress});

%%%%% Setting the expression of the ODE for the stretch w.r.t. temperature.
dydT = -dphi + (1-heat_phi)*alpha_a + (1/lf)*la*dphi;
```

VITA

Brent Louis Volk is the third son in his family, and brother to Eric and Chris. He is married to his wife Abby. He was raised in Arlington, Texas, and attended Lamar High School. After graduating high school, Brent attended Texas A&M University and completed a B.S. in aerospace engineering in May of 2007. He then enrolled in the graduate program in aerospace engineering at Texas A&M University in the fall of 2007, where he has worked under the guidance of Dr. Dimitris C. Lagoudas. His research interests include the material characterization and modeling of active materials, particularly shape memory polymers and shape memory alloys. An extended resume can be found at <http://smart.tamu.edu>. Mr. Volk can be reached at his permanent address:

2400 Central Park Lane
Apartment 203
College Station, TX, 77840

His email address is blvolk@gmail.com.

The typist for this thesis was Brent Louis Volk.